UNIVERSITY OF CALIFORNIA,
IRVINE

Large Amplitude Oscillatory Shear (LAOS) Rheology of Pickering Emulsions

THESIS

submitted in partial satisfaction of the requirements

for the degree of

MASTER OF SCIENCE

In Chemical Engineering

by

Kunal Choudhuri

Thesis Committee:

Associate Professor Ali Mohraz, Chair

Assistant Professor Mikael Nilsson

Professor Albert Yee

2016

Table of Contents

Page

Table of Figures

Acknowledgements

It was a great privilege for me, to work in The Colloid Sciences Laboratory, University of California Irvine as a graduate researcher. The exposure and the experience that I have gained are invaluable and I am sure that they will be of immense help to me in the future.

I avail this opportunity to express deep sentiments of gratitude to my committee chair, Professor Ali Mohraz for introducing me to the fascinating world of colloid science. I extend my sincere thanks to him for providing me excellent infrastructure facilities to carry out the present work, for eliciting novel perspectives towards the whole approach of the project and encouraging me to think independently as a researcher. This work would not have been possible without his guidance and encouragement.

I would like thank my committee members, Professor Mikael Nilsson and Professor Albert Yee for kindly serving in my committee. I would like to appreciate their support and personal attention throughout the period of my thesis project.

I am greatly indebted to my colleagues from CSL for their valuable support, encouragement and inspiring valuable suggestions throughout my research work. I gratefully acknowledge the help of Max Kaganyuk for training me on using the various instruments and his advice on crucial research work. The numerous discussions on research topics with him had enabled me to gain valuable scientific insights. I would like to thank Todd Thorson, Joseph Goodrick and Dr. Jessica Witt for helping me to complete this project work.

Last, but not least, I owe my gratitude to my family and friends for all the love and affection they have showered upon me.

KUNAL CHOUDHURI

Abstract of the Thesis

Large Amplitude Oscillatory Shear Rheology of Pickering Emulsions

By

Kunal Choudhuri

Master of Science in Chemical Engineering

University of California Irvine, Irvine, 2016

Associate Professor Ali Mohraz, Chair

Emulsions are a class of disperse systems consisting of two immiscible liquids. The liquid droplets (the disperse phase) are dispersed in a liquid medium (the continuous phase). In order to disperse two immiscible liquids, a third component is required, namely the emulsifier. The choice of emulsifier is crucial not only for the formation of the emulsion but also for its long term stability [1]. Pickering emulsions are emulsions of any type, either oil-in-water (o/w), water-in-oil (w/o), or even multiple, stabilized by solid particles in place of surfactants. Pickering emulsions are named after S.U. Pickering whose paper is considered the first report of o/w emulsions stabilized by solid particles adsorbed at the surface of oil droplets [2]. The 'surfactant-free' character of these emulsions makes them attractive to several applications fields, in particular cosmetic and pharmaceutical applications where surfactants often show adverse effects [3].

Typically in Pickering emulsions, the droplet interfaces are stabilized by the presence of particles. These particles can modify the flow properties or rheology of the emulsions by modifying the interaction between the droplets. Hence an understanding of emulsion flow properties is of fundamental interest and of value for many applications [4]. This research work is focused on studying and analyzing the Large Amplitude Oscillatory Shear (LAOS) Rheology of Pickering emulsions stabilized by Poly(methyl methacrylate) or PMMA particles. With the help of the MITlaos framework, intra-cycle nonlinearities such as strain stiffening/softening and shear thickening/thinning have been studied for these Pickering emulsions. Firstly, the repeatability aspect of the experimental protocol has been studied followed by the LAOS analyses at three different strain percentages. The analyses have been compared for the slip v/s no-slip cases as well and the elastic and viscous nonlinearities have been quantified. Finally, the prospect of analyzing the LAOS Rheology at two different volume fractions of particles have been performed. In these experiments, elastic and viscous nonlinearities are not observed at low strains but they become more prominent as the strain percentages are increased. Through the use of Chebyshev

decomposition of the stress response and alternate moduli to quantify the nonlinearities, we gain physical insight about the sample behavior as it is subjected from low to higher strains/strain-rates. These physical insights can be obscured by conventional rheology characterization test protocols like Small Amplitude Oscillatory Shear (SAOS) techniques.

Another aspect of the thesis work is aimed to combine rheology with imaging using a 20X objective lens on the Discovery Hybrid Rheometer (TA-Instruments, DHR-3). This imaging allowed me to correlate between the droplet deformations and the large amplitude rheology. At low strains, the droplet deformations are reversible, as observed from the comparison of the images taken before and after the sample is subjected to shear. At large strains, however, the droplet deformations are irreversible. As the emulsion yields from being 'solid-like' to 'liquid-like' in response to the increasing strain, the permanent droplet deformations become kore prominent. The observations of the imaging studies using the DHR are complemented by the results of the LAOS analyses.

Chapter 1

Introduction

As compared to surfactant based emulsions, the droplets are stabilized by colloidal particles in Pickering emulsions. The interfacial attachment energy for a surfactant molecule is several k_BT, therefore the interfacial population is always in a dynamic equilibrium with a population in the host solvent. Colloidal particles, on the other hand, need to overcome an energy barrier of hundreds or thousands of k_BT to detach from the interface [4]. Once covered in particles, these Pickering emulsions are extremely stable owing to this huge energy barrier. Another advantage of these Pickering emulsions is that the interactions between colloidal particles are very well understood and can be tuned according to the requirements. There are several ways of tuning the interactions like chemical modification, index matching and the addition of salt or non-adsorbing polymers. Due to these reasons, Pickering emulsions find widespread applications in the pharmaceutical and cosmetic industries.

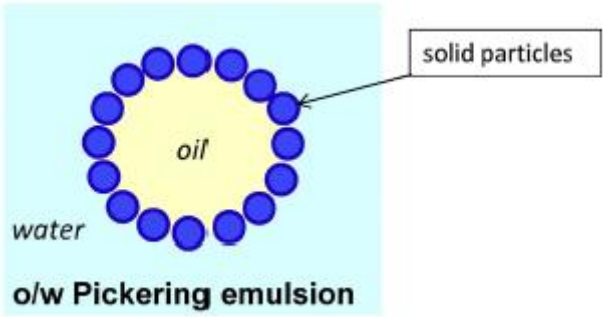

Figure 1: The solid particles adsorbed at the oil-water interface stabilize the oil-in-water Pickering emulsion. (Courtesy: Yves Chevalier and Marie-Alexandrine Bolzinger, Elsevier 2013)

To describe the behavior of a single particle at the liquid-liquid interface, the expression for the adhesion energy as a function of the contact angle can be given by [5]-

$$\Delta E = \pi R^2 \gamma_{OW} (1 - |\cos\theta|)^2$$

Here R is the radius of the particle, γ_{OW} refers to the interfacial tension at the oil-water interface and the contact angle is given by θ. The convention to measure θ from the more polar liquid (water in this case) has been used [6]. Hence we have $0° \leq \theta < 90°$ for hydrophilic particles and $90° < \theta \leq 180°$ for hydrophobic particles.

The oscillatory shear tests can be used to study the rheology of soft materials where a material is subjected to a sinusoidal deformation and the mechanical response is recorded as a function of time. If we find a linear viscoelastic response, it can be quantified by two material measures- the elastic storage modulus G'(ω) and the viscous loss modulus G''(ω), where ω refers to the angular frequency of oscillation. In the linear viscoelastic region, the strain amplitude is small enough such that the elastic and loss moduli are independent of the strain amplitude [7]. Owing to the firm theoretical foundations, linear viscoelasticity tests, also called Small Amplitude Oscillatory Shear tests (SAOS tests), are excellent ways to probe the rheological characterization of complex fluids and soft materials. However, as the amplitude of the applied strain is increased at a constant frequency, a transition between the linear and non-linear regions is observed beyond the SAOS regime. The nonlinear region is characterized by the storage and loss moduli being functions of the strain amplitude Υ_0, namely G'(Υ_0) and G''(Υ_0). Here Υ_0 refers to the strain amplitude. At larger strain amplitudes, the nonlinear behavior is more apparent and hence nonlinear dynamic tests are typically referred to as Large Amplitude Oscillatory Shear (LAOS) tests [7]. Despite the fact that SAOS tests are efficient tools to comprehend the relationship between microstructure and rheology of complex fluids, it is important to realize that the linear viscoelastic tests have a meaning only when the total deformation is quite small. The deformations can be often large and rapid in processing operations and thus linear viscoelastic tests are not sufficient to characterize the rheology in these nonlinear situations [7]. It is therefore understood that studying the nonlinear viscoelastic response of soft materials is of paramount importance.

There are several ways to characterize the nonlinear rheology of soft materials. In the present thesis work, the MITlaos protocol developed by Randy H. Ewoldt, A.E. Hosoi and Gareth McKinley (*J. Rheol. 52 (6), 1427-1458 November/December (2008*)) has been used to study and characterize the LAOS response of Pickering emulsions. The protocol uses Chebyshev coefficients and alternate moduli to quantify the nonlinearities observed in a material response. Through the use of this protocol a deeper insight is obtained regarding the rheology of Pickering emulsions as compared to the conventional test protocols like SAOS analyses. A detailed explanation of the LAOS protocol and the descriptions of the various quantification methods has been covered in Chapter 2 of the thesis report.

The experimental system used in the thesis work is the utilization of nearly monodisperse PMMA particles which stabilize an aqueous phase-in-organic phase Pickering emulsion. While dodecane has been used as the oil phase, de-ionized water nearly saturated with sodium iodide has been chosen to be the aqueous phase. The addition of sodium iodide in water helps us to increase the refractive index of water to match that of the solid particles. As the first step of the experiments, the repeatability aspect of the LAOS tests has been addressed. By comparing the results of four LAOS analyses at Υ_0=0.6 and ω=1 radian/sec, the repeatability limit is calculated. It is shown that the values of two parameters used to quantify nonlinearity are within the repeatability limit and hence the robustness of the LAOS protocol to characterize intra-cycle nonlinearity is determined. The next part of the research is focused on performing the LAOS analyses at three strain

percentages and angular frequencies. At small strain amplitudes, a linear viscoelastic response is observed as evident from the Lissajous curves of the stress v/s strain response. In this context both elastic and Lissajous plots have been plotted to characterize and visualize the intracycle nonlinearities. As the strain amplitude is progressively increased, the deviation of these curves from the elliptical nature is observed. With the help of a Pipkin diagram, the Lissajous curves have been plotted as a function of both the strain amplitude and the oscillating frequency. However, the elastic Lissajous curve again takes an elliptical shape at a high strain amplitude (Υ_0=7 and ω=7.5 radians/sec). This can be attributed to the phenomena of slip, which disrupts any relaxation mechanisms at such high angular frequencies. The observations of the Lissajous curves are complemented with the results of the LAOS analyses obtained by the rheological experiments performed on the TA-Instruments AR-G2 Rheometer. Using simultaneous rheology and imaging, I have been able to capture the images of the emulsion taken before and after the LAOS tests and the two images were compared. The imaging was performed using a 20X objective lens on the TA Instruments Discovery Hybrid Rheometer (DHR-3). In the linear regime when the strain amplitudes are small, the microstructure deformations are reversible and no noticeable change is observed between the images taken before and after the tests. As the strain is increased, the microstructure changes become irreversible and we observe that the droplets do not come back to their original configurations. The observation can be explained by the phenomena of 'caging' where the droplets are trapped in cages by their neighbors at low strains, but they escape from their cages once the amplitude is increased. Realizing that slip is an important factor which can determine the rheology of emulsions, the LAOS analyses of the Pickering emulsions were also compared between the slip and no-slip cases. The phenomena of slip is prevented by coating the bottom glass surface and the top geometry surface with a transparent nail polish. The prevention of slip is proved by the help of imaging where we compare the slip v/s no-slip case under identical conditions of strain percentage and frequency. Finally the particle volume fraction is varied and rheological analyses are performed for two volume fractions of 2% and 5% for the case of three strain percentages and two angular frequencies. The details of the sample preparation and the LAOS analyses are covered in Chapter 3.

Chapter 2

The MITlaos Framework

Introduction

In this chapter, the MITlaos framework developed by Randy H. Ewoldt, A.E. Hosoi and Gareth H. McKinley (*J. Rheol. 52 (6), 1427-1458 November/December (2008*)) has been discussed in detail. In the present research work, MITlaos is used as a tool to characterize nonlinear viscoelasticity in LAOS. The main aim of the framework was to develop to tool which could probe the complex viscoelastic response of soft materials in the most appropriate way [8].

In the linear region when the strain amplitude is small, the viscoelastic moduli G'(ω) and G''(ω) are used to characterize the material. However, in the nonlinear regime, the moduli are not defined owing to the fact that a nonlinear stress response is not a single harmonic sinusoid [8]. For the quantification of LAOS tests, Fourier Transform (FT) Rheology is one of the most commonly used methods. Considering a sinusoidal strain input $\Upsilon=\Upsilon_0 \sin(\omega t)$, the Fourier series can be used to represent the stress response σ in the following way,

$$\sigma(t;\omega,\gamma_0) = \gamma_0 \sum_{n\ odd} \{G_n'(\omega,\gamma_0)\sin n\omega t + G_n''(\omega,\gamma_0)\cos n\omega t\}$$

In this Fourier series representation, only the odd harmonics are included [8]. This is because the stress response is assumed to be of odd symmetry with respect to the directionality of shear strain, which means that if the coordinate system were to be reversed, the material response would not change. This FT Rheology technique is mathematically robust and reduces to the linear viscoelastic framework when the strains are small. However this framework suffers from two major drawbacks [8]-

- Although the Fourier Transform technique is an excellent indicator of nonlinearity, the FT framework does not result in a clear physical interpretation of the higher order coefficients.
- The use of first harmonic coefficients G_1' and G_1'' as measures of the viscoelastic moduli in the nonlinear regime is arbitrary and is unable to capture the nonlinearities which are apparent in the raw data signal.

As an example to illustrate how the first harmonic moduli G_1' and G_1'' fail to capture the nonlinearities in the stress response signal, Figures 2 and 3 are shown. These figures refer to the oscillatory strain sweeps of pedal mucus from *Limax maximus* at a frequency of ω=3 rad/sec [9]. Figure 2 shows the typical rheometric measures of viscoelastic moduli while figure 3 represents the raw data measured by the torque transducer where the stress response is plotted against the induced strain [8].

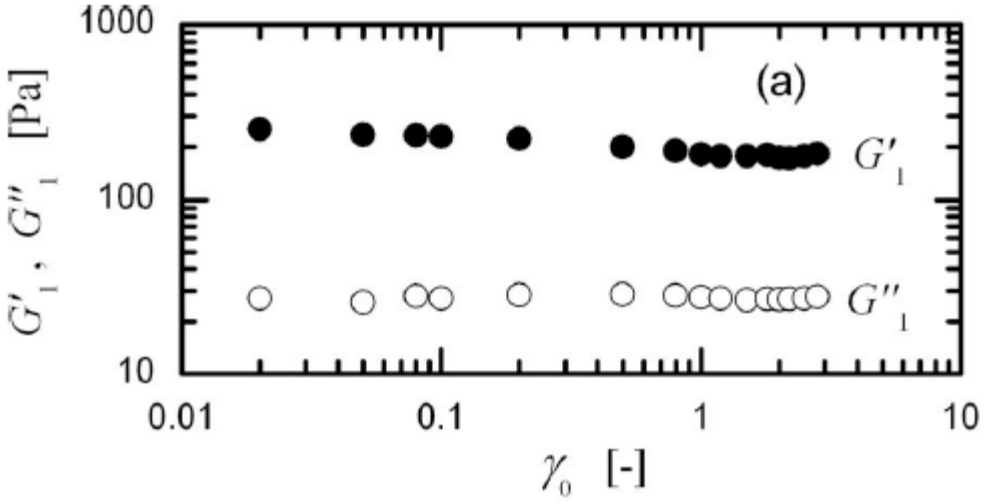

Figure 2: The typical output from a rheometer of the fluid viscoelasticity as described by the first harmonic Fourier moduli (Courtesy: Randy H. Ewoldt, A.E. Hosoi and Gareth H. McKinley (J. Rheol. 52 (6), 1427-1458 November/December (2008))

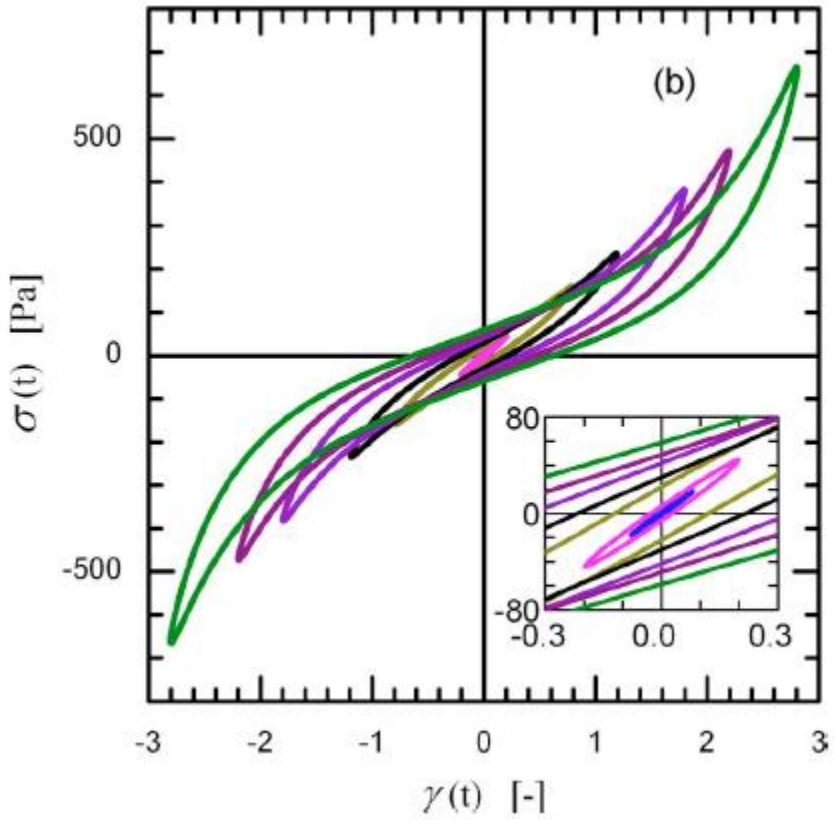

Figure 3: The raw data is plotted as σ(t) vs ϒ(t) also called Lissajous plot. Here, nonlinear characteristics are observed which can be typically hidden by the first harmonic moduli.

(Courtesy: Randy H. Ewoldt, A.E. Hosoi and Gareth H. McKinley (*J. Rheol. 52 (6), 1427-1458 November/December (2008*))

As evident from Figure 2, the elastic modulus G_1' decreases slightly with strain amplitude which depicts a minor softening behavior. As compared to this, Figure 3 reveals a nonlinear response implying strain stiffening [8]. In the linear regime, the Lissajous plots are elliptical in shape as shown in the inset of Figure 3. As the strain amplitude is increased, the nonlinearities creep in and the elliptical nature of the curve begins to get distorted. The strain stiffening response is understood if we project the center portion of the ellipse and find out that the shear stress is greater at larger strains as compared to the stress response at low strains. This apparent disparity between the two figures underscores the need of a protocol which could capture the intra-cycle nonlinearities. Thus the MITlaos framework is a quantitative measure which can easily describe and identify such nonlinear behavior.

Theory

Part 1: Interpretation of higher harmonics in in the stress response

For proper interpretation of the LAOS data in a physically meaningful manner, the nonlinear stress response is decomposed into a superposition of an elastic stress σ'(x) and a viscous stress σ'(y) [Cho *et al*. (2005)]. This decomposition is an extension of the method of orthogonal stress decomposition. Here x= $\frac{\gamma}{\gamma_0}$ =sin ωt and y=$\frac{\dot{\gamma}}{\dot{\gamma}_0}$ = cos ωt. The total oscillatory stress thus is the summation of the elastic stress and the viscous stress; σ (t) =σ' (t) +σ'' (t). It should be noted here that σ' exhibits odd symmetry with respect to x and even symmetry with respect to y while σ'' exhibits even symmetry with respect to x and odd symmetry with respect to y [8].

$$\sigma' = \frac{\sigma(\Upsilon, \dot{\Upsilon}) - \sigma(-\Upsilon, \dot{\Upsilon})}{2} = \Upsilon_0 \sum_{n\ odd} G_n'(\omega, \Upsilon_0) \sin \omega t$$

$$\sigma'' = \frac{\sigma(\Upsilon, \dot{\Upsilon}) - \sigma(\Upsilon, -\dot{\Upsilon})}{2} = \Upsilon_0 \sum_{n\ odd} G_n''(\omega, \Upsilon_0) \cos \omega t$$

In this manner, the elastic and viscous stresses can be related to the Fourier decomposition. A polynomial regression fit is suggested to these lines of elastic and viscous stresses by Cho *et al*. Using the process of elimination the authors argue that the set of Chebyshev polynomials of the first kind is the most logical choice for understanding the LAOS data [8]. This choice is based on the fact that these functions are bounded, exhibit symmetry about x=0, are orthogonal on the domain [-1,+1] and can be related to the Fourier coefficients which have dominated the LAOS rheology. Using these basis functions, the elastic and viscous contributions to the stress response can be described as [8]-

$$\sigma'(x) = \Upsilon_0 \sum_{n:odd} e_n(\omega, \Upsilon_0) T_n(x)$$

$$\sigma''(y) = \dot{\Upsilon}_0 \sum_{n:odd} v_n(\omega, \Upsilon_0) T_n(y)$$

Here, $T_n(x)$ is the n-th order Chebyshev polynomial of first kind, while e_n and v_n are referred to as the elastic and viscous Chebyshev coefficients respectively. In the linear region, $e_3/e_1 \ll 1$ and $v_3/v_1 \ll 1$ such that $e_1 \rightarrow G'$ and $v_1 \rightarrow \frac{G''}{\omega}$. As a result of this Chebyshev decomposition of the stress response, we can conclude that $e_3 > 0$ corresponds to intracycle strain stiffening of the elastic stress while $e_3 < 0$ describes strain softening. Similarly, a positive value of the viscous coefficient $v_3 > 0$ indicates shear thickening of the viscous stress while a negative value corresponds to a shear thinning behavior [8]. The relationships between the Chebyshev and the Fourier coefficients can be described as follows-

$$e_n = G_n'(-1)^{(n-1)/2} \qquad n: odd$$

$$v_n = \frac{G_n''}{\omega} = \eta_n' \qquad n: odd$$

Hence, the third order Fourier coefficients can now be given a physical interpretation exactly in a similar fashion as the third order Chebyshev coefficients. With the aid of this MITlaos framework, the Fourier coefficients can be used to calculate physically meaningful measures of nonlinearity, i.e. the elastic and viscous Chebyshev coefficients [8].

Part 2: Meaningful viscoelastic moduli in the nonlinear regime

As explained in the introduction section of this chapter, the first harmonic moduli G_1' and G_1'' are often unable to describe the nonlinearities in the raw data response. This protocol aims to define alternate viscoelastic moduli in the nonlinear regime which have distinct physical interpretations and complement the often reported first order Fourier coefficients [8]. These moduli are chosen in such a way that they reduce to the material functions G' and G'' in the linear regime but capture the physical insight of the material nonlinearities which can be obscured by G_1' and G_1''. Accordingly, the authors here define a set of elastic moduli which are derived geometrically and then relate their values to both the traditional Fourier Transform Rheology descriptions and the Chebyshev stress decompositions [8].

$$G_M' = \left.\frac{d\sigma}{d\Upsilon}\right|_{\Upsilon=0} = \sum_{n\ odd} nG_n' = e_1 - 3e_3 + \cdots$$

$$G_L' = \left.\frac{\sigma}{\Upsilon}\right|_{\Upsilon=\pm\Upsilon_0} = \sum_{n\ odd} G_n'(-1)^{(n-1)/2} = e_1 + e_3 + \cdots$$

Here, G'_M is the minimum-strain modulus or tangent modulus at ϒ=0 and G'_L is the large-strain modulus or secant modulus calculated at the maximum strain [8]. In the linear viscoelastic region, $G'_M = G'_L = G'_1$=G'(ω). For a sinusoidal strain input, at the point where the strain is zero, the strain-rate is at a local maximum and hence the viscous contribution to the stress is locally constant. This implies that any change in stress should be related only to elasticity. Similarly, for ϒ=Υ_0, the strain rate is zero implying that the instantaneous viscous stress at this point is also 0. Therefore, the resulting stress is because of only the elastic characteristics of the material. For a large imposed strain amplitude, $G'_L > G'_M$ indicates that the material is strain stiffening within the given cycle while $G'_L < G'_M$ is an indicator of intracycle strain softening [8].

In line with the large-strain and minimum-strain elastic moduli, a pair of viscous moduli have also been defined in a similar fashion [8].

$$\eta'_M = \left.\frac{d\sigma}{d\dot{\Upsilon}}\right|_{\dot{\Upsilon}=0} = \frac{1}{\omega}\sum_{n\ odd} nG''_n\,(-1)^{(n-1)/2} = v_1 - 3v_3 + \cdots$$

$$\eta'_L = \left.\frac{\sigma}{\dot{\Upsilon}}\right|_{\dot{\Upsilon}=\pm\dot{\Upsilon}_0} = \frac{1}{\omega}\sum_{n\ odd} G''_n = v_1 + v_3 + \cdots$$

Here, η'_M refers to the minimum-rate dynamic viscosity while η'_L corresponds to the large-rate dynamic viscosity. In the linear regime, each of these moduli reduce to the value of $\eta' = \frac{G''}{\omega}$. As before, $\eta'_L > \eta'_M$ indicates that the material suffers from intracycle shear thickening while $\eta'_L < \eta'_M$ is an indicator of a shear thinning behavior within the given cycle [8].

Example

As an example of LAOS Rheology and the interpretation of the results of the MITlaos software, I have prepared a water-in-oil emulsion stabilized by PMMA particles. The details of the sample preparation is explained in Chapter 3 of this report. The sample was loaded onto a TA-Instruments AR-G2 Rheometer and the rheological test was performed using a cone-and-plate geometry (Cone angle of 1.988 degrees, diameter 40mm and truncation gap of 60 micro-meters). The LAOS test was done at a strain percentage of 700 and an oscillating frequency of 7.5 rad/sec. The raw displacement and torque data were collected from the rheometer. In order to reduce the noise, the average of every 10 points for the displacement and torque was calculated. Then this data was fed to the MITlaos software for the LAOS analysis. The figure below shows the overview plot of the test which helps us to characterize the intracycle nonlinearities. The interpretation of the plot is described as follows-

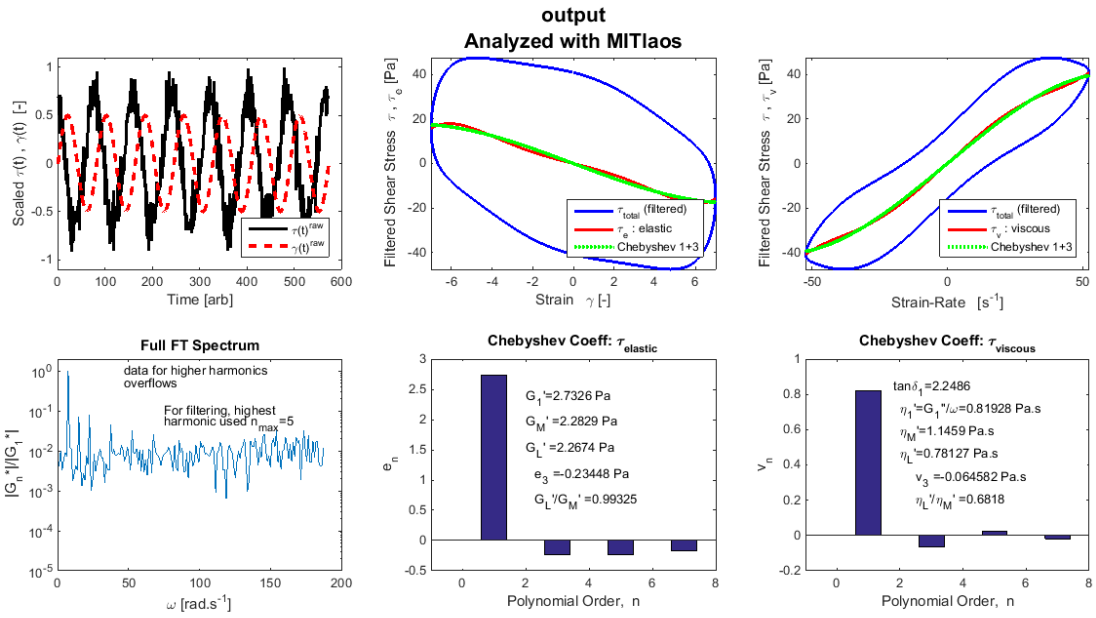

Figure 4: Overview plot of the LAOS analysis at 700% strain and 7.5 rad/sec angular frequency

Interpretation of the plot-

First row (from left to right)-

The first figure indicates the plots of raw strain and stress with respect to an arbitrary time. The second plot refers to the Lissajous plot where the total and elastic stresses are plotted with respect to the strain. The blue line indicates the total stress while the red line indicates the elastic stress. The use of the first and third elastic Chebyshev coefficients to express the elastic stress, shown by the green line, is extremely good as is seen by the almost overlapping nature of those two lines. The third plot refers to the Lissajous plots of total and viscous stresses with respect to the strain-rate. As before, the first and third viscous Chebyshev coefficients are able to represent the viscous stress quite well.

Second row (from left to right)-

The first figure indicates the full Fourier Transform spectrum of the stress. The normalized Fourier coefficients are plotted and I have chosen the highest odd harmonic used in stress reconstruction to be 5. Beyond that, the spectrum essentially enters the noise region. The second plot refers to the values of the elastic Chebyshev coefficients with respect to the polynomial order and also indicates the values of G_L' and G_M'. This plot gives important information regarding the quantitative degrees of intra-cycle non-linearity observed in the emulsion. The negative value of the third elastic Chebyshev coefficient (denoted by e_3), indicates an intra-cycle strain-softening behavior of the emulsion at large amplitudes. The value of G_L' being less than G_M' indicates that the material tends to "soften" at large amplitudes, a fact that is in harmony with the negative value of e_3. The third plot indicates the viscous Chebyshev coefficients with respect to the

polynomial order. The interpretation of this plot is similar to the previous one. We observe a negative value of the third viscous Chebyshev coefficient indicating the intra-cycle shear thinning behavior of the material at high strain-rates. The ratio of $\frac{\eta_L'}{\eta_M'}$ being less than 1 indicates the same shear thinning behavior as predicted by the value of v_3.

One important observation in the plot is that a higher value of η_M' as compared to η_L' indicates that at small instantaneous strain-rates (corresponding to strains near the maximum strain), the deformed material tends to be more dissipative. Another vital observation is that the elastic Lissajous plot takes an elliptical shape which resembles a linear viscoelastic response. The ratio of $\frac{G_L'}{G_M'}$ takes a value of 0.99325, which is very close to 1, evocative of a linear behavior. This response can possibly be attributed to the phenomenon of slip at the surfaces at such a high strain percentage and angular frequency. The slip essentially ruptures any relaxation mechanism of the material such that the response becomes linear. These vital physical insights into the material behavior can be completely hidden by the conventional test protocols. Through the interpretation of the plot, crucial information about the intracycle nonlinearities can be obtained. This underscores the importance of the MITlaos framework in understanding the Large Amplitude Oscillatory Shear Rheology of soft materials.

Chapter 3

Results and Discussions

Introduction

In this chapter the emulsion sample preparation as well as the LAOS tests have been described in detail. In Part 1 of this chapter, the sample preparation is explained and the repeatability aspect of the LAOS analysis is studied in part 2. By performing the analysis at a strain percentage of 60% and an angular frequency of 1 rad/sec, we use the concept of repeatability limit for understanding the repeatability criteria of the tests. In part 3, the LAOS analysis is performed at three different strain percentages of 1%, 60% and 700% and at angular frequencies of 3, 5 and 7.5 rad/sec. In part 4 of this chapter, the effect of slip on the large amplitude rheology of these emulsions is analyzed. By preventing wall slip at the top and bottom surfaces, the LAOS analyses are compared in both the cases of slip and no-slip. In both parts 3 and 4, we take the help of simultaneous imaging and rheology using a TA Instruments DHR-3 Rheometer. This imaging helps us to relate microstructure deformations with the large amplitude rheological characterization using the MITlaos software. Finally part 5 of this chapter deals with the effect of variation of particle volume fraction on the LOAS analyses. We have used two volume fractions of 2% and 5% of PMMA particles in the emulsion and studied how the MITlaos response varies with particle volume fraction.

Part 1- Sample Preparation

Stabilizing Particles- The particles used in the Pickering emulsion system consist of graft co-polymer chains of poly-(dimethylsiloxane)-g-poly (methyl methacrylate), also represented as PDMS-g-PMMA. These partially hydrophobic particles tend to stabilize a water-in-oil emulsion and have a diameter of 1.3 microns. Unless stated, I have used a particle volume fraction of 5% throughout the course of my research work.

Liquid phases- The oil phase was taken to be dodecane (Chemical Formula- $C_{12}H_{26}$). De-ionized water also called DI water was used as the aqueous phase. To visualize the microstructure of the emulsion by confocal microscopy, the refractive indices of the liquid phases had to be matched with that of the particles. In order to bring up the refractive index of water, sodium iodide was dissolved into the water at a total concentration of 60% by mass. The aqueous phase to oil phase ratio was kept at 50:50.

Procedure- The PMMA particles are first dispersed into the two phase liquid mixture followed by vortex mixing for 10 seconds. Then the sample was kept in the sonication bath (Branson 1510) for 1 hour. Next the ultrasonic probe (Branson Sonifier 250) was operated on the sample at 2W for a period of 2 minutes with 80% duty cycle. After preparing the emulsion it was centrifuged (VWR Clinical 200) at 1500 rpm for 6 minutes. This was done to remove some of the continuous phase and make the material a bit more viscoelastic. After removing the oil, the aqueous phase

concentration was raised to 56.4% and the particle volume fraction increased to 5.6%. It was observed that centrifuging at higher rpm values was causing the droplets to be deformed. I have attached four 20X images of the emulsions. Figure 5 shows the 20X confocal images of these concentrated emulsions while Figure 6 depicts the 20X images on the DHR.

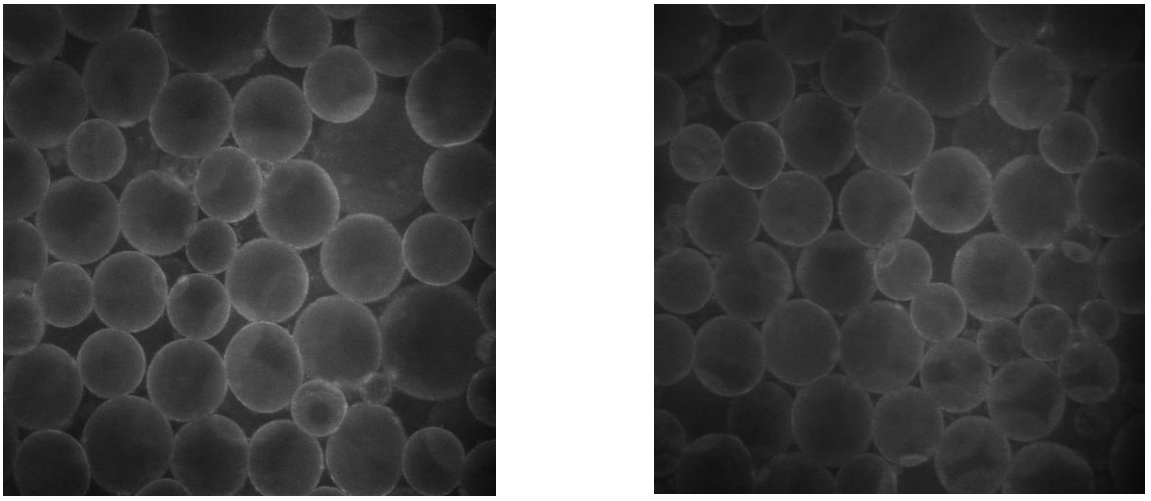

Figure 5: 20X confocal images of the Pickering emulsion

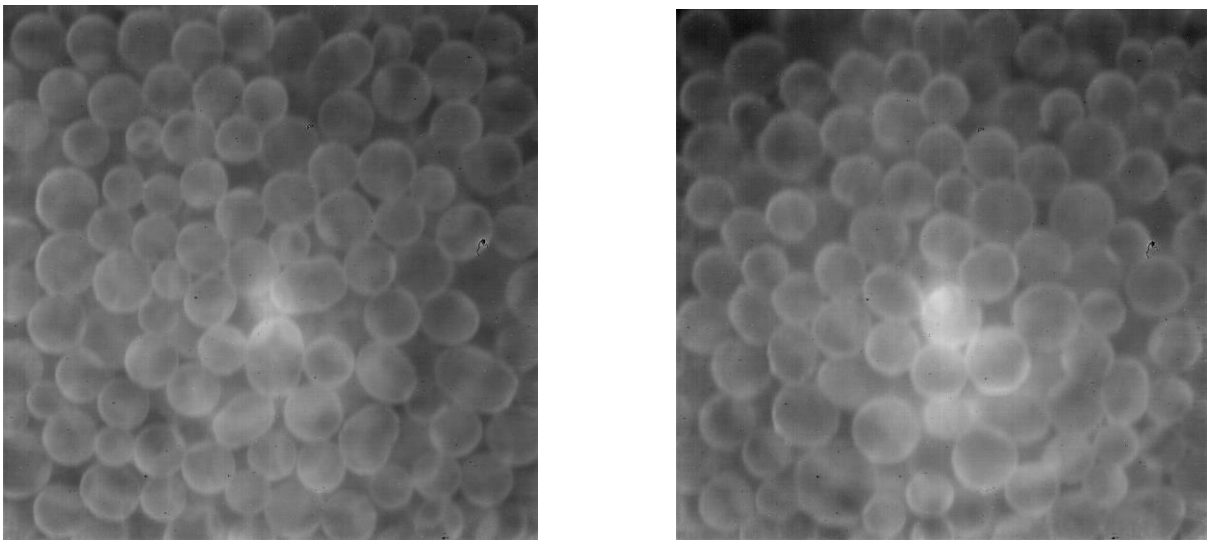

Figure 6: 20X images of the emulsion captured on the DHR

Part 2: Repeatability of the LAOS Tests

The primary objective of this section is to check whether the LAOS tests using the MITlaos framework are repeatable or not. Although they are useful in characterizing the nonlinear rheology of emulsions, the repeatability of the experiments is an important aspect and is a primary requirement of any robust rheology characterization technique. Keeping that in view the sample was prepared according to the protocol explained in the previous section and the rheological characterization as described below-

Rheology- I used the cone and plate geometry on the DHR with a cone diameter of 40 millimeters and the angle of the cone being 2.026 degrees. The truncation gap was 62 micro-meters. The frequency of operation was kept at 1 rad/sec and the strain percentage was 60%.

Three separate LAOS analyses were performed using the same methods of sample preparation and were subjected to identical rheological tests. The repeatability limit was calculated for two parameters; $\frac{G_L'}{G_M'}$ and $\frac{\eta_L'}{\eta_M'}$ in the case of three tests. It is finally shown that the absolute difference between any two values of a parameter lies within this limit from which the repeatability aspect of the MITlaos protocol is ascertained. Before proceeding to the test results, a brief explanation of the concept of repeatability is introduced.

Generally, during experiments, two kinds of error occur- random and systematic. A random error is associated with the fact that when a measurement is repeated, it will generally provide a measured value that is different from the previous value. It is random in that the next measured value cannot be predicted exactly from previous values. The concept of random error is closely related to the concept of precision. The higher the precision of a measurement technique, the smaller is the standard deviation in its readings. In the case of a good measurement technique, the difference in the values should be small enough for the particular purpose for which we want the measurements. Repeatability of an experiment can be described as the closeness of agreement between independent results obtained with the same method on identical test material, under the same conditions [10]. To provide a quantitative measure of repeatability, the repeatability limit is defined as the value less than or equal to which the absolute difference between two test results obtained under repeatability conditions may be expected to be with a probability of 95% [11]. On the assumption that under repeatability conditions, individual test results follow a standard deviation σ, the differences between pairs of such results will follow a normal distribution with mean 0 and standard deviation $\sqrt{2}\sigma$ [11]. For all normal distributions, 95% of values lie within 1.96 standard deviations of the mean. Hence, the repeatability limit r is given by-

$$r=2.8\ \sigma \text{ [12]}$$

Finally, to put it simply, approximately 95% of all pairs of test results can be expected to differ in absolute value by less than r. Two test results from the same laboratory would be considered

suspect if they differed in absolute values by more than r [12]. Using the above framework, let us find out the repeatability limit of the two parameters $\frac{G_L'}{G_M'}$ and $\frac{\eta_L'}{\eta_M'}$

A. $\frac{G_L'}{G_M'}$: The analysis of the three results are as follows-

Values of the parameter in the 3 experiments: 1.8224, 2.1678, 2.5008
Standard Deviation: 0.33922
r: 0.9498
Absolute differences between pairs of values: 0.3454, 0.33, 0.6784

B. $\frac{\eta_L'}{\eta_M'}$: The analysis of the three results are as follows-

Values of the parameter in the 3 experiments: 0.53438, 0.56519, 0.5863
Standard Deviation: 0.02611
r: 0.073
Absolute differences between pairs of values: 0.031, 0.02, 0.052

The overview plots of the LAOS tests from the three experiments is shown in Appendix 1. As is clear from the calculations above, in both the cases, the absolute values of the differences are less than r. So the values are within the repeatability limit and can be considered precise. The differences between any pair of values being less than the limit indicate that the LAOS analysis is indeed a robust technique for measurement of intra-cycle non-linearity. Hence, it can be concluded that the LAOS technique is reproducible and can serve as an essential tool for rheological characterization of samples. However, it should be noted that the tests have been carried out in identical circumstances (like temperature). Under proper operating conditions, the LAOS can serve as a powerful tool in the future for the Colloid Sciences Laboratory. Although the method works well when the sample size is relatively large, I have used three experiments to calculate the repeatability limit in order to show how this concept can be used to provide reliable information on which precision statements can be based.

Part 3: Analysis of LAOS with the variation of strain percentage and frequency

In this section we see how the LAOS analysis changes with the variation of strain percentage and frequency. With the aid of simultaneous imaging and rheology using the DHR, we can correlate between the microstructure deformation and large amplitude rheology. First an amplitude sweep curve of the emulsion is shown, followed by the elastic and viscous Lissajous plots at 3 strain percentages and frequencies. Finally, the 20X images are presented which helps us to explain some of the LAOS results that we observe.

If the overall goal of the research is to correlate between the micro-structure deformations and large amplitude rheology, it is a good idea if we compare what's happening at low strain amplitudes to the observations at higher amplitudes. By observing the amplitude sweep curve (as shown in figure 7), we find that a strain percentage of 1 is in the linear region while a strain percentage of 700 ensures that we are looking at analyses in the nonlinear regime. We choose another strain percentage at 60, in between these two values, for a better analysis of the material in between low strains and extremely high strains. The details of the experimental tests are explained as follows-

Firstly, the sample is prepared according to the protocol described in Part 1 of this chapter. For the analysis of the amplitude sweep curve, the sample was loaded onto the TA Instruments AR-G2 Rheometer. I have used a cone and plate geometry on the AR-G2 with a cone diameter of 40 millimeters and the angle of the cone being 2.026 degrees. The truncation gap was 62 micro-meters. The amplitude Sweep was performed from a strain percentage of 0.01 to 1000%. The angular frequency was kept at 3 rad/sec and 6 points per decade were used. The plots of G' (storage modulus) and G'' (loss modulus) with the strain percentage is plotted as shown in Figure 7. From the plot we observe that the storage modulus is essentially constant till a strain of approximately 1% after which it begins to dip sharply. On the other hand, the decrease in the loss modulus is a little less gradual till the yield point which is defined as the point where the two moduli cross each other. After the yield point is reached (the point where the two moduli cross each other), both the Storage and Loss Moduli decrease sharply. By analyzing the plot, we find that the strain percentage of 1 can be considered to be in the linear viscoelastic region while at 700% strain, we can expect to capture rich nonlinearities. The amplitude sweep curve is shown below-

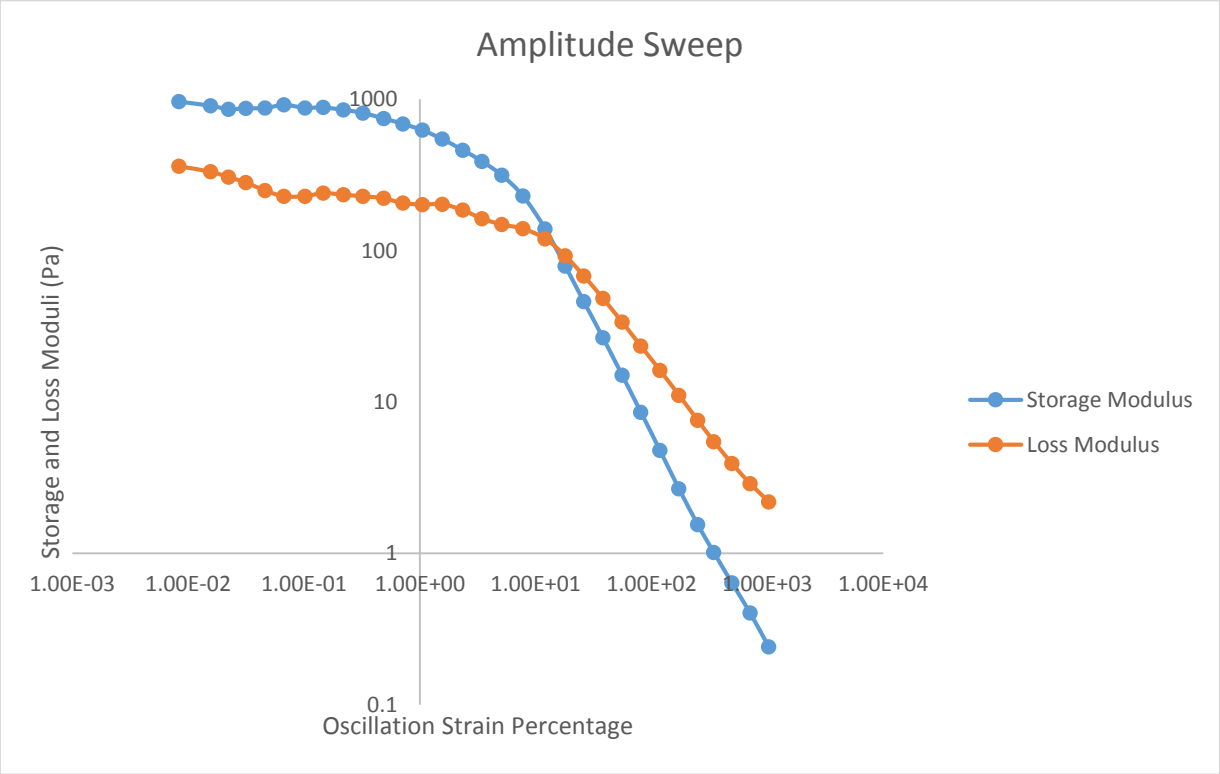

Figure 7: Amplitude Sweep curve of Pickering emulsion

For the purpose of LAOS experiments, the sample was loaded onto the AR-G2 Rheometer. The cone and plate geometry with the specifications described earlier was used for the rheological characterization. The tests were performed at strain percentages of 1, 60 and 700 and at angular frequencies of 3, 5 and 7.5 rad/sec. The data collected from the tests were fed to the MITlaos software for the analysis. I have attached the overview plots of the tests in Appendix 2. For the purpose of the analysis in the present section, I have plotted the elastic and viscous Lissajous curves as shown in Figures 8 and 9 respectively. These curves represent the stress-strain plots at the three strain percentages and frequencies in a two-dimensional space. The plots can be used to visualize the nonlinear behavior owing to the distortion from their elliptical nature in the nonlinear regimes. A further analysis is explained in the following paragraphs. I have also plotted the values of $\frac{G_L'}{G_M'}$ and $\frac{\eta_L'}{\eta_M'}$ at the 3 angular frequencies for the three strain percentages (Figures 10 and 11). These graphs can help us to visualize how the parameters change as the frequency is varied at a particular strain percentage. Finally for the purpose of imaging, 20X images of the sample were captured on the DHR for the three strain percentages but at an oscillatory frequency of 0.5 rad/sec. The choice of this frequency allows us to track droplet motion properly, as at higher frequencies, the droplets are seen to get dragged as spheres instead of deforming in response to shear. In the case of imaging, the images taken before and after the rheology test are placed side by side in each of the three strains. This comparison of the images taken before

and after the test are useful to understand the droplet deformations and provide us a way to correlate between these deformations and large amplitude rheology. The comparison of the images for strains of 1%, 60% and 700% are shown in figures 12, 13 and 14.

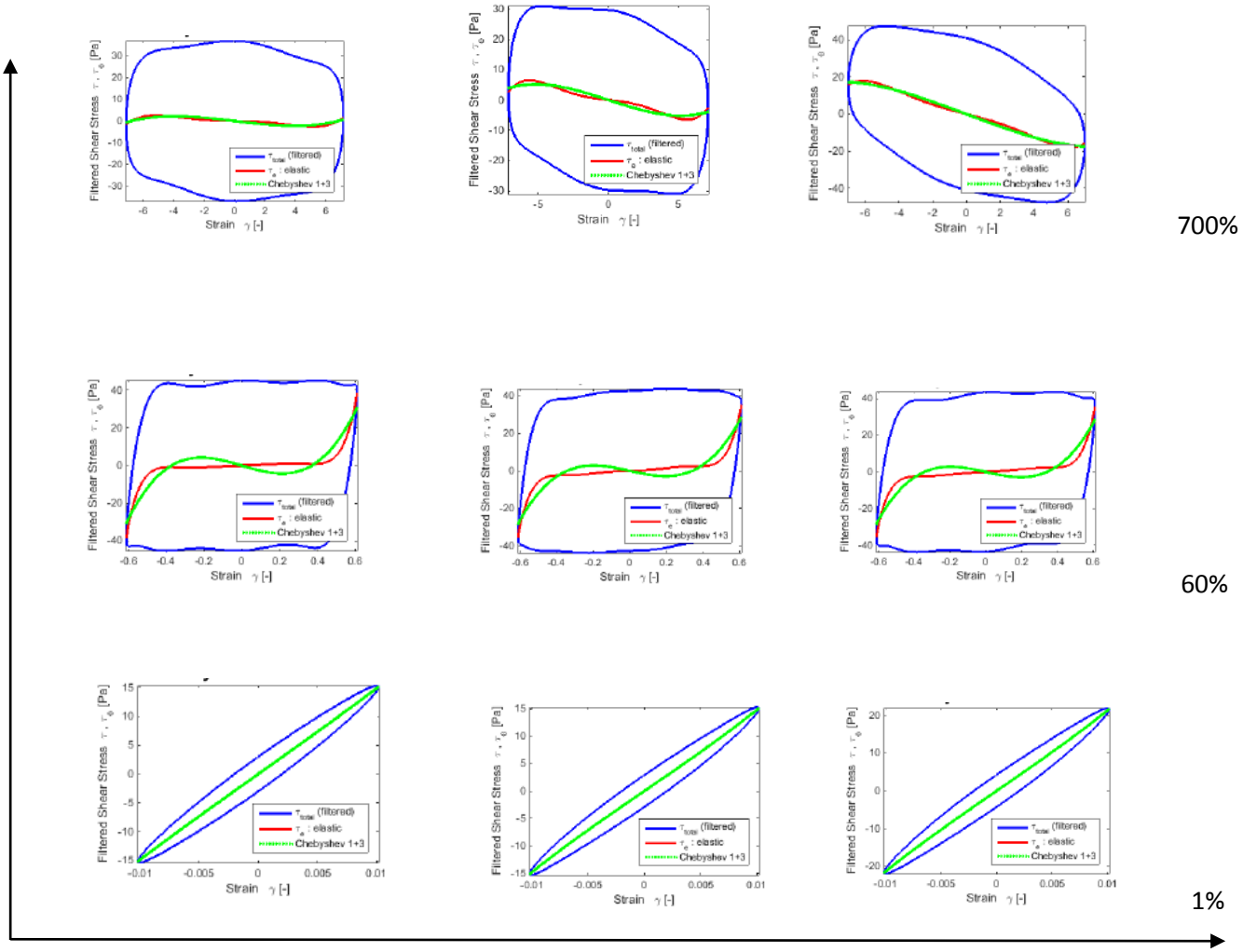

Figure 8: Elastic Lissajous plots showing stress-strain curves derived from the MITlaos analysis. We plot the curves at each pair of strain percentage and frequency.

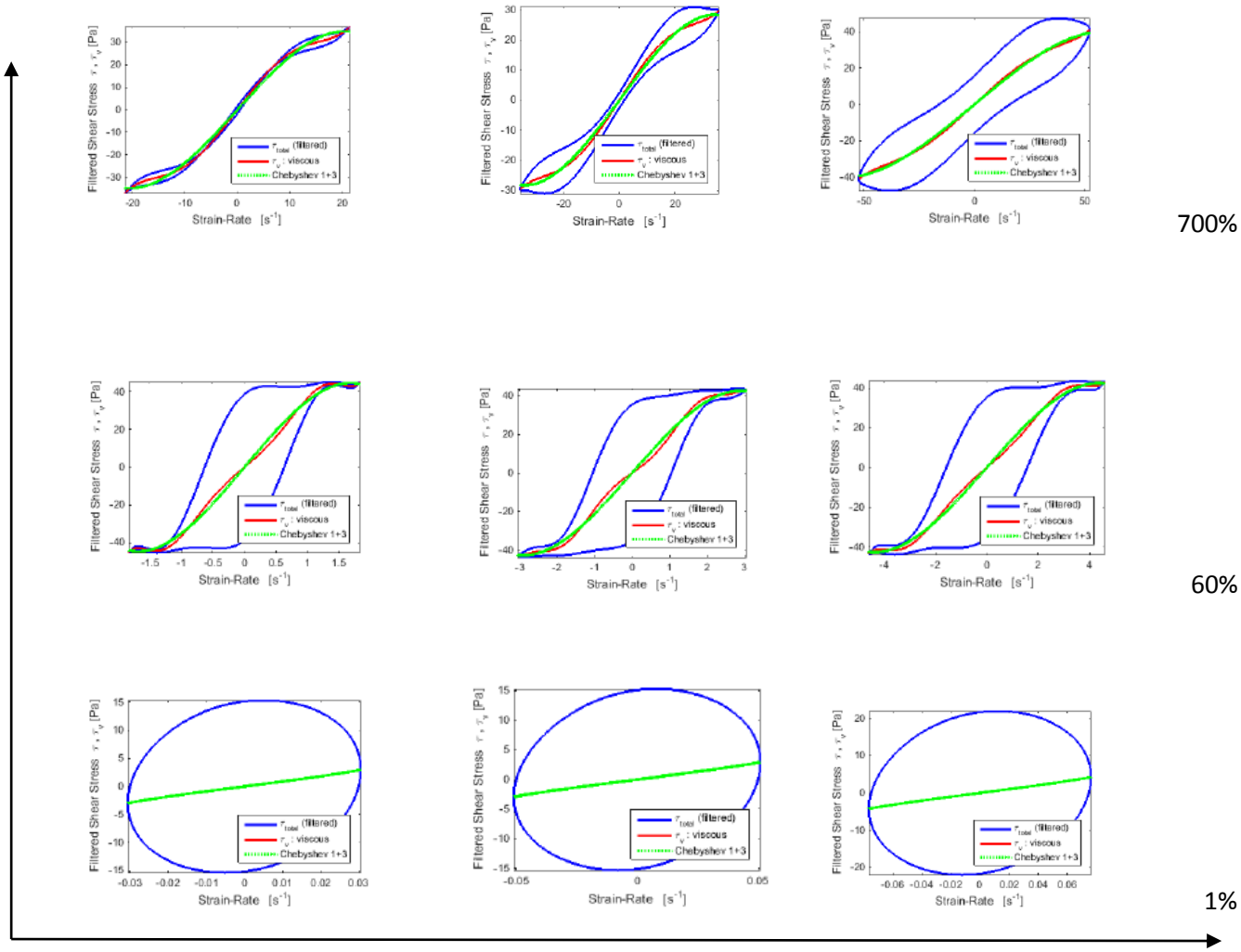

Figure 9: Viscous Lissajous plots showing stress v/s strain-rate curves derived from the MITlaos analysis. We plot the curves at each pair of strain percentage and frequency.

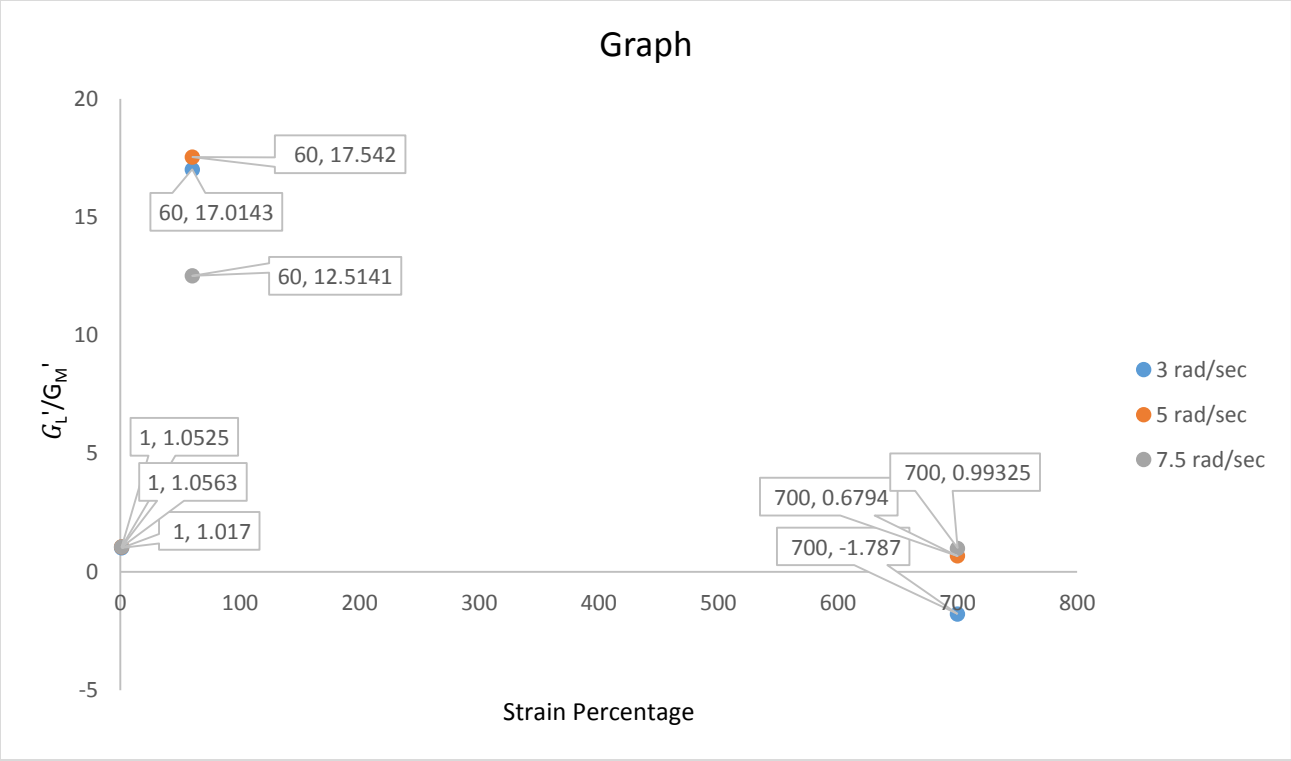

Figure 10: The variation of the ratio $\frac{G_L'}{G_M'}$ as a function of strain percentage for 3 frequencies.

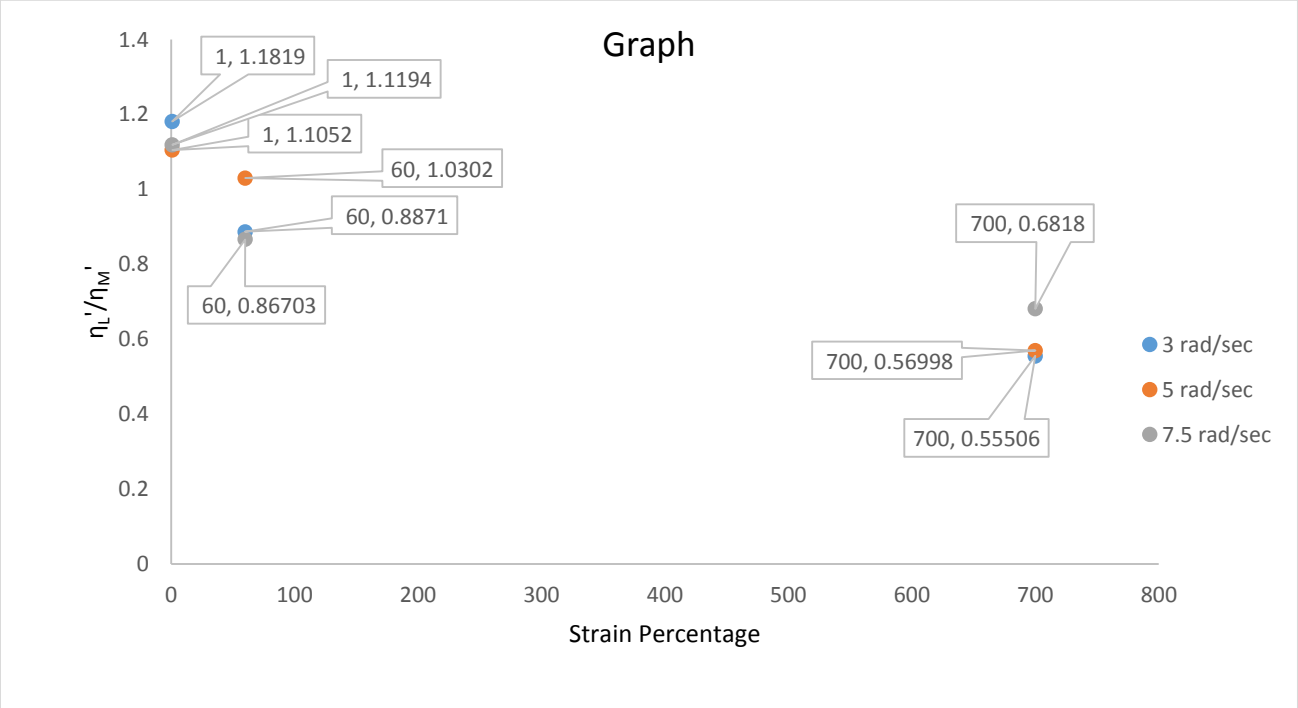

Figure 11: The variation of the ratio $\frac{\eta_L'}{\eta_M'}$ as a function of strain percentage for 3 frequencies.

Observations-

1% Strain- The elastic and viscous Lissajous plots are similar to the ones commonly observed in the linear region. The linear nature in this case is demonstrated by the elliptical plots of the stress with the strain and strain-rate, as is predicted by the amplitude sweep curve. The plots of elastic and viscous stresses are straight lines with no such non-linearity observed at high strains/strain-rates (as shown in figures 8 and 9). The absence of any observable non-linearity is demonstrated by the values of G_L' and G_M'. In the linear region, G_L'= G_M'=G'. The ratios of $\frac{G_L'}{G_M'}$ is close to 1 in all the three frequencies and we are not able to discern any significant nonlinearity in the material. The same interpretations can be applied for the viscous case (as shown in figures 10 and 11). After imaging of the sample was performed along with the rheology, we find that images before and after the tests are the same (as shown in figure 12). Thus, we can relate the lack of the microstructure changes to the linear viscoelasticity observed from the LAOS analysis. It could be further explained that the droplets are trapped in cages by their neighbors at such low strains and fail to break away from these cages. By performing simultaneous imaging and rheology, we have been able to establish the correlation between lack of deformation of droplets to linear viscoelasticity at 1% Strain.

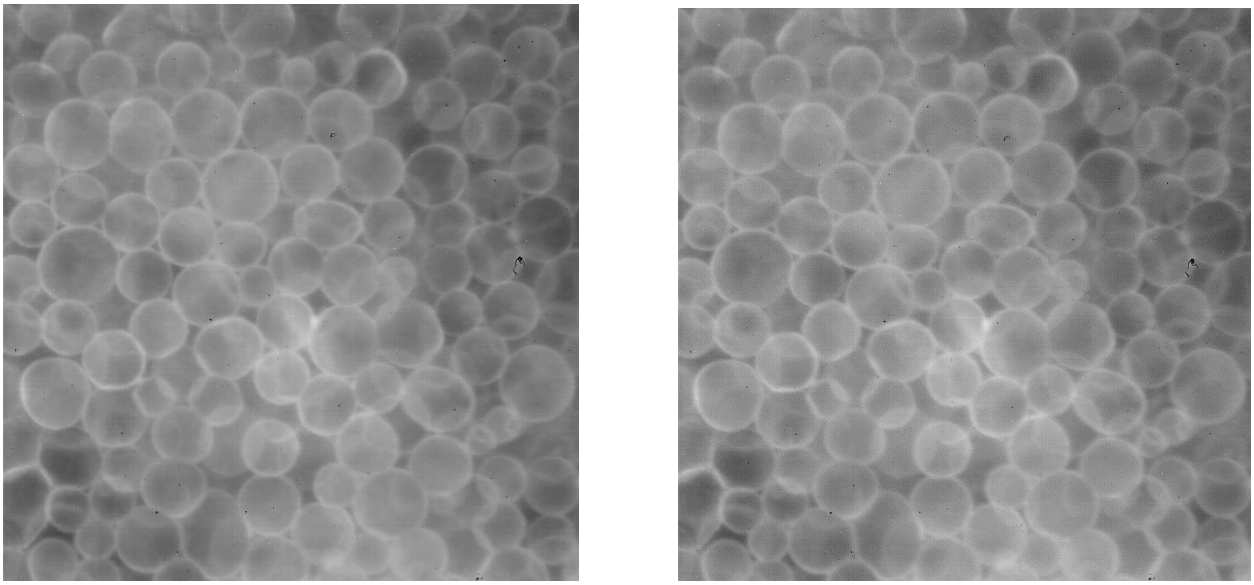

(A) (B)

Figure 12: Comparison of images taken before and after the LAOS test at 1% strain and 0.5 rad/sec frequency. Figure (A) shows the image of the sample before the test while figure (B) depicts the image of the sample after the test.

60% Strain- The Lissajous plots are no more elliptical in shape and indicate that we are in the non-linear regime. Here, we find sharp intra-cycle strain stiffening and shear thinning behavior at large strains and strain-rates (as shown in figures 8 and 9). The values of $\frac{G_L'}{G_M'}$ are much more greater than 1 now in all the three frequencies indicating the strain stiffening behavior (as shown in figure 10). The ratio $\frac{G_L'}{G_M'}$ goes down a bit at a frequency of 7.5 rad/sec. This observation can be attributed to the phenomenon of slip where all the relaxation mechanisms are disrupted and the response approaches a linear behavior. However, at a strain of 60% the slip might not be sufficient enough to produce a completely linear response but the lowering of the ratio at a frequency of 7.5 rad/sec seems to indicate the onset of slip. On the other hand, the ratios of the viscous moduli, $\frac{\eta_L'}{\eta_M'}$ are not too much away from 1 in the three frequencies (as shown in figure 11). Hence from the above values it can be predicted that the elasticity of the material suffers from a greater extent of nonlinearity as compared to the viscosity. By comparison of the images taken before and after the test (shown in figure 13), it is interesting to note that the droplets do not deform much. This could be possible as we are not able to capture the irreversible droplet deformations at such low frequencies. The LAOS analysis of the sample at 60% strain and 0.5 rad/sec could reveal important information in this regard, but performing such an experiment is not discussed in this present research work.

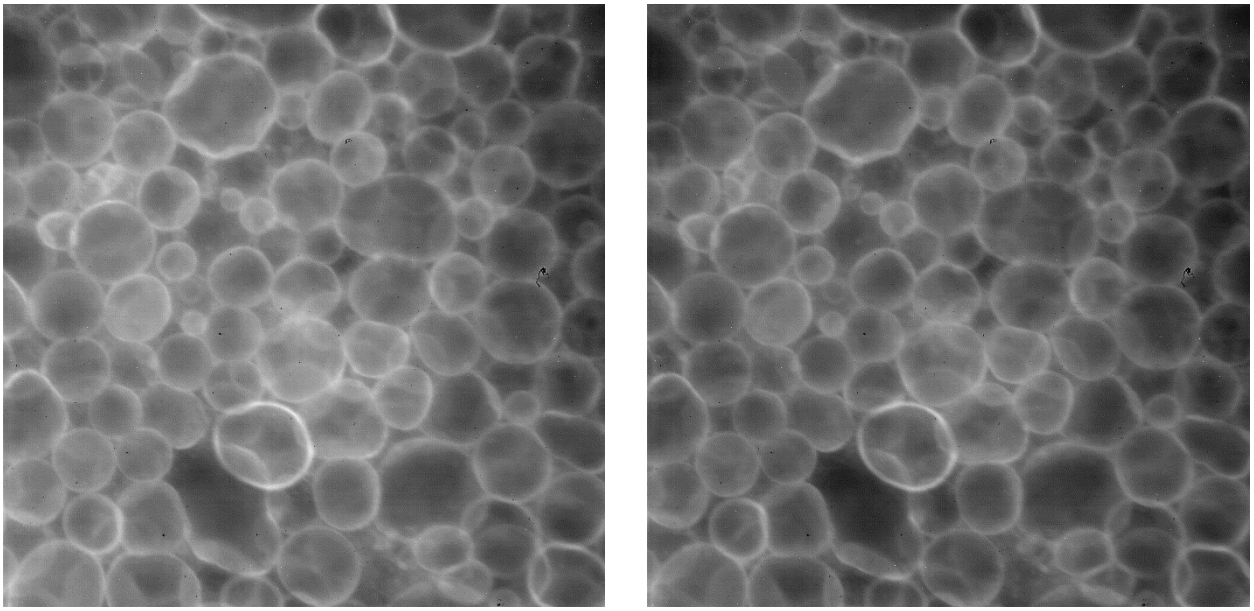

(A) (B)

Figure 13: Comparison of images taken before and after the LAOS test at 60% strain and 0.5 rad/sec frequency. Figure (A) shows the image of the sample before the test while figure (B) depicts the image of the sample after the test.

700% Strain- The elastic and viscous Lissajous plots tend to take an elliptical shape as the frequency is progressively increased from 3 rad/sec to 7.5 rad/sec (as shown in figure 8 and 9). This trend is also seen in the values of $\frac{G_L'}{G_M'}$ and $\frac{\eta_L'}{\eta_M'}$ (as shown in figures 10 and 11) where the values of these parameters approach 1 with the increase of frequency. As $\frac{G_L'}{G_M'}$ = $\frac{\eta_L'}{\eta_M'}$=1 in the linear viscoelastic regime, it can be said that the material approaches a linear behavior at higher frequencies. A possible explanation of this behavior can be made on the grounds of slip. It can be said that slip disrupts all relaxation mechanisms of this material such that only the Newtonian solvent dissipates energy and the viscous response becomes linear at such high frequencies [8]. This is the reason why the values of these two parameters approach 1 as the frequency is increased. Another vital observation is that the elastic Lissajous plot at frequencies of 5 and 7.5 rad/sec, take an inverted nature. In other words, in these plots, the elastic stress takes a negative value as the strain is increased from 0 to the maximum strain amplitude. This could be because of the phase difference between the stress and strain, which could possibly mean that the material is not able to come back to its original position and becomes more dissipative. It is influenced by slip and continues to deform in the same direction. In other words, it offers no restoring force. Finally we observe that the value of $\frac{G_L'}{G_M'}$ takes a negative value at frequency of 3

rad/sec (-1.787). This is because of the negative value of G_L' at this frequency and could possibly mean that the material is unloading stress faster than the new deformation is being accumulated [8]. With a slight deforming strain, the material is influenced by slip and loses the ability to regain its original configuration. A comparison of the images taken before and after the rheology experiment indicate that the droplets tend to deform irreversibly at such high strains. This might be due to the cage-breaking phenomena; whereby the droplets are no longer trapped by their neighbors. The irreversible deformation of these droplets can be correlated with the elastic and viscous nonlinearities observed at low frequencies. This shows us that the material does not come back to its original position after the removal of deformation as the droplets move away from their trapped cages and begin to flow.

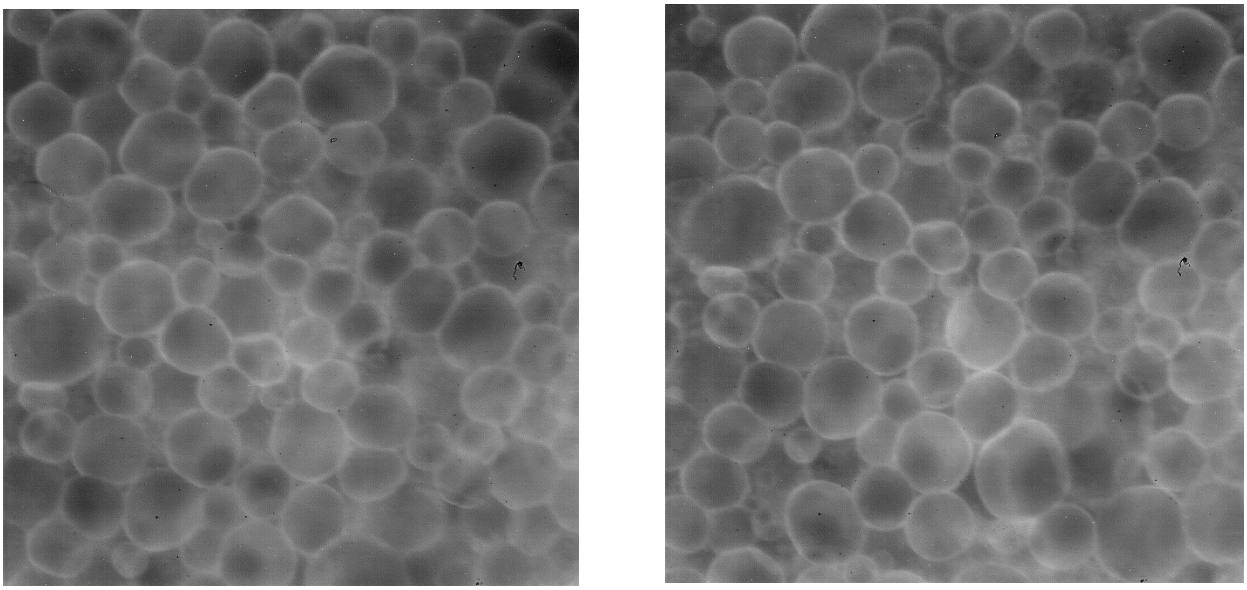

(A) (B)

Figure 14: Comparison of images taken before and after the LAOS test at 700% strain and 0.5 rad/sec frequency. Figure (A) shows the image of the sample before the test while figure (B) depicts the image of the sample after the test.

Part 4- Analysis of effect of slip on LAOS studies

In this section we analyze how slip is affecting the large amplitude rheology of Pickering emulsions. The no-slip boundary condition of fluid flow past a solid surface states that flowing fluid comes to rest just at the point where it meets the solid surface. There is no relative motion of the fluid to the impenetrable boundary that it flows past; molecules at the boundary move on average with the same velocity as that boundary, and is therefore zero at a solid [13]. The no-slip is a fundamental assumption and a generally-accepted boundary condition in rheology and fluid mechanics with strong experimental support. However, the violations of this condition are widely recognized in many situations, especially in the flow of non-Newtonian fluids [14]. Under the influence of slip, the droplets get dragged as spheres instead of deforming in response to shear.

For preventing the slip on the glass surface, it was painted with a layer of Sally Hansen transparent nail polish. It was left to dry for 2 hours. As a cone and plate geometry was used for the purpose of rheological analysis, the surface of the cone was also painted with a thin layer of the same transparent nail-polish and left to dry for 2 hours. It was supposed that such an operating protocol could make the colloids stick to the glass surface. In order to illustrate the prevention of slip using this method, 20X images of the sample before and after the test were captured. The sample was prepared according to the protocol described in part 1. The sample was loaded onto the DHR, and the 20X imaging was performed simultaneously with the rheological tests. The frequency of operation was 0.5 rad/sec and the test was performed over a period of 60 seconds with a strain percentage of 700%. Figure 15 shows the imaging of the sample before and after the rheology experiment when the surfaces have not been treated. Figure 16 illustrates the sample images before and after the test, but this time the surfaces have been treated to avoid slip. By looking at image 15, we find that the images taken before and after the test are not same. This is because the droplets are not stuck to the surface and are definitely moving. At a strain of 700%, we find some irreversible droplet deformations caused due to this motion. With the help of this experiment we illustrate what slip is exactly doing to the bottom surface and how it can be readily observed. On the other hand, figure 16 indicates that the images before and after the test are the same. This is probably because the droplets are hardly moving and the first layer appears to be stuck to the surface. As we are imaging the first layer on the DHR, this experiment seems to indicate that we have been able to prevent the slip problem. However it is interesting to note that the droplets don't get deformed much.

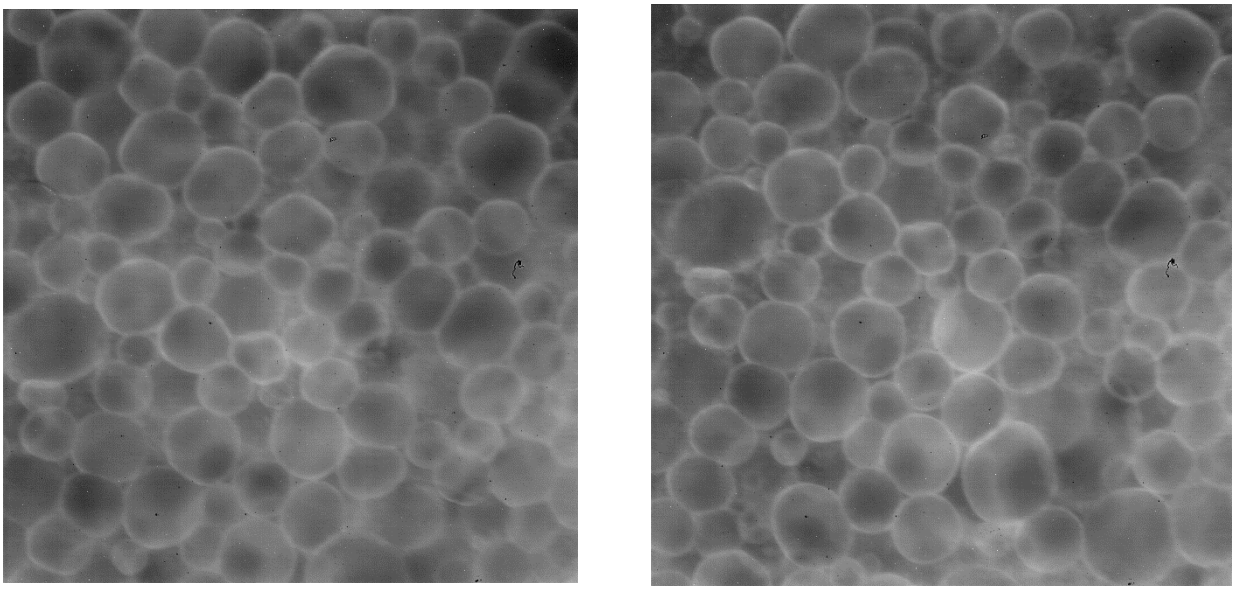

(A) (B)

Figure 15: Comparison of images taken before and after the LAOS test at 700% strain and 0.5 rad/sec frequency where the surfaces have not been treated. Figure (A) shows the image of the sample before the test while figure (B) depicts the image of the sample after the test.

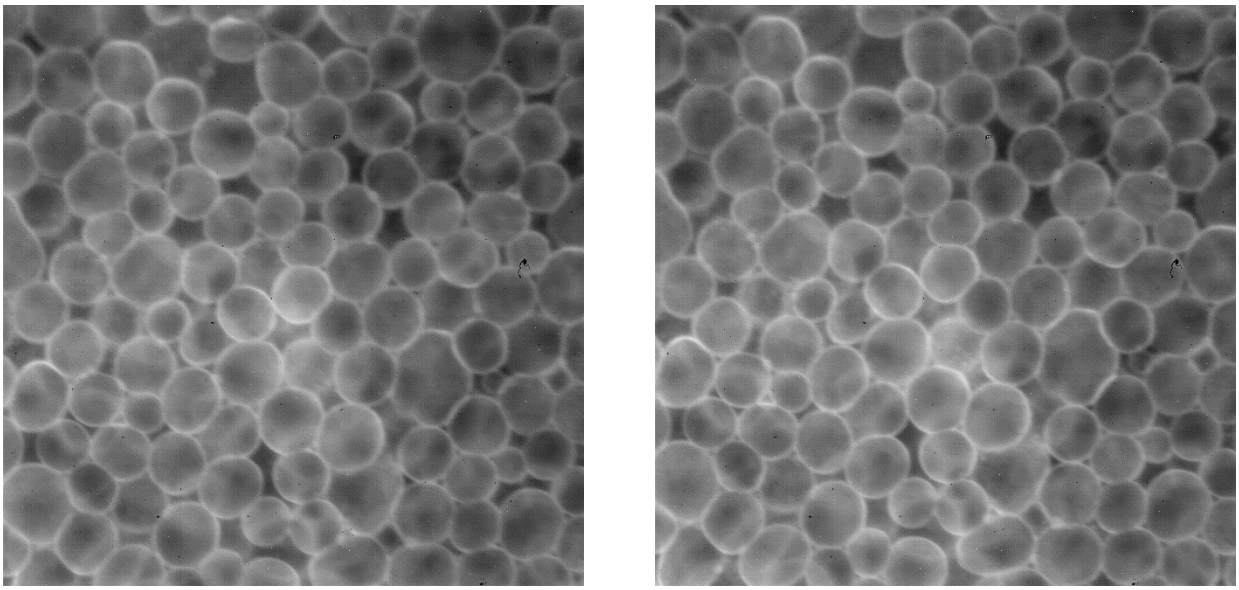

(A) (B)

Figure 16: Comparison of images taken before and after the LAOS test at 700% strain and 0.5 rad/sec frequency where the surfaces been treated to prevent slip. Figure (A) shows the image of the sample before the test while figure (B) depicts the image of the sample after the test.

Firstly, we analyze the amplitude sweep curves in both the cases of slip and no-slip. For the analysis of the amplitude sweep curves, the sample (prepared according to the protocol described earlier this chapter) was loaded onto the TA Instruments DHR-3 Rheometer. I have used a cone and plate geometry on the DHR with a cone diameter of 40 millimeters and the angle of the cone being 2.026 degrees. The truncation gap was 62 micro-meters. The amplitude Sweep was performed from a strain percentage of 0.01 to 1000%. The angular frequency was kept at 5 rad/sec and 6 points per decade were used. The plots of G' (storage modulus) and G'' (loss modulus) with the strain percentage is plotted as shown in Figure 17. While figure 17 (A) denotes the amplitude sweep curve for the case of untreated surfaces, figure 17 (B) illustrates the sweep curve for the case where the top and bottom surfaces have been treated to prevent slip.

From figure 17 we observe that the storage and loss moduli are constant till a strain percentage of 1 in both (A) and (B) after which the storage moduli starts to decrease sharply. After the yield point is reached, both the moduli start to decrease with the loss modulus dominating the storage modulus. An interesting point to be noted here is that the yield strain in case (A) occurs at a strain percentage of 10, while the yield strain in (B) is at a strain percentage of 24. As the yield point is defined as the point where the two moduli cross each other, the corresponding strain at this point can be described as the strain where the droplets tend to move out of their cages and start to “flow”. In the case where we have slip, the droplets are not stuck to the surfaces and are moving with response to shear. Compared to the case where we have prevented slip, the droplet motion is restricted as they are stuck to the surfaces. Hence, it requires more strain in the latter case to drive the droplets out of their cages and make them flow. Eventually when the material yields to the applied shear, it starts to flow, but it requires more strain to induce the flow behavior in case (B).

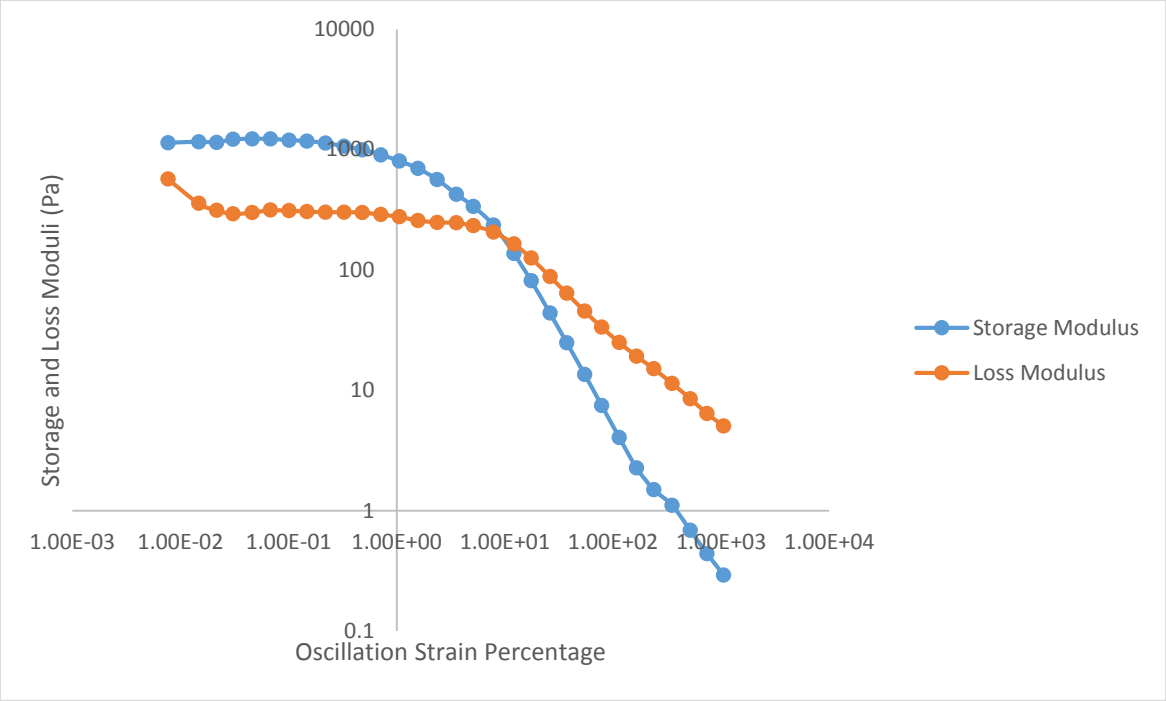

(A)

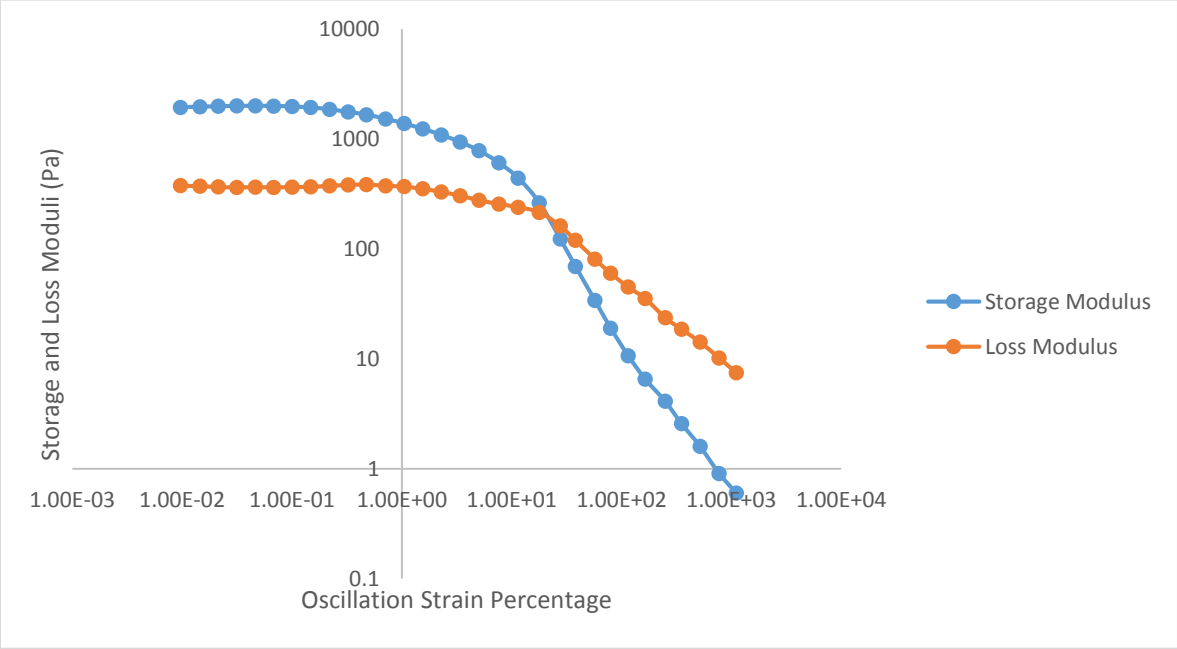

(B)

Figure 17: Amplitude Sweep curves of the Pickering emulsion at a frequency of 5 rad/sec. Figure (A) shows the sweep for the case where the surfaces are not treated while (B) shows the curve for the case where slip is prevented.

For the purpose of LAOS experiments, the sample was loaded onto the TA-instruments DHR-3 Rheometer. The cone and plate geometry with the specifications described earlier was used for the rheological characterization. The tests were performed at strain percentages of 1, 60 and 700 and at an angular frequency of 5 rad/sec in both the cases of slip and no-slip. The data collected from the tests were fed to the MITlaos software for the analysis. I have attached the overview plots of the tests in Appendix 3. For the purpose of analysis in the present section, I have plotted the elastic and viscous Lissajous curves as shown in Figures 18 and 19 respectively. The plots of slip and no-slip cases are presented in the same graph for better comparison of results. I have also plotted the values of $\frac{G_L'}{G_M'}$ and $\frac{\eta_L'}{\eta_M'}$ for the slip and no-slip cases at the three strain percentages (Figures 20 and 21). These graphs can help us to visualize how the parameters change with the presence/absence of slip at a particular strain percentage.

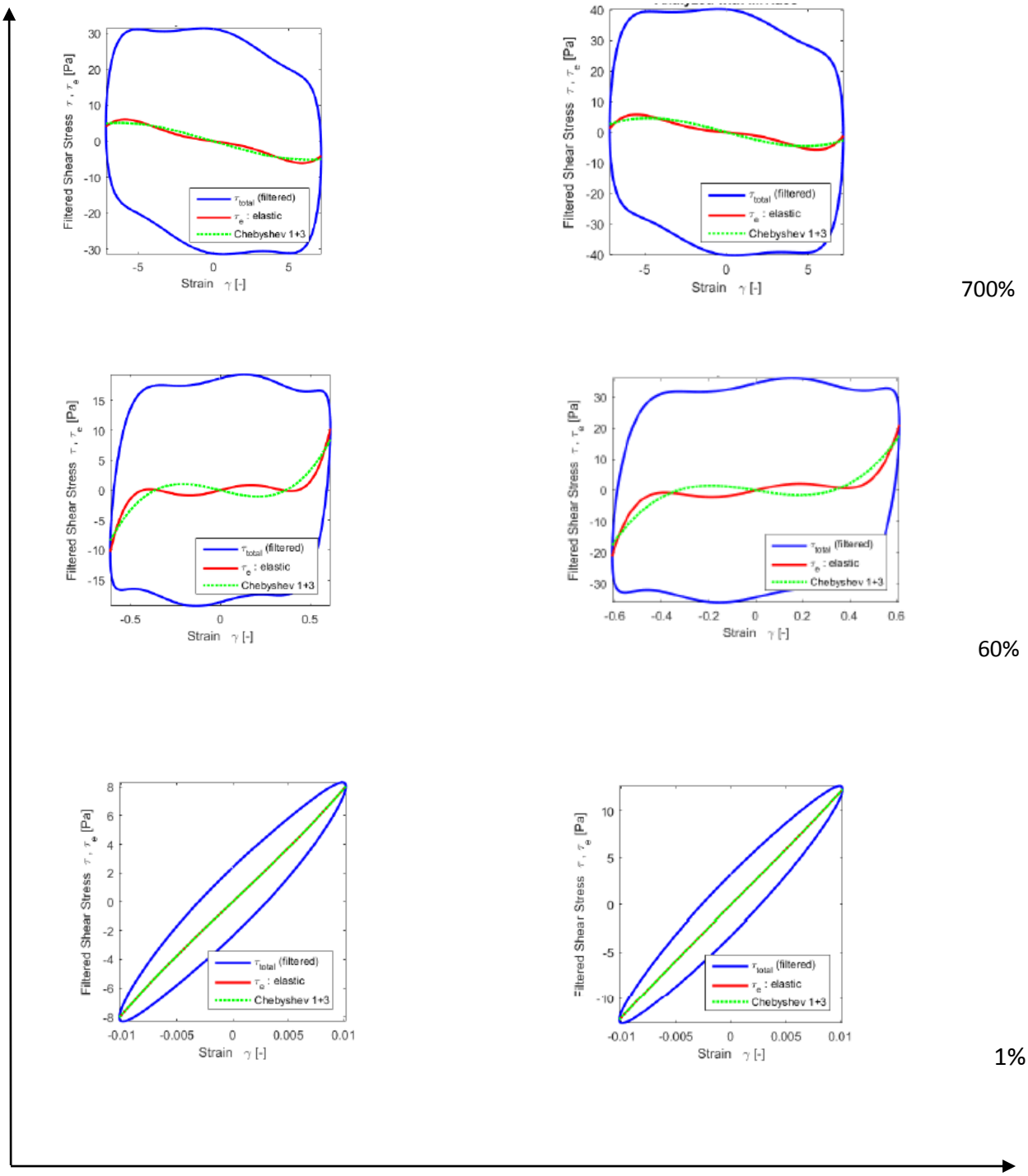

Figure 18: Elastic Lissajous plots showing stress-strain curves derived from the MITlaos analysis. We plot the curves at each strain percentage for both the cases of slip and no-slip.

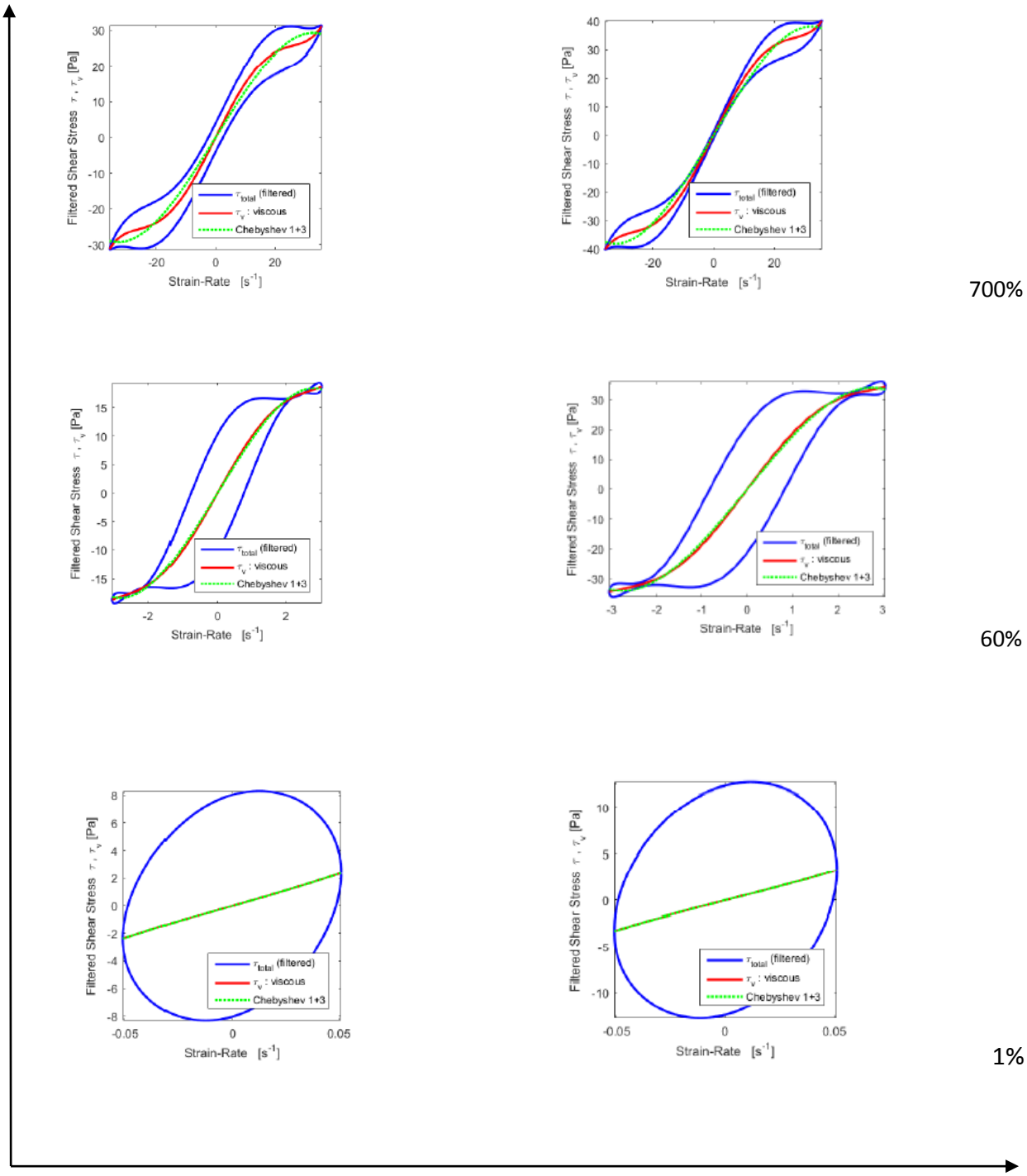

Figure 19: Viscous Lissajous plots showing stress v/s strain-rate curves derived from the MITlaos analysis. We plot the curves at each strain percentage for both the cases of slip and no-slip.

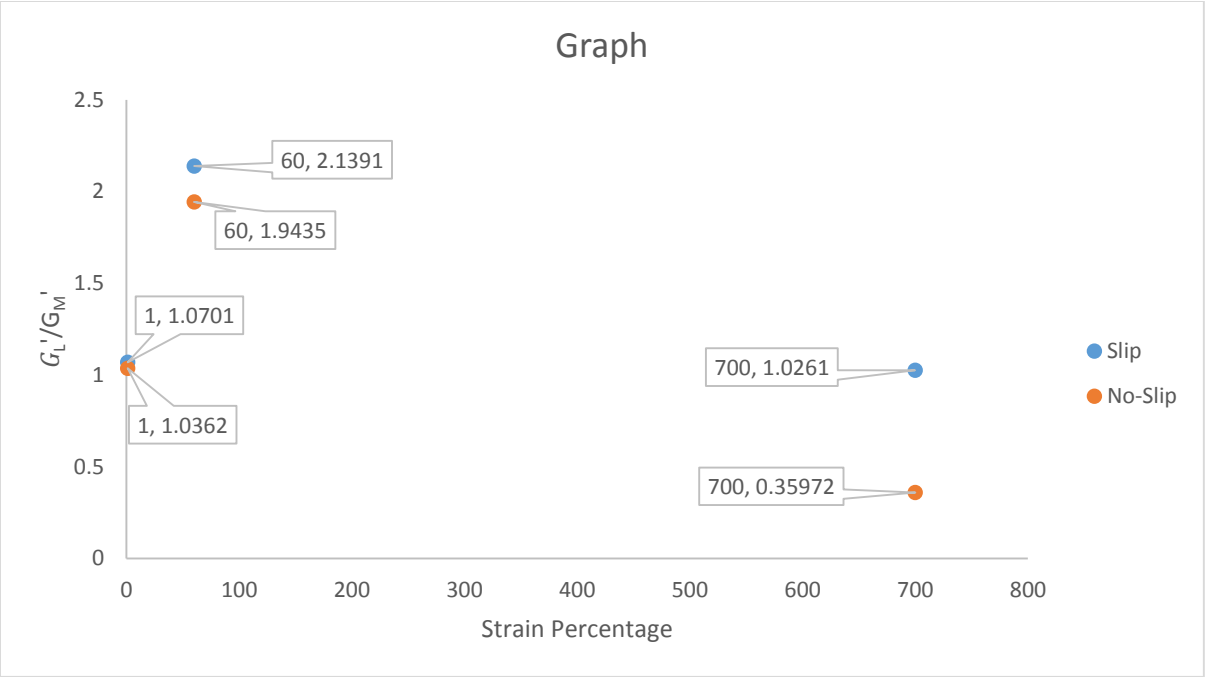

Figure 20: The variation of the ratio $\frac{G_L'}{G_M'}$ as a function of strain percentage for slip and no-slip.

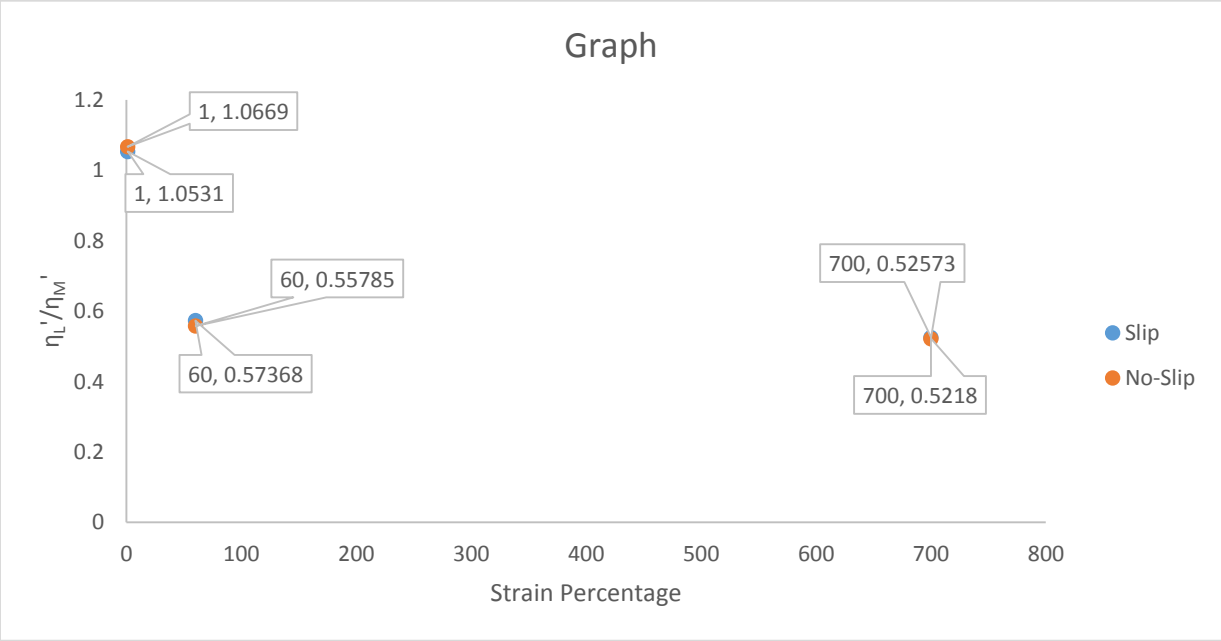

Figure 21: The variation of the ratio $\frac{\eta_L'}{\eta_M'}$ as a function of strain percentage for slip and no-slip.

As seen from figure 18 and 19, the Lissajous curves are perfect ellipses for a strain percentage of 1 but they deviate from their elliptical nature and enter the nonlinear regime at a strain percentage of 60. At this strain, we observe an intracycle strain stiffening and shear thinning behavior in both the cases of slip and no-slip owing to values of $\frac{G_L'}{G_M'}$ >1 and values of $\frac{\eta_L'}{\eta_M'}$ less than 1 (from figures 20 and 21). The Lissajous plots at a strain percentage of 700% are non-elliptical and thus evocative of intracycle nonlinearities. From the values of $\frac{\eta_L'}{\eta_M'}$ as a function of strain percentage it is observed that the values are nearly equal for the slip and no-slip cases across the three strain percentages. One interesting that can be observed from figure 20 are the values of $\frac{G_L'}{G_M'}$ in case of slip and no-slip at a strain percentage of 700. The value rises from 0.35972 in case of no-slip to a value of 1.0261 in the case of slip. As we know, a value of $\frac{G_L'}{G_M'}$ near 1 indicates that the response is linear viscoelastic. Hence, it means that at a strain percentage of 700, the response is approaching a linear behavior in the case of slip. This seems to agree with our previous argument that in case of slip, all the relaxation mechanisms are disrupted and the response is linear. Comparing that with the case of no-slip, the value of $\frac{G_L'}{G_M'}$ =0.35972 indicates that the material is suffering from intracycle strain softening (and hence referring to a nonlinear behavior) and the relaxation mechanisms are not disrupted. This seems to confirm that we have been able to avoid slip using our protocol and the above observation supports our initial observation using imaging on the DHR.

Part 5- LAOS Analysis with the variation of particle volume fraction

In this section we see how the LAOS analysis changes with the variation of particle volume fraction. We have chosen two particle volume fractions for the purpose of our analysis- 2% and 5%. The samples are prepared and LAOS analysis is performed with the aid of the MITlaos software. First amplitude sweep curves for both the volume fractions are plotted and analyzed. Then the elastic and viscous Lissajous plots are illustrated at three strain percentages of 1%, 60% and 700% and at two angular frequencies of 1 rad/sec and 5 rad/sec. The average droplet radius was calculated for the case of both 2% and 5% volume fractions. While the average droplet radius was found to be 28.3 microns for the case of 5%, it was equal to 39.5 microns in case of 2% volume fraction of particles. Below are shown two 20X confocal images of the Pickering emulsion consisting of 2% volume fraction of particles.

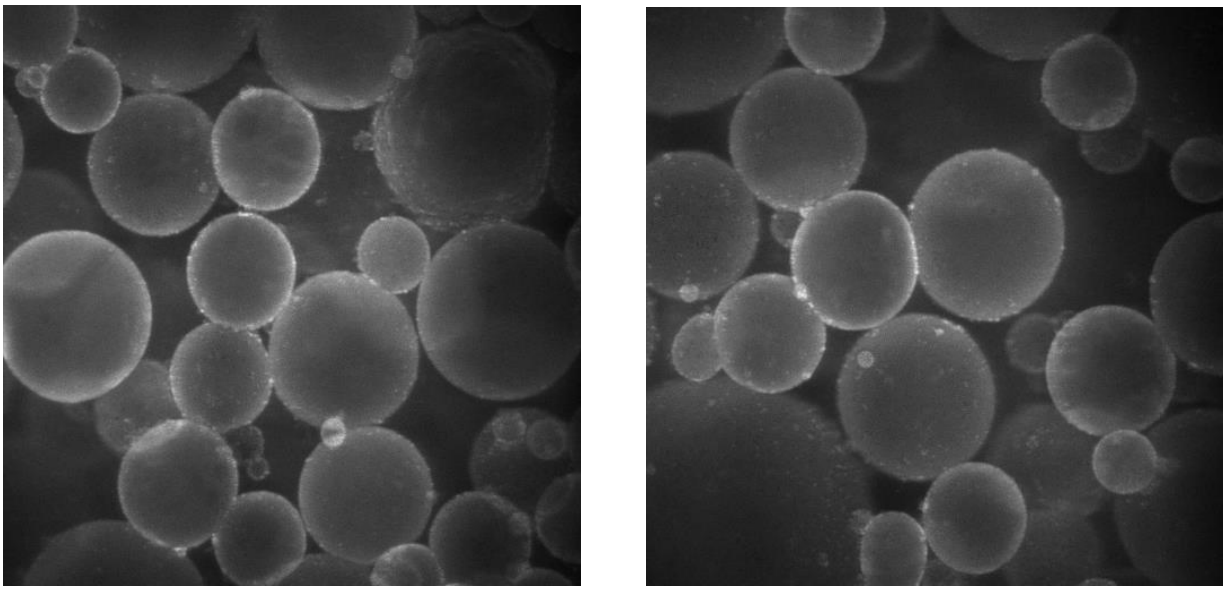

Figure 22: 20X confocal images of the Pickering emulsion stabilized by 2% volume fraction of PMMA particles

Firstly, we analyze the amplitude sweep curves in both the cases of 2% and 5% particle volume fractions. For the analysis of the amplitude sweep curves, the sample (prepared according to the

protocol described earlier this chapter) was loaded onto the TA Instruments DHR-3 Rheometer. I have used a cone and plate geometry on the DHR with a cone diameter of 40 millimeters and the angle of the cone being 2.026 degrees. The truncation gap was 62 micro-meters. The amplitude Sweep was performed from a strain percentage of 0.01 to 1000%. The angular frequency was kept at 5 rad/sec and 6 points per decade were used. The plots of G' (storage modulus) and G'' (loss modulus) with the strain percentage is plotted as shown in Figure 23. While figure 23 (A) denotes the amplitude sweep curve for the case of 2% volume fraction, figure 23 (B) illustrates the sweep curve for the case where the particle volume fraction is 5%.

From figure 23 we observe that the storage and loss moduli are constant till a strain percentage of 1 in both (A) and (B). After the yield point is reached, both the moduli start to decrease with the loss modulus dominating the storage modulus. On careful observation, we find that the crossover point between the storage and loss moduli (also called the yield point) occurs at a strain of 10% in the case of 5% volume fraction while it occurs at a strain of 48.5% in the 5% volume fraction case. As discussed previously, the corresponding strain at the yield point (also called the yield strain) can be correlated to the strain required to drive the droplets out of their cages and make them flow. As we know, smaller droplets break their bonds at lower strain [4] and on an average the droplets are smaller in the case of 5% volume fraction particles as compared to the 2% case. Using this idea, we have a possible explanation for the observation. In the case of 5% volume fraction, the droplets break their bonds and move out of their cages at a lesser strain as compared to the ones at 2% volume fraction owing to the smaller droplet size. Hence the yield strain is lower in the case of 5% volume fraction.

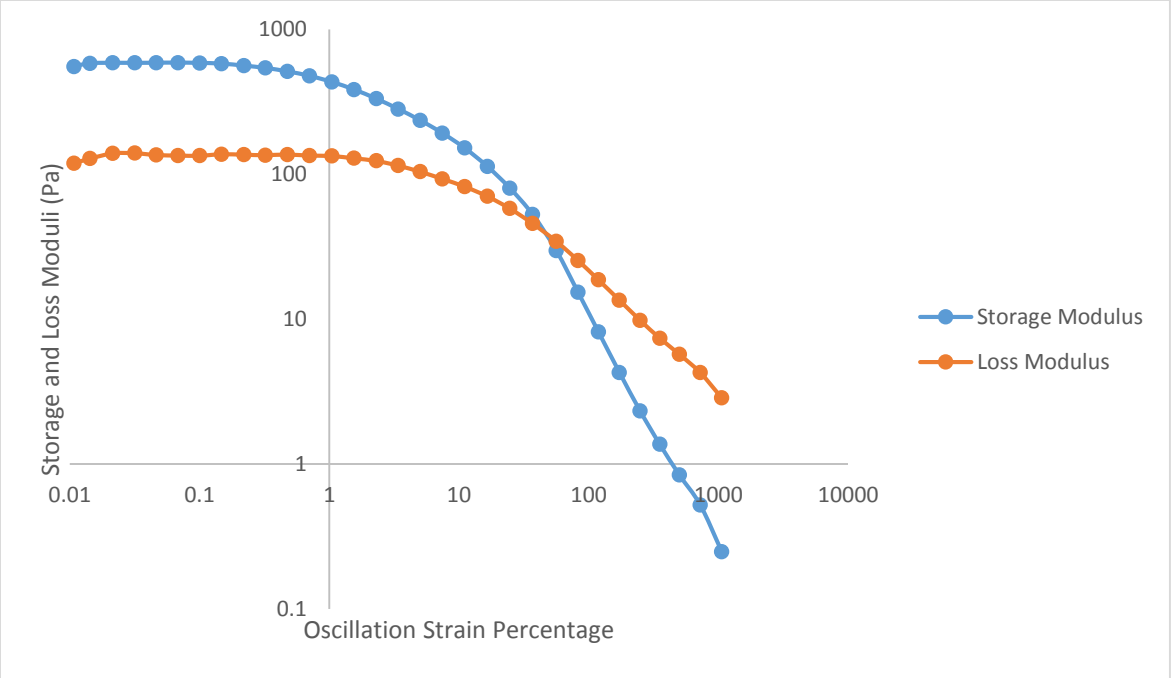

(A)

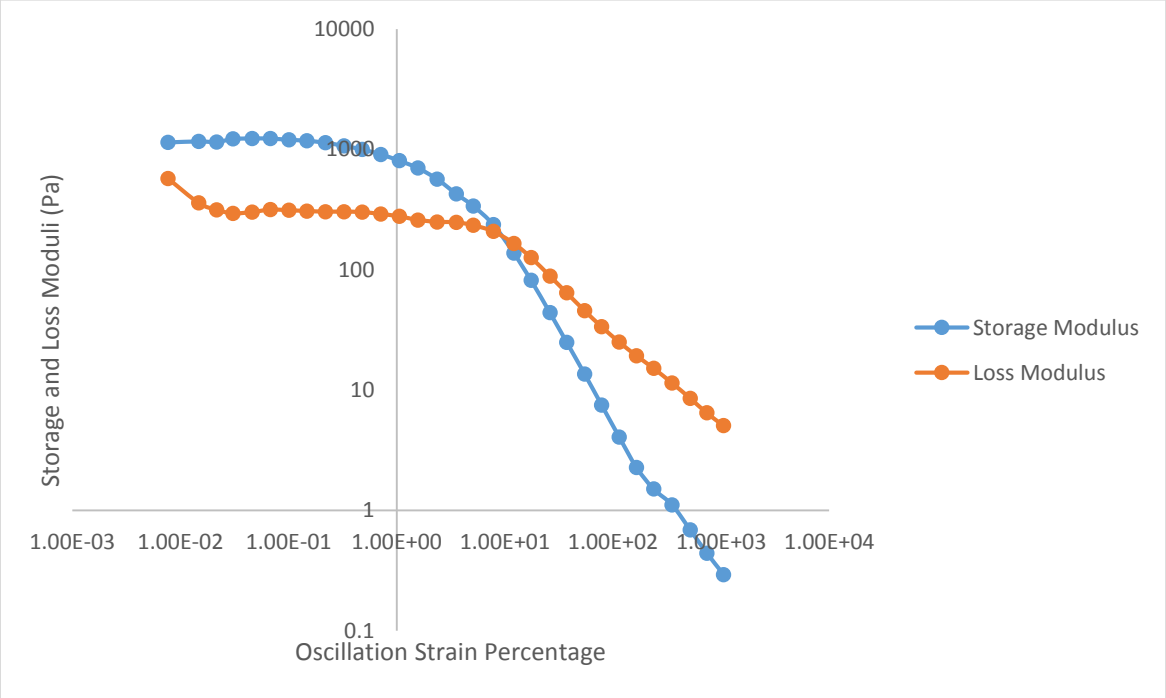

(B)

Figure 23: Amplitude Sweep curves of the Pickering emulsion at a frequency of 5 rad/sec. Figure (A) shows the sweep for the case where the particle volume fraction is 2% while (B) shows the curve for the 5% case.

For the purpose of LAOS experiments, the sample was loaded onto the TA-instruments DHR-3 Rheometer. The cone and plate geometry with the specifications described earlier was used for the rheological characterization. The tests were performed at strain percentages of 1, 60 and 700 and at angular frequencies of 1 and 5 rad/sec in both the cases of 2% and 5% volume fractions. The data collected from the tests were fed to the MITlaos software for the analysis. I have attached the overview plots of the tests in Appendix 4. For the purpose of analysis in the present section, I have plotted the elastic and viscous Lissajous curves as shown in Figures 24 and 25 (for a frequency of 1 rad/sec) and figures 26 and 27 (at a frequency of 5 rad/sec). The plots of 2% and 5% volume fraction cases are presented in the same graph for better comparison of results. I have also plotted the values of $\frac{G_L'}{G_M'}$ and $\frac{\eta_L'}{\eta_M'}$ for the two volume fractions at the three strain percentages and two frequencies (Figures 28, 29, 30 and 31). These graphs can help us to visualize how the parameters change with the volume fraction at a particular strain percentage and frequency.

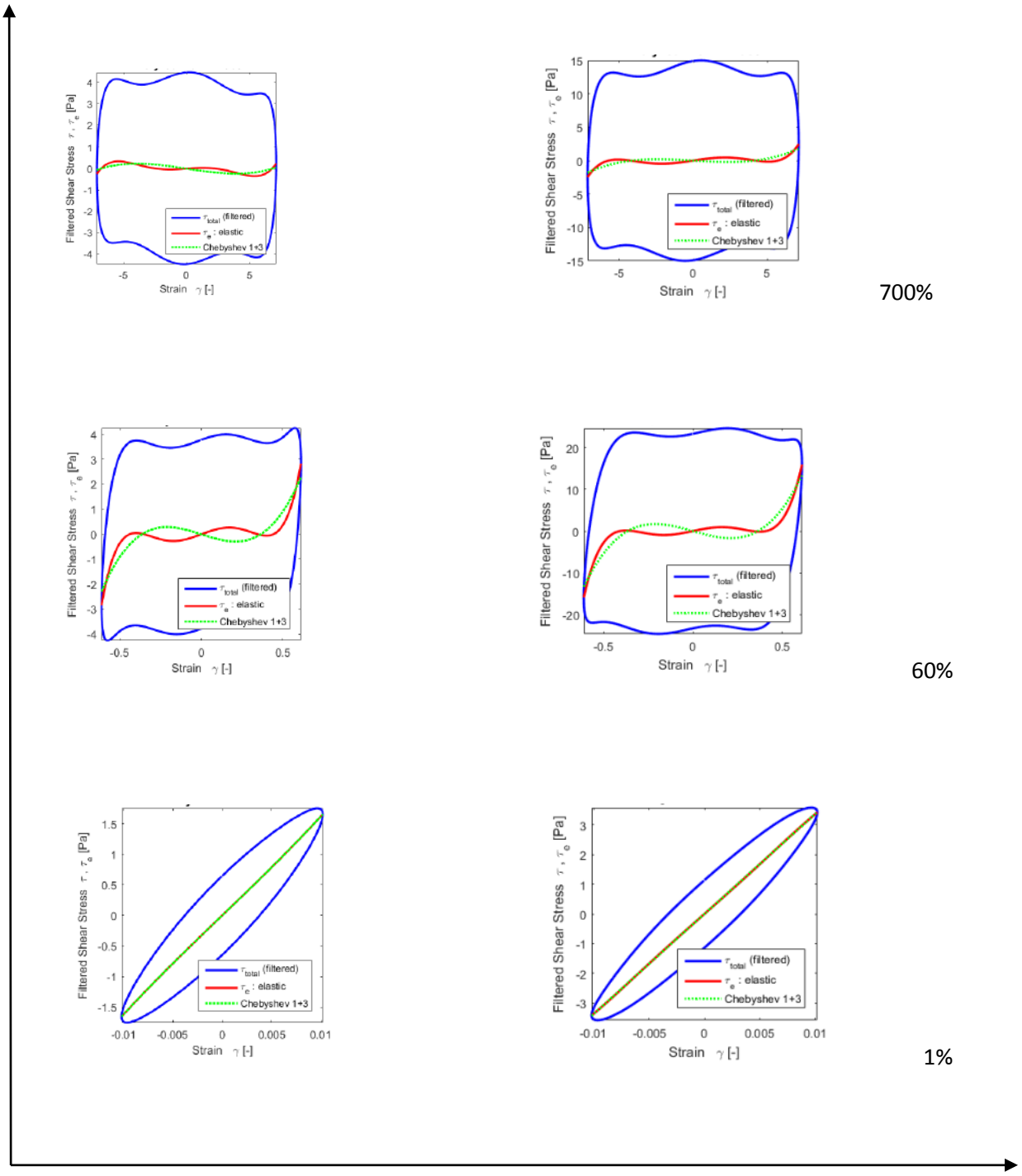

Figure 24: Elastic Lissajous plots showing stress-strain curves at 1 rad/sec derived from the MITlaos analysis. We plot the curves at each strain percentage for both the cases of 2% and 5% volume fraction of particles.

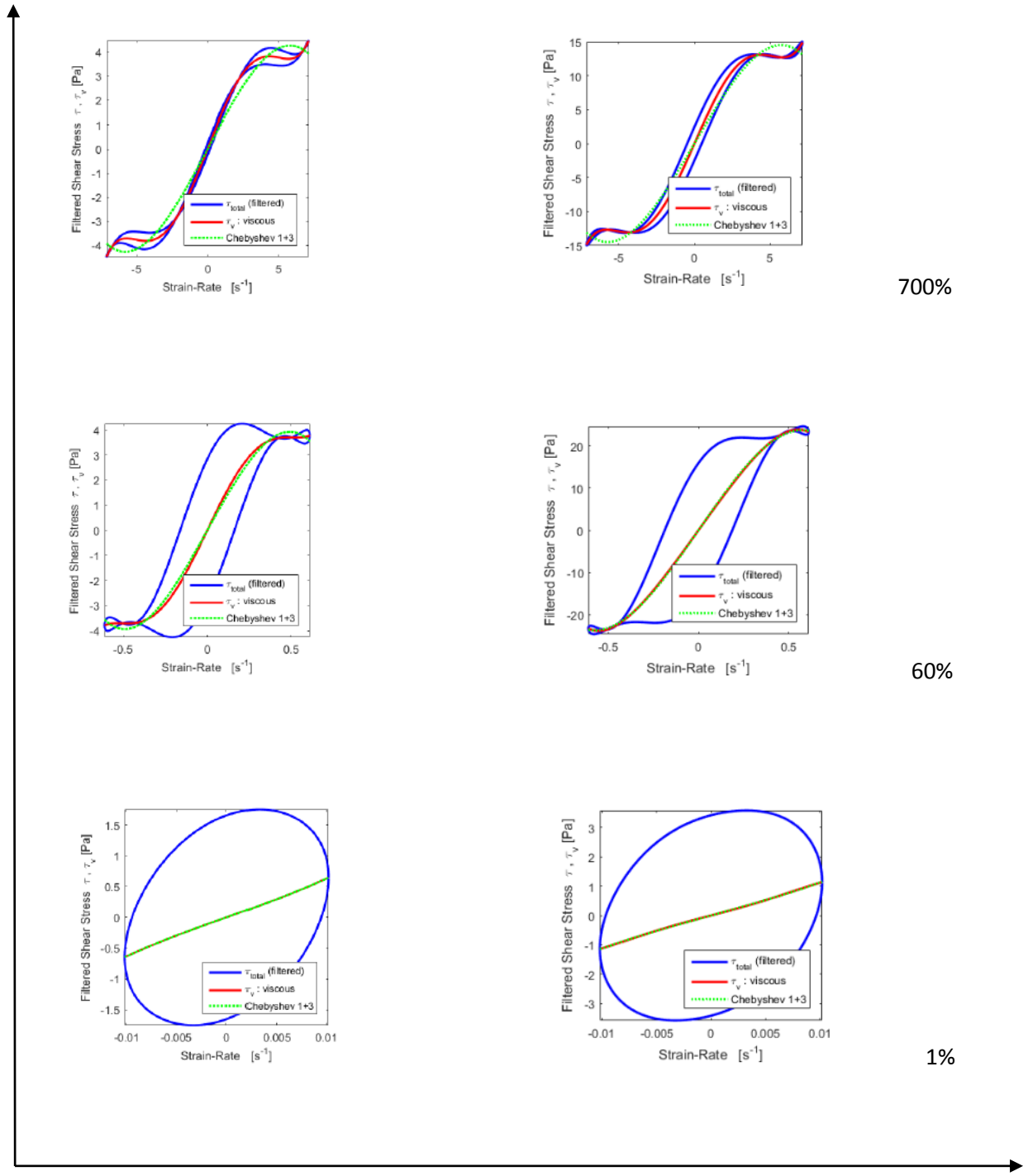

Figure 25: Viscous Lissajous plots showing stress vs strain-rate curves at 1 rad/sec derived from the MITlaos analysis. We plot the curves at each strain percentage for both the cases of 2% and 5% volume fraction of particles.

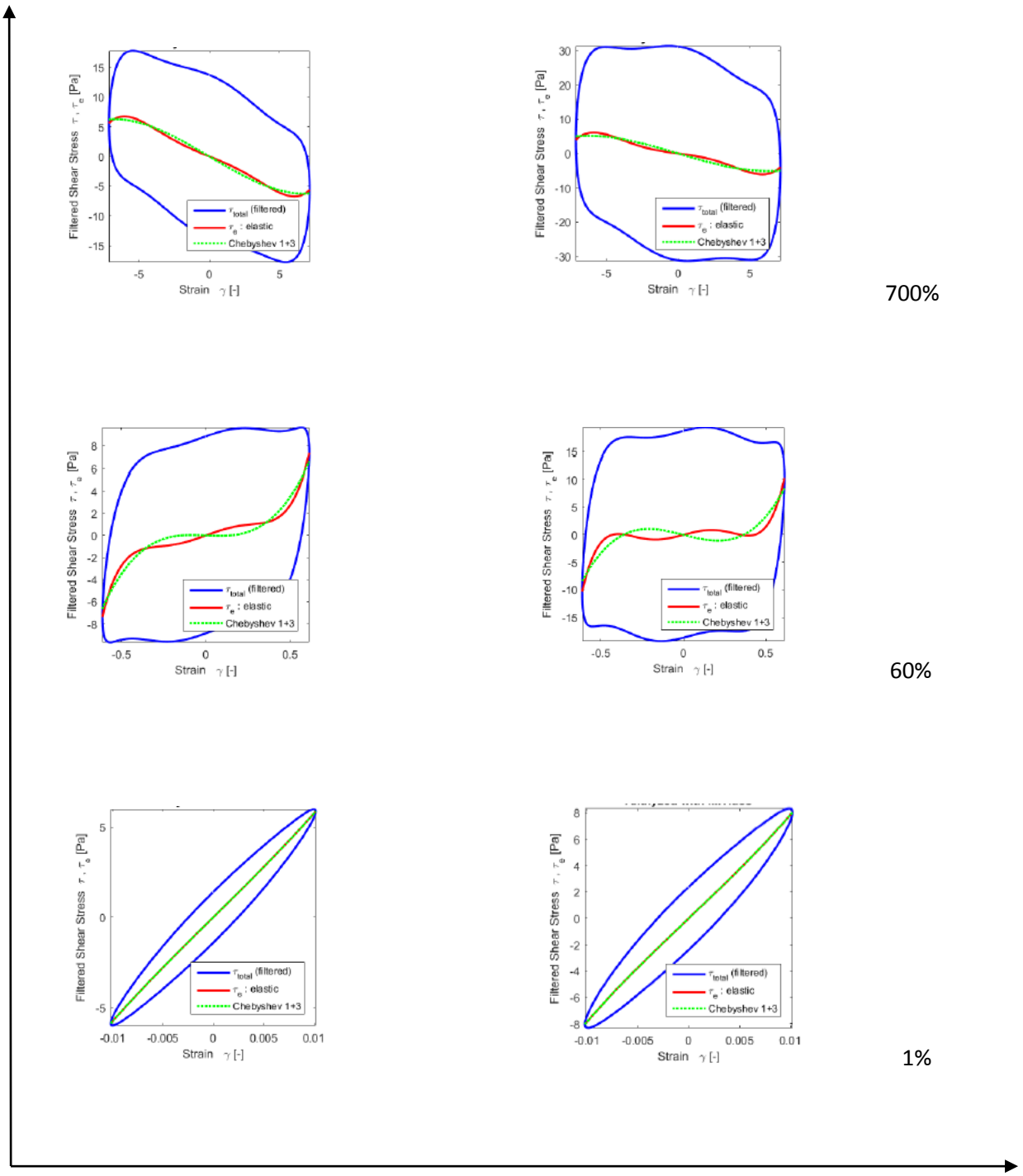

Figure 26: Elastic Lissajous plots showing stress-strain curves at 5 rad/sec derived from the MITlaos analysis. We plot the curves at each strain percentage for both the cases of 2% and 5% volume fraction of particles.

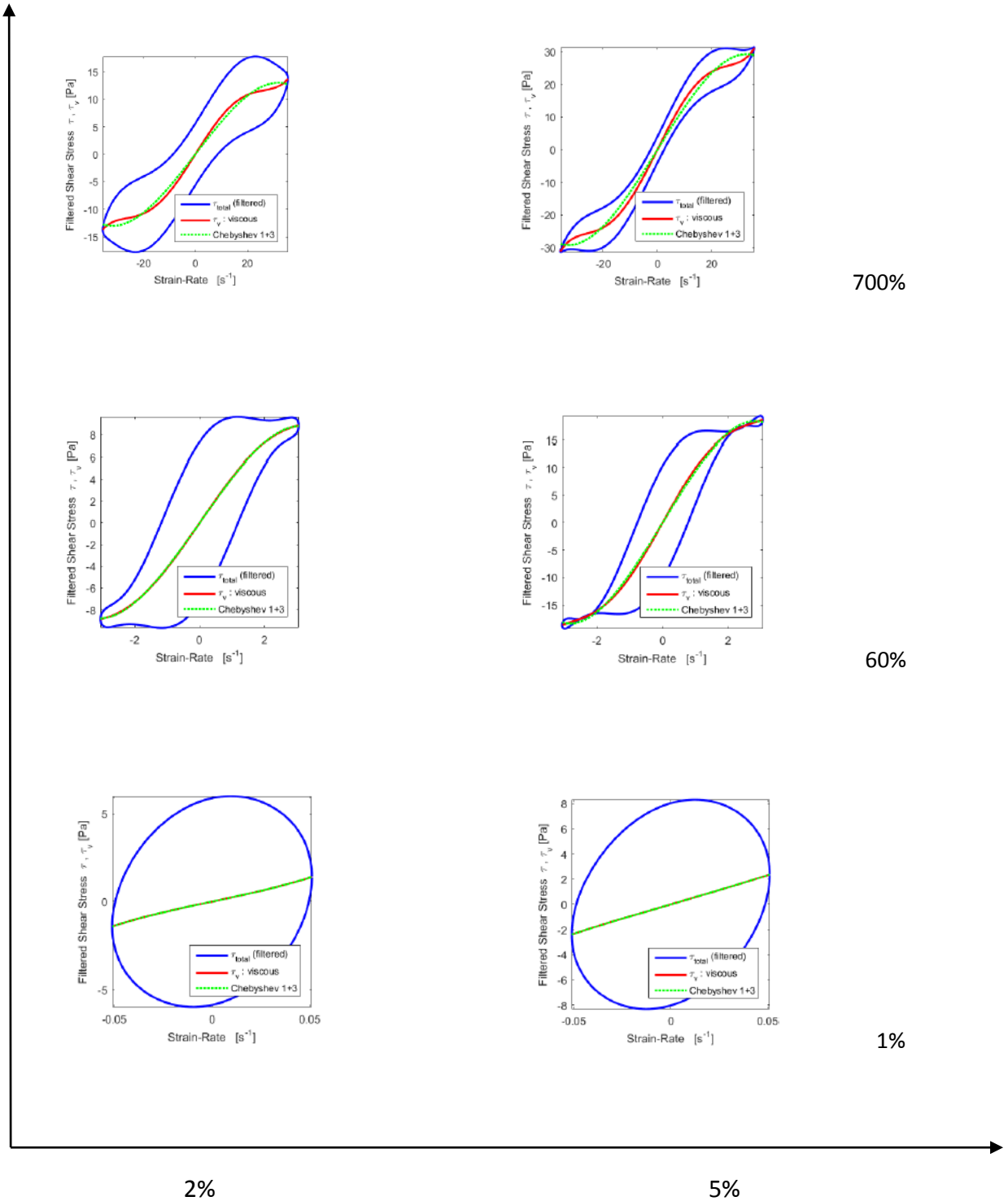

Figure 27: Viscous Lissajous plots showing stress vs strain-rate curves at 5 rad/sec derived from the MITlaos analysis. We plot the curves at each strain percentage for both the cases of 2% and 5% volume fraction of particles.

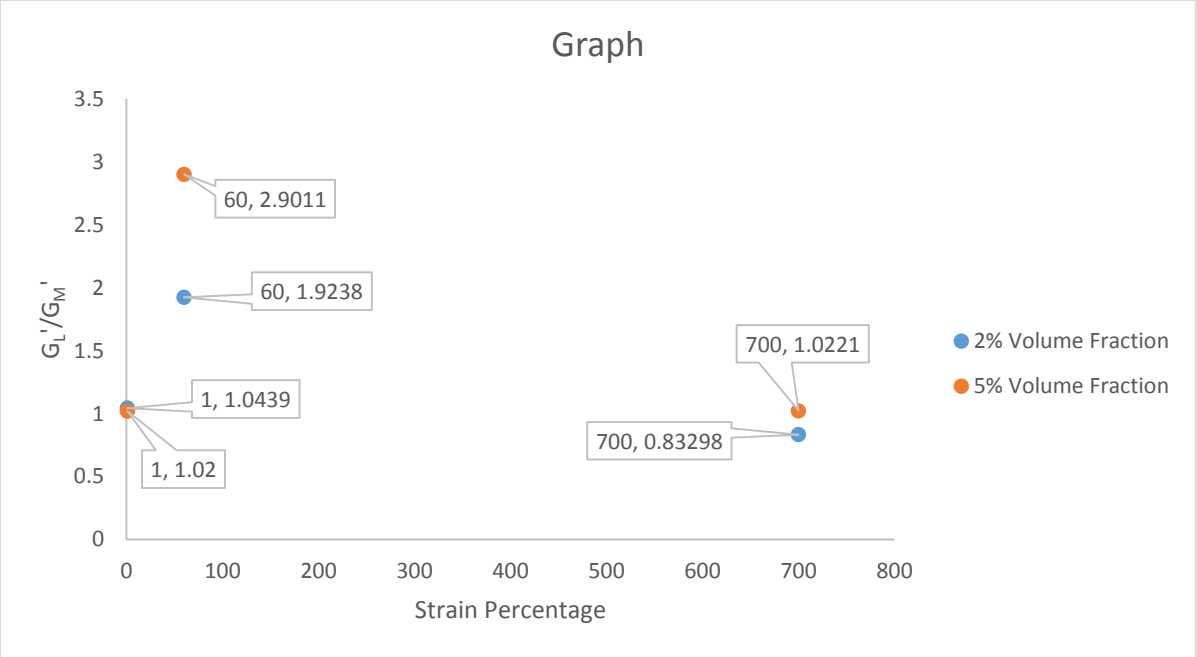

Figure 28: The variation of the ratio $\frac{G_L'}{G_M'}$ as a function of strain percentage for the 2 volume fractions at 1 rad/sec.

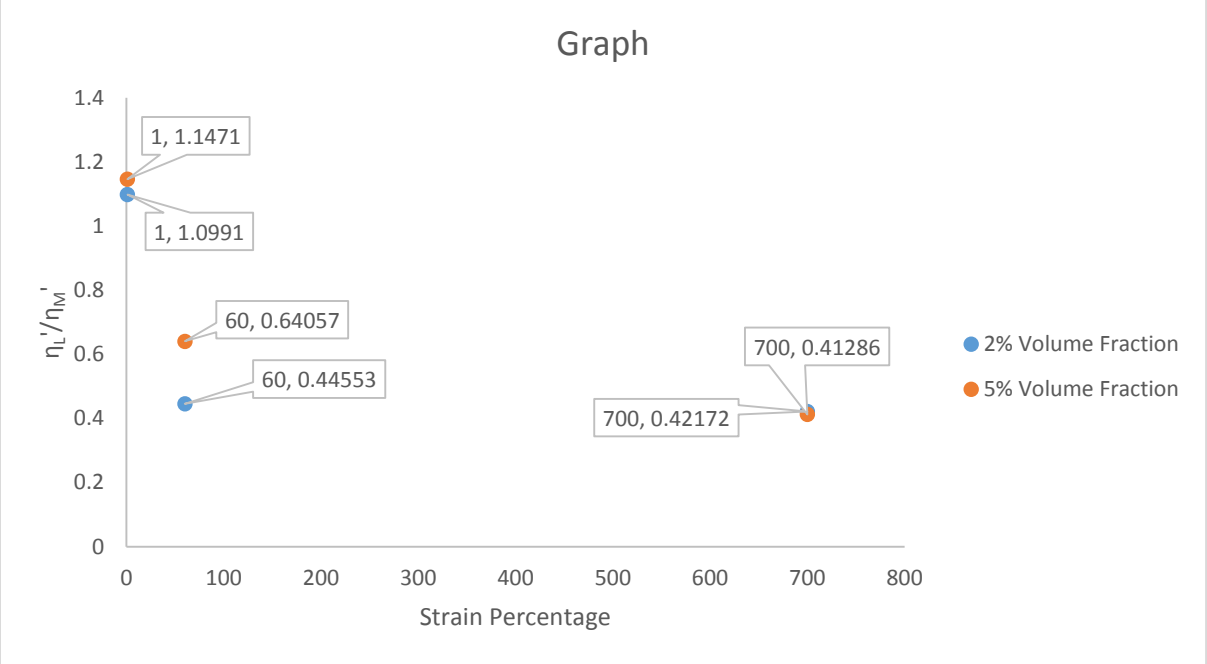

Figure 29: The variation of the ratio $\frac{\eta_L'}{\eta_M'}$ as a function of strain percentage for the 2 volume fractions at 1 rad/sec.

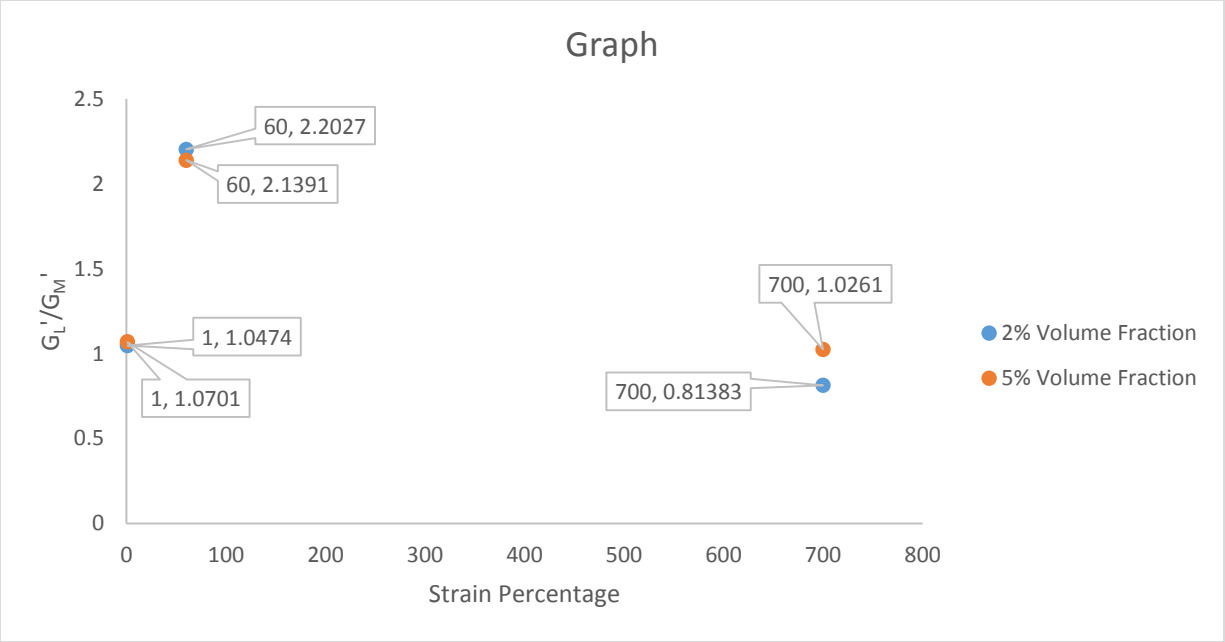

Figure 30: The variation of the ratio $\frac{G_L'}{G_M'}$ as a function of strain percentage for the 2 volume fractions at 5 rad/sec.

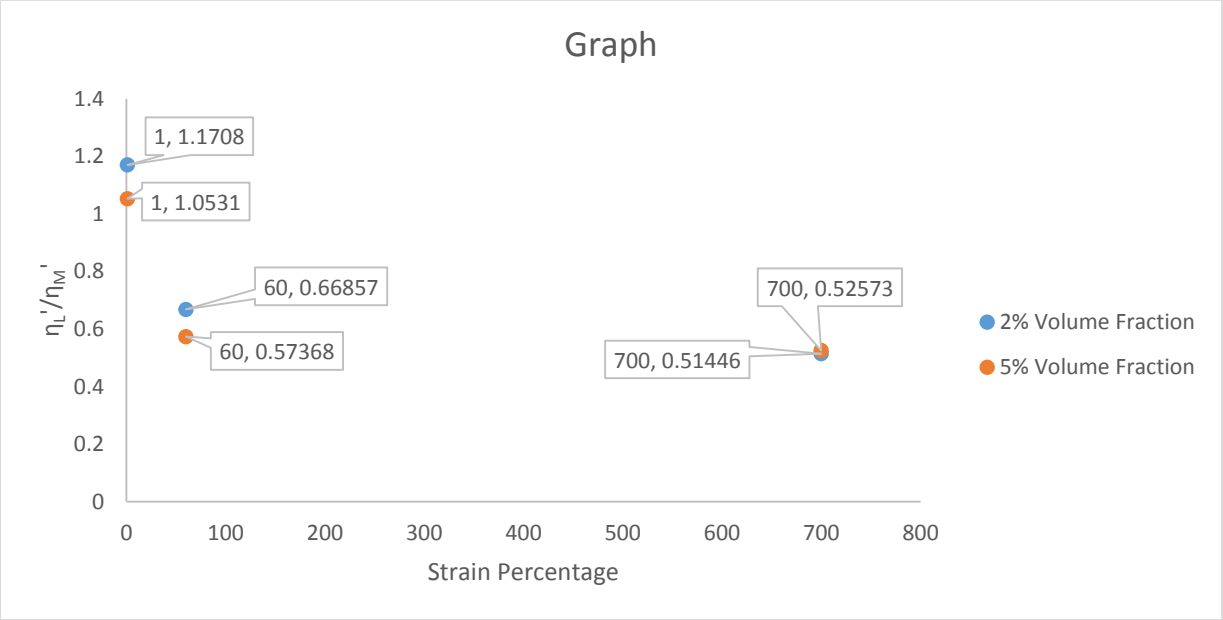

Figure 31: The variation of the ratio $\frac{\eta_L'}{\eta_M'}$ as a function of strain percentage for the 2 volume fractions at 5 rad/sec.

From the above results, we find that at a strain percentage of 1, the elastic and viscous Lissajous plots are nearly elliptical for both volume fractions evocative of a linear viscoelastic response. The values of $\frac{G_L'}{G_M'}$ and $\frac{\eta_L'}{\eta_M'}$ are close to 1 in all the cases indicating that we are observing in the linear regime. At a strain percentage of 60, we find an intracycle strain stiffening and shear thinning behavior. Of particular interest is the difference in the values of $\frac{G_L'}{G_M'}$ at a strain of 60%, 1 rad/sec for the 2% and 5% volume fractions. $\frac{G_L'}{G_M'}$ takes a value of 1.9238 in case of 2% volume fraction while it takes a value of 2.9011 for 5% volume fraction at this strain percentage and frequency. This could be probably because at this strain percentage and frequency, the bigger droplets (from the 2% volume fraction) are deviating less from linearity as compared to the smaller droplets (from 5% volume fraction). As the value of this parameter equals 1 in the linear regime, it can be concluded that a strain percentage of 60 and an angular frequency of 1 rad/sec does not introduce as much elastic nonlinearity in the 2% case as in the case of 5% owing to the fact that bigger droplets break their bonds less easily as compared to smaller droplets. It is interesting to note that the values of $\frac{G_L'}{G_M'}$ are very close to each other for the 2 volume fractions at the same strain percentage but at a frequency of 5 rad/sec. This angular frequency might be producing sufficient elastic nonlinearities in both the volume fractions. As we have noticed in previous cases, the linear response is observed at a strain of 700% in case of higher frequencies. From the elastic Lissajous plots, we observe that the curves tend to approach an elliptical nature as the frequency is increased from 1 rad/sec to 5 rad/sec. This could mean that the response is affected by slip and all material relaxation mechanisms are beginning to get disrupted so that a linear response is observed. However it is interesting to note that at a strain of 700%, the elastic Lissajous plot of the 2% volume fraction case assumes a more elliptical shape at a frequency of 5 rad/sec as compared to the 5% case.

CONCLUSIONS

The report focusses on a novel method to probe the nonlinear viscoelastic response of Pickering emulsions in a physically meaningful way. Through the use of the MITlaos protocol, the higher order Fourier coefficients can be physically interpreted and the use of tangent and secant moduli for characterizing nonlinear rheology is explained. Through the use of this framework, we obtain a better knowledge of the material response as compared to the conventional test protocols like SAOS. The repeatability aspect of the protocol as discussed in the report proves that MITlaos is indeed a robust technique and can serve as a powerful tool in the future for the Colloid Sciences Laboratory. The analysis of LAOS over a range of strain percentages and frequencies help us to determine the material behavior at both low and high strain percentages and frequencies. The observation of a linear behavior at high strain and frequency seems to indicate that the influence of slip might be affecting the relaxation mechanism of the material. With the aid of simultaneous imaging and rheology on the DHR, we had correlated the relationship between the droplet deformations and the LAOS response. An attempt to prevent slip using a transparent nail polish has been discussed in this report. To an extent we have been able to tackle slip as the material response assumes a less linear behavior at a strain of 700% as compared to the case where the surfaces were not treated. Also with the help of imaging we observed that the droplet motion is restricted when we treat the surfaces given by the comparison of images taken before and after the rheology analysis. Finally the LAOS response is probed by varying the particle volume fraction.

As a next step in the research, the phenomenon of slip could be studied in much more detail. As we had based some of our arguments on the basis of slip, future research can be performed to see how exactly is slip disrupting the relaxation mechanisms and what are the structural implications of the same. For the purpose of imaging, using a mixture of fluorescent and non-fluorescent particles can help us to image deeper than the first layer on the DHR and analyze the difference between the slip at bottom and top surfaces. Using Pearson correlation coefficient to quantify the irreversible microstructure deformations can be useful in this regard.

APPENDIX 1

Repeatability of LAOS tests at 60% Strain and 1 rad/sec frequency

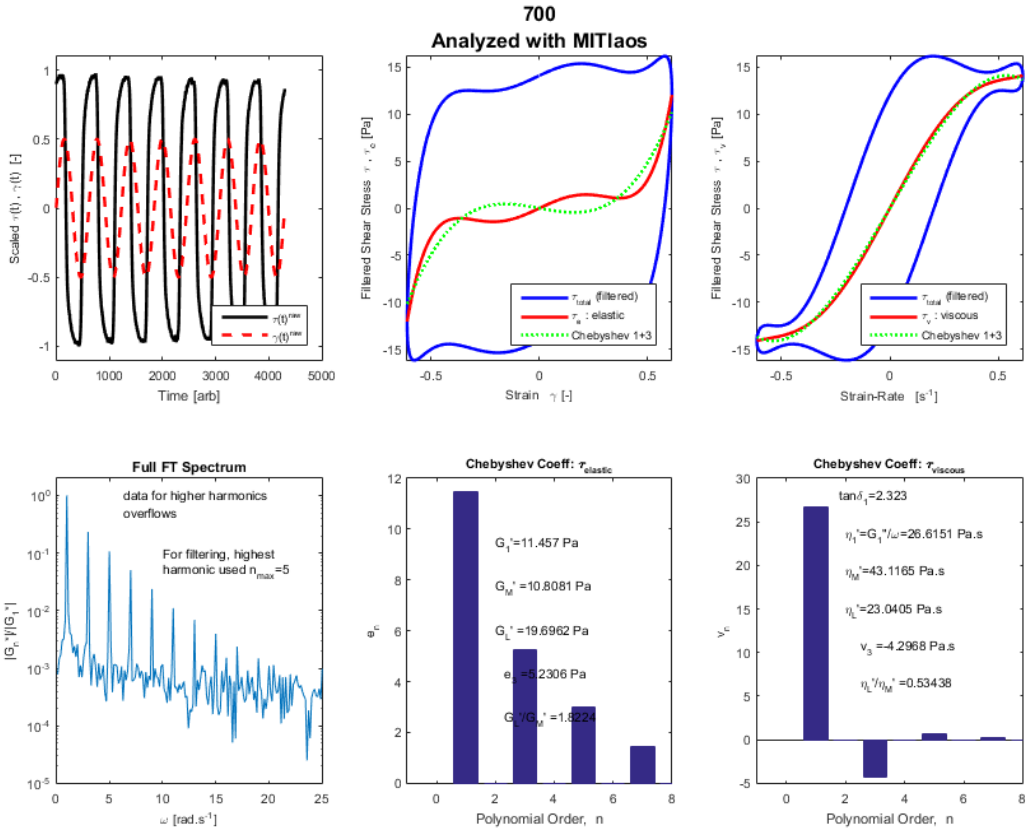

Overview Plot 1

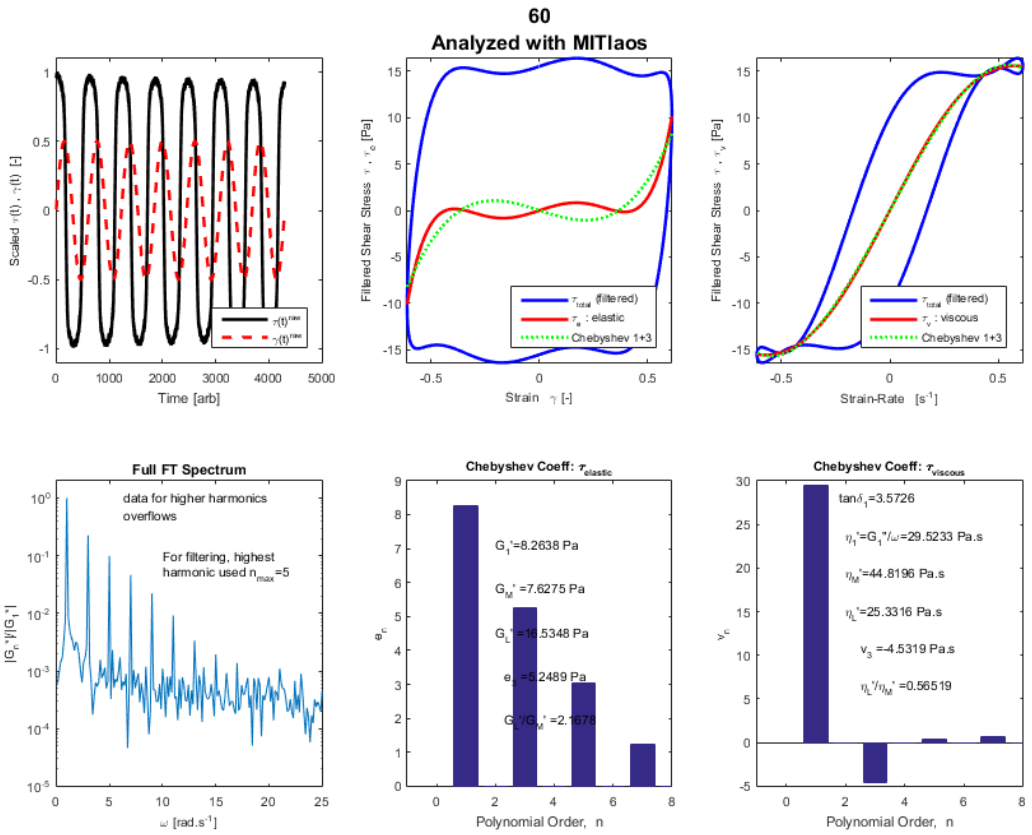

Overview Plot 2

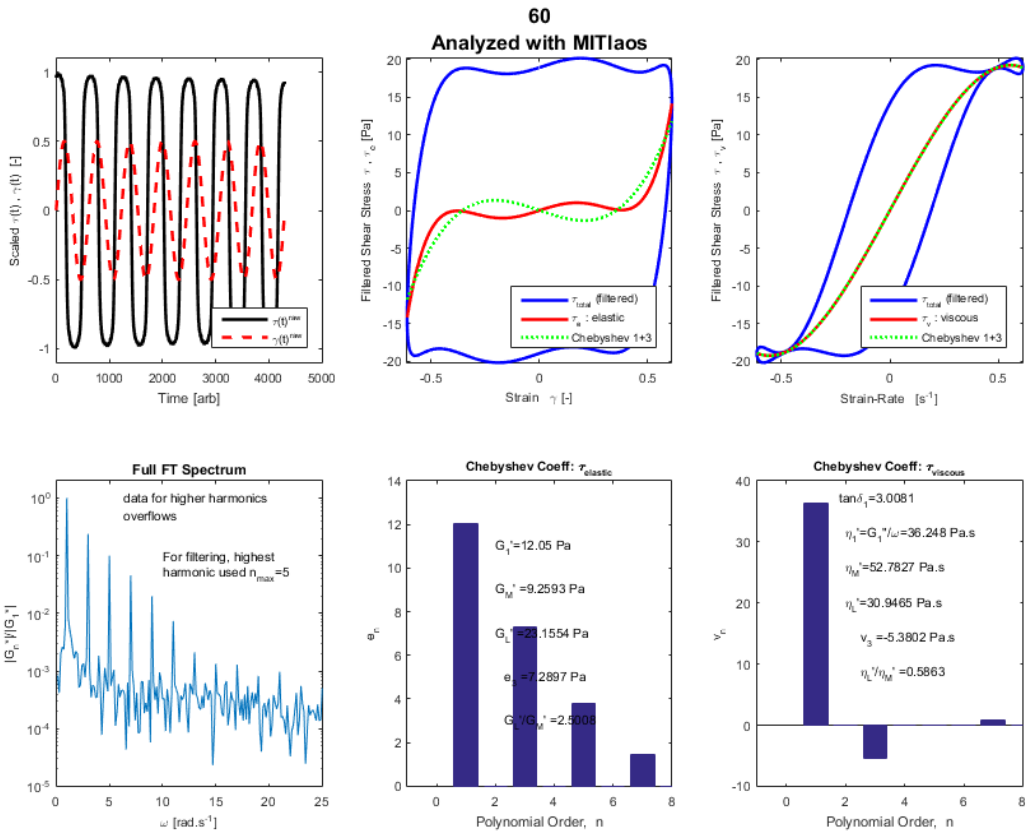

Overview Plot 3

APPENDIX 2

LAOS Analysis with the variation of strain percentage and frequency

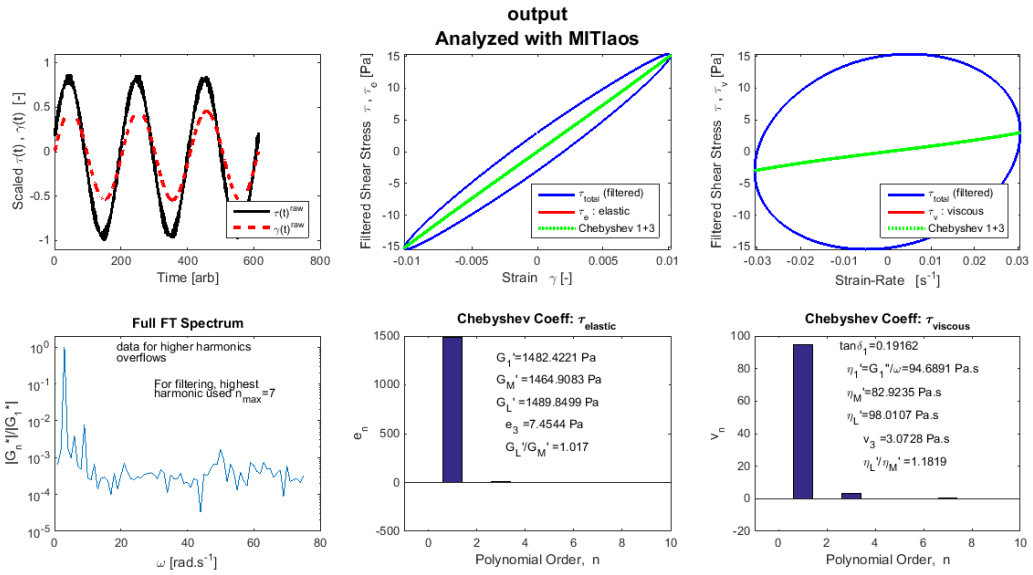

Strain 1%, frequency 3 rad/sec

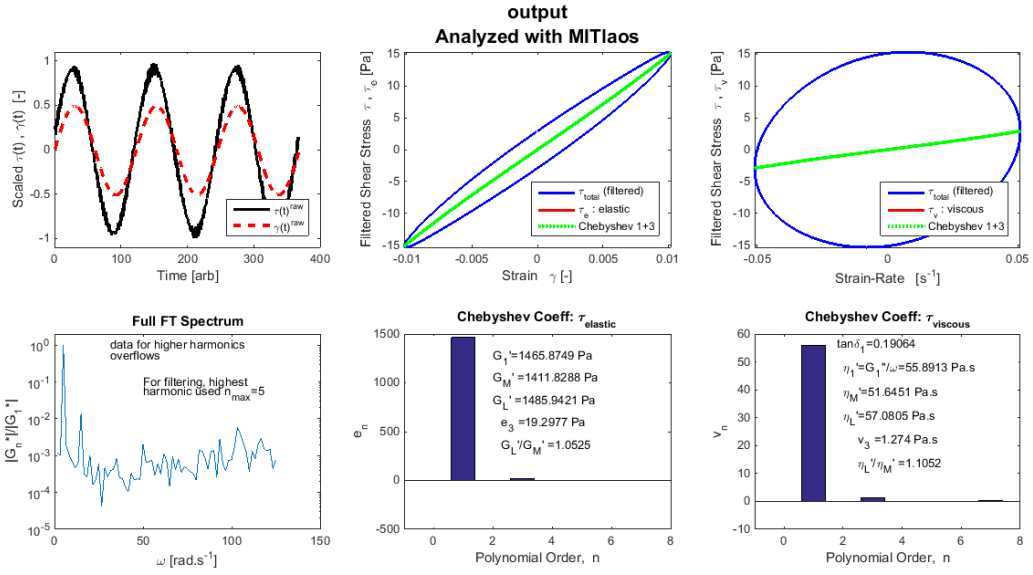

Strain 1%, frequency 5 rad/sec

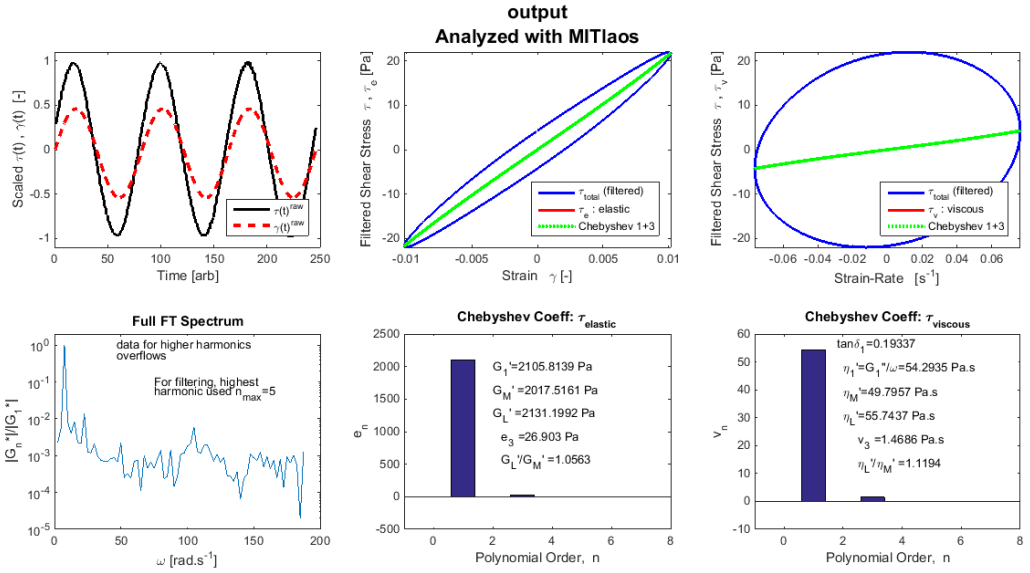

Strain 1%, frequency 7.5 rad/sec

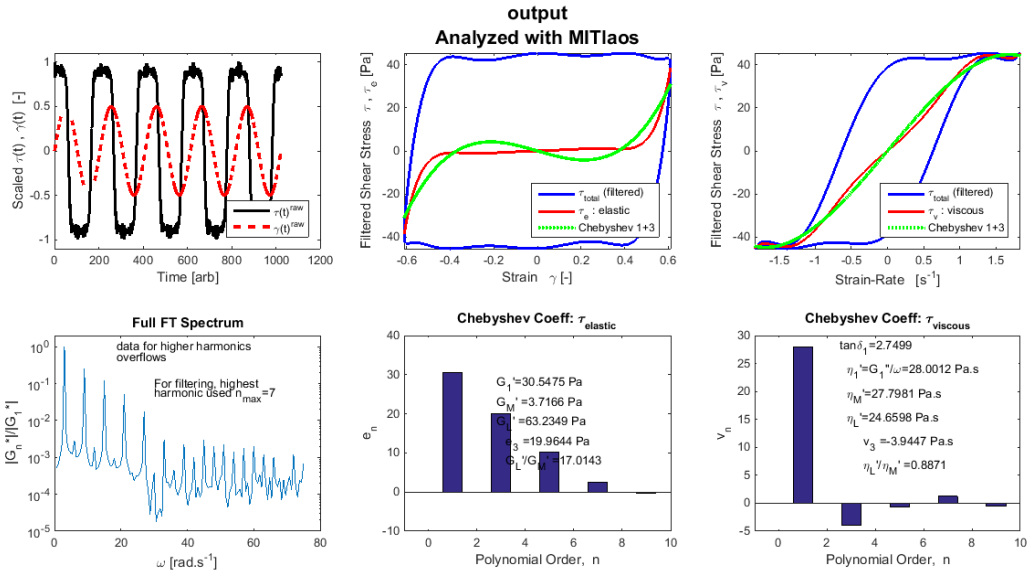

Strain 60%, frequency 3 rad/sec

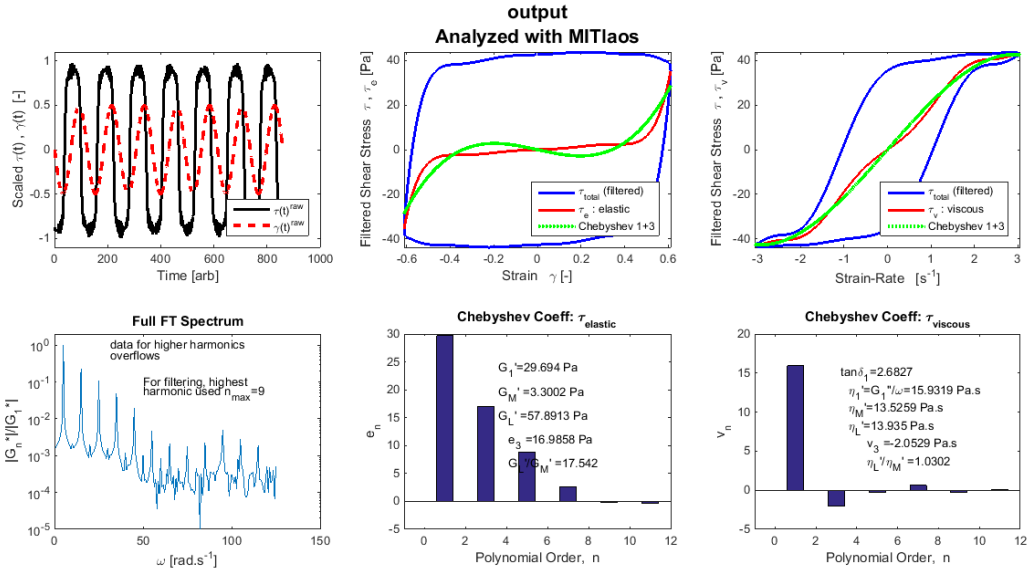

Strain 60%, frequency 5 rad/sec

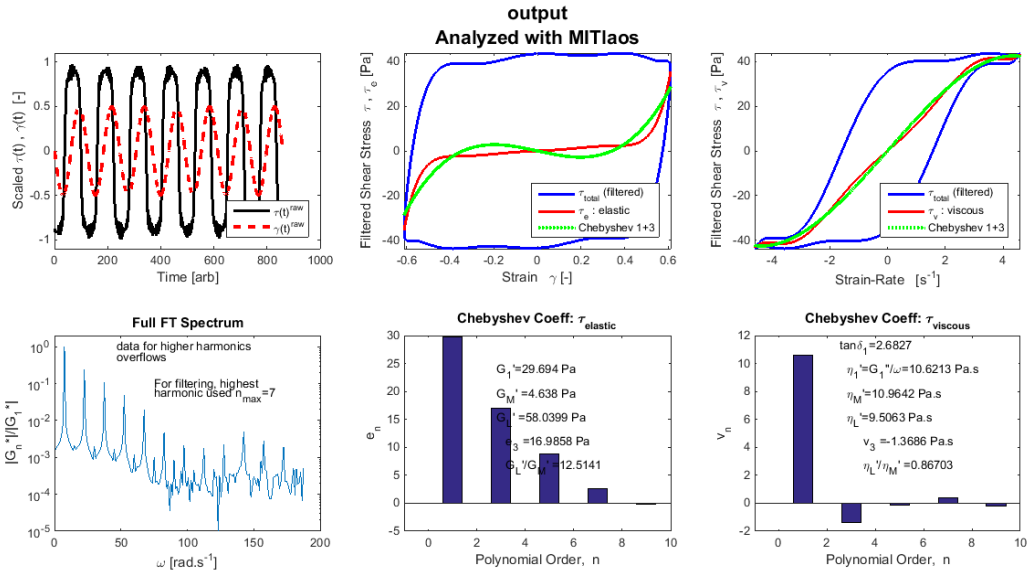

Strain 60%, frequency 7.5 rad/sec

Figure 4

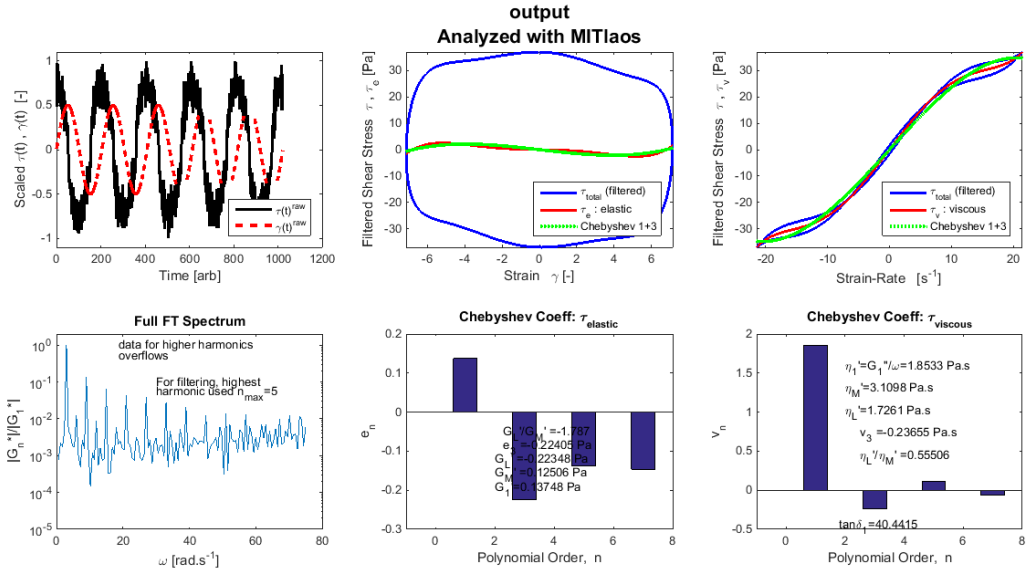

Strain 700%, frequency 3 rad/sec

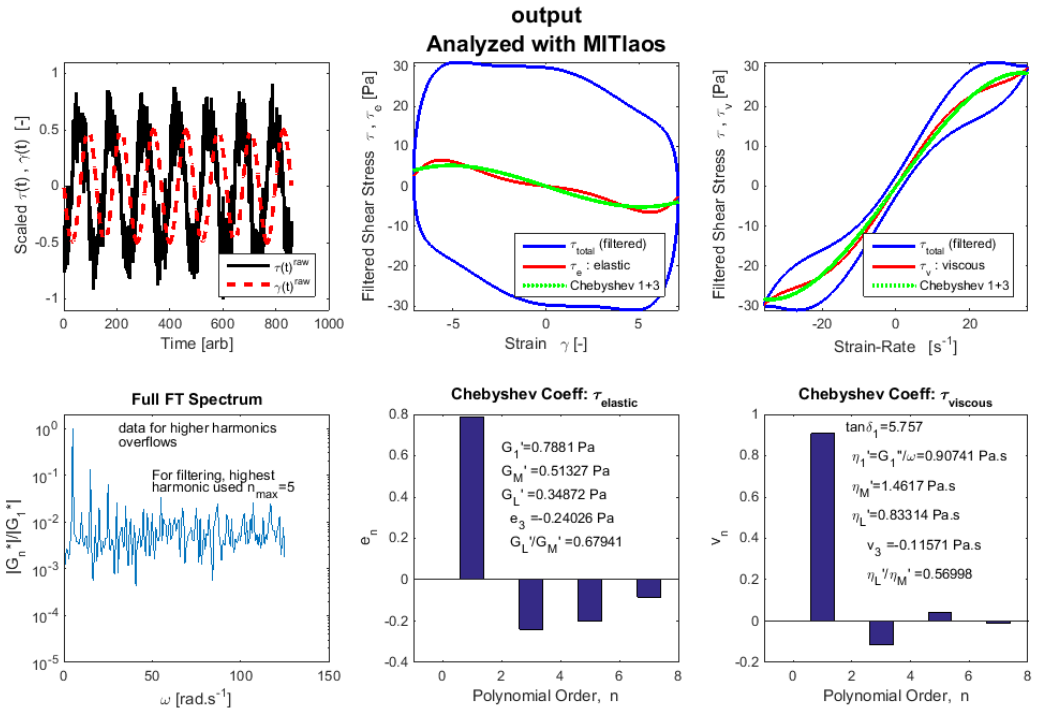

Strain 700%, frequency 5 rad/sec

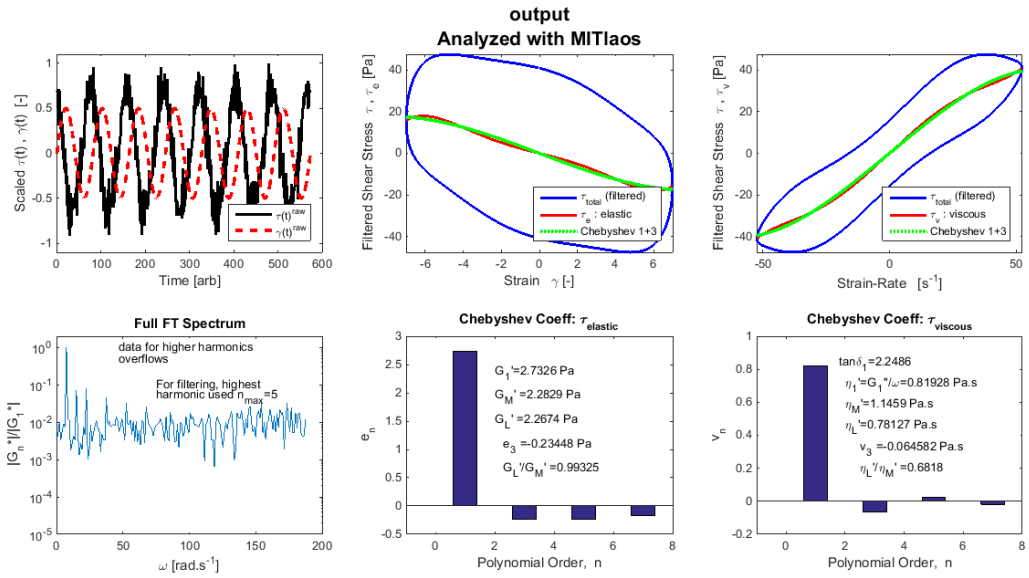

Strain 700%, frequency 7.5 rad/sec

APPENDIX 3

Analysis of effect of slip on LAOS studies

1. Slip Condition

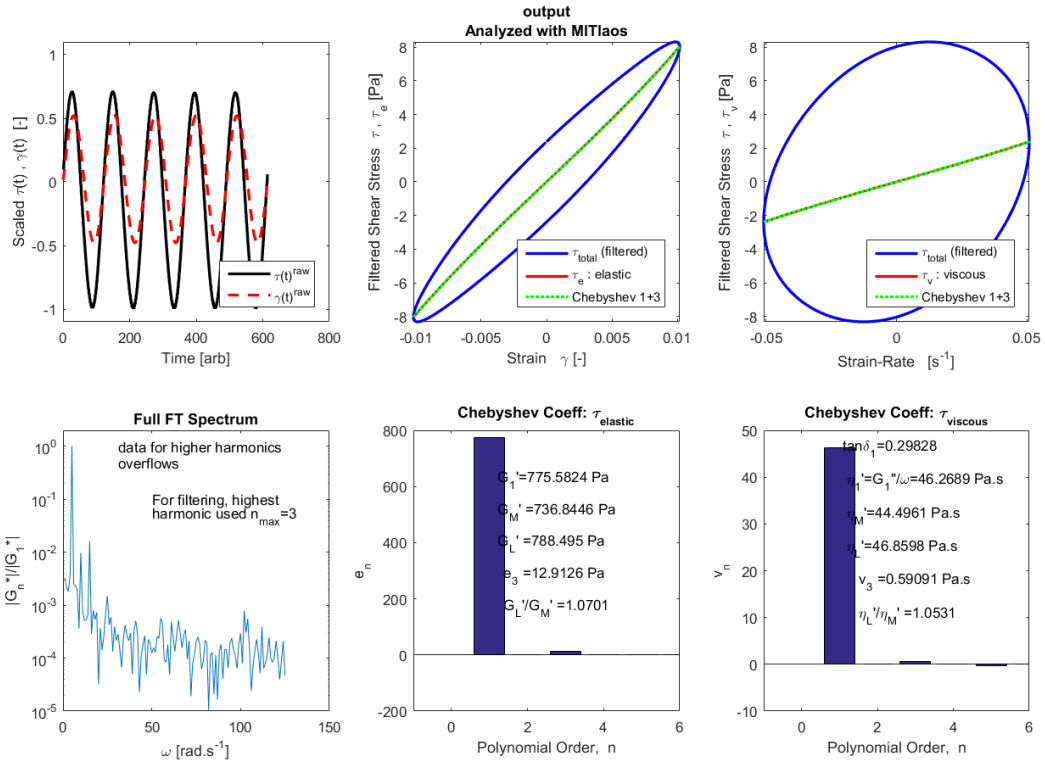

Strain 1 %, frequency 5 rad/sec

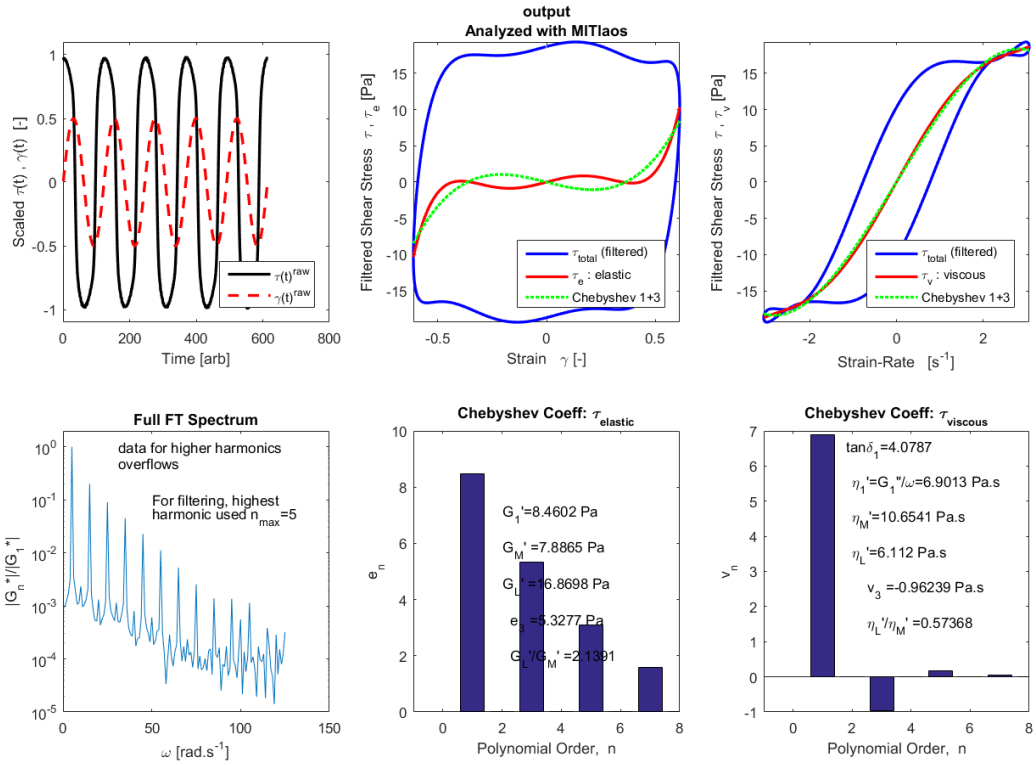

Strain 60%, frequency 5 rad/sec

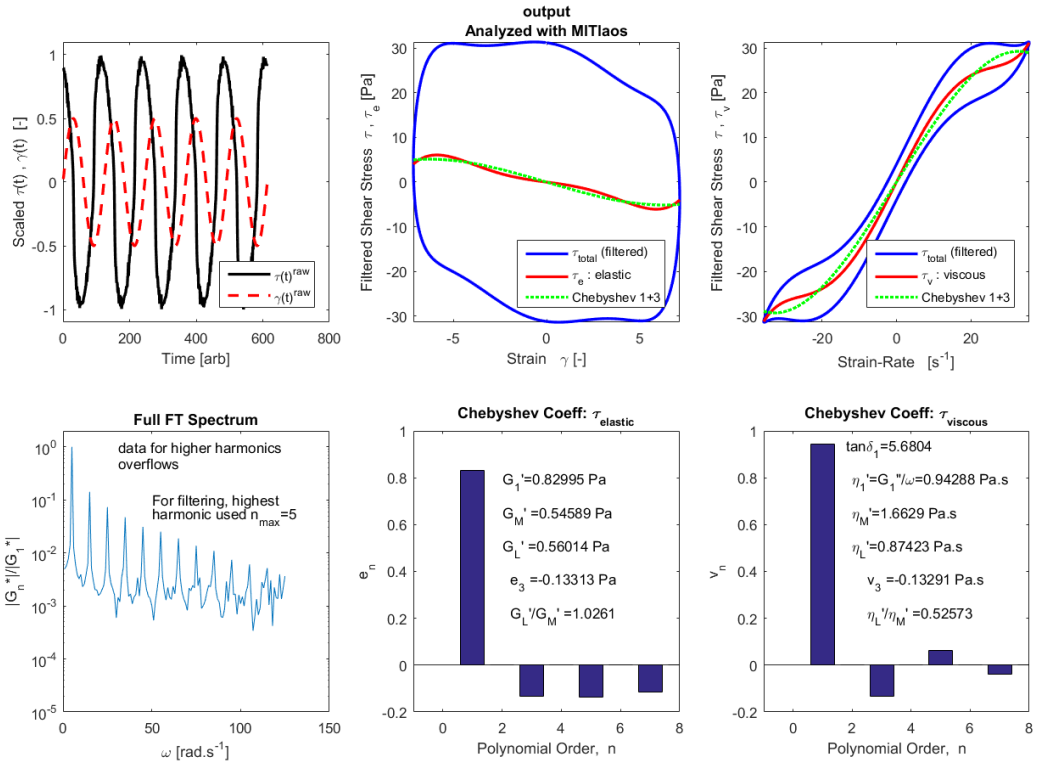

Strain 700%, frequency 5 rad/sec

2. No-Slip Condition

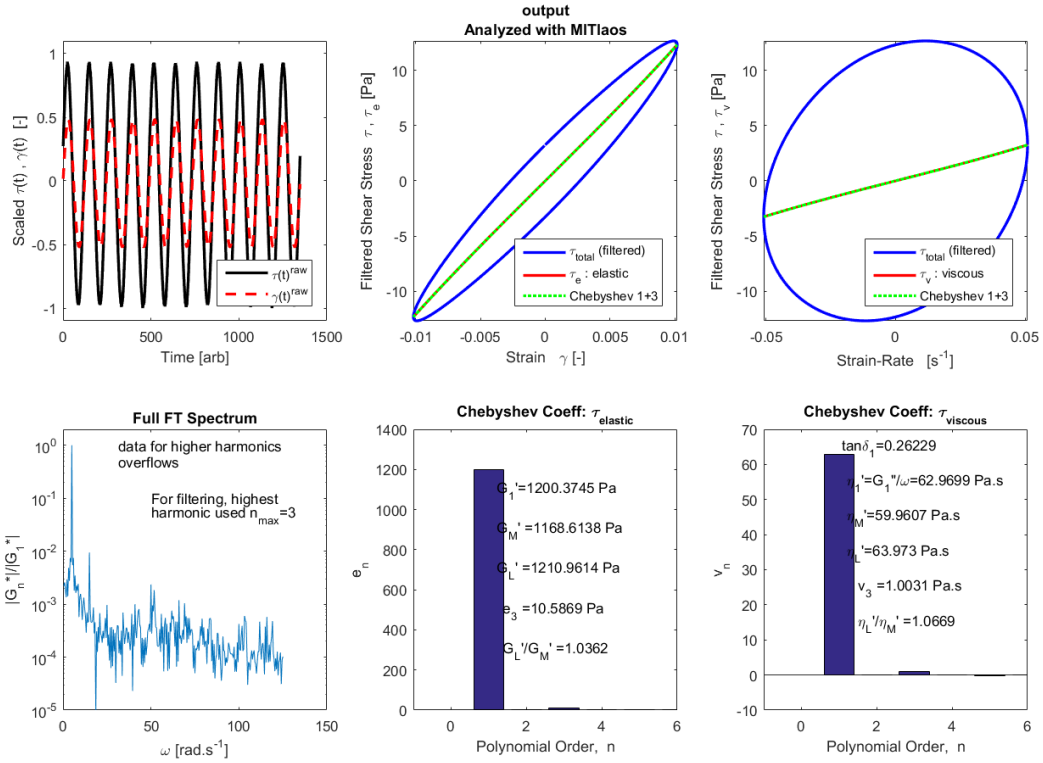

Strain 1%, frequency 5 rad/sec

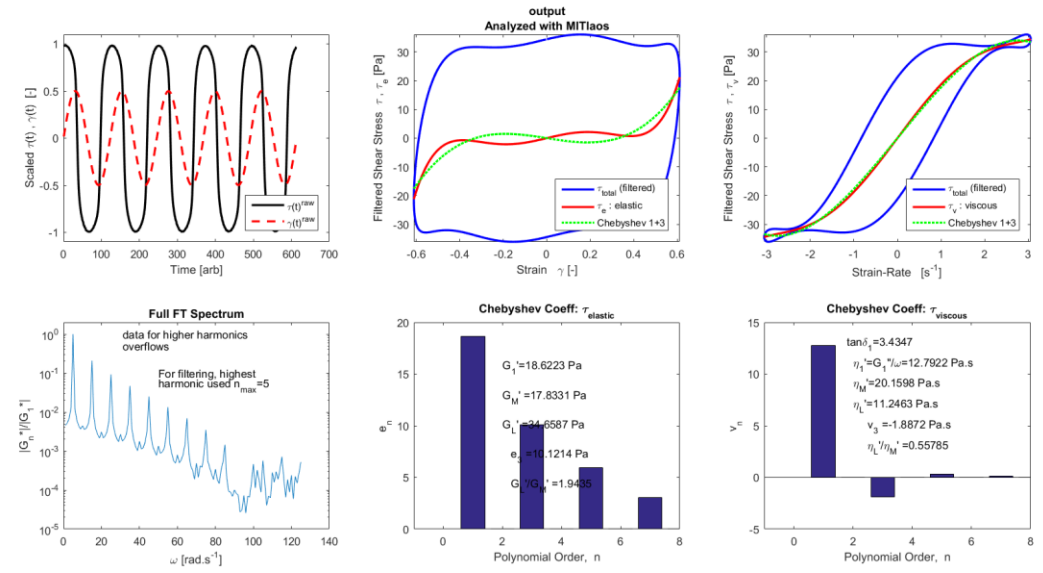

Strain 60%, frequency 5 rad/sec

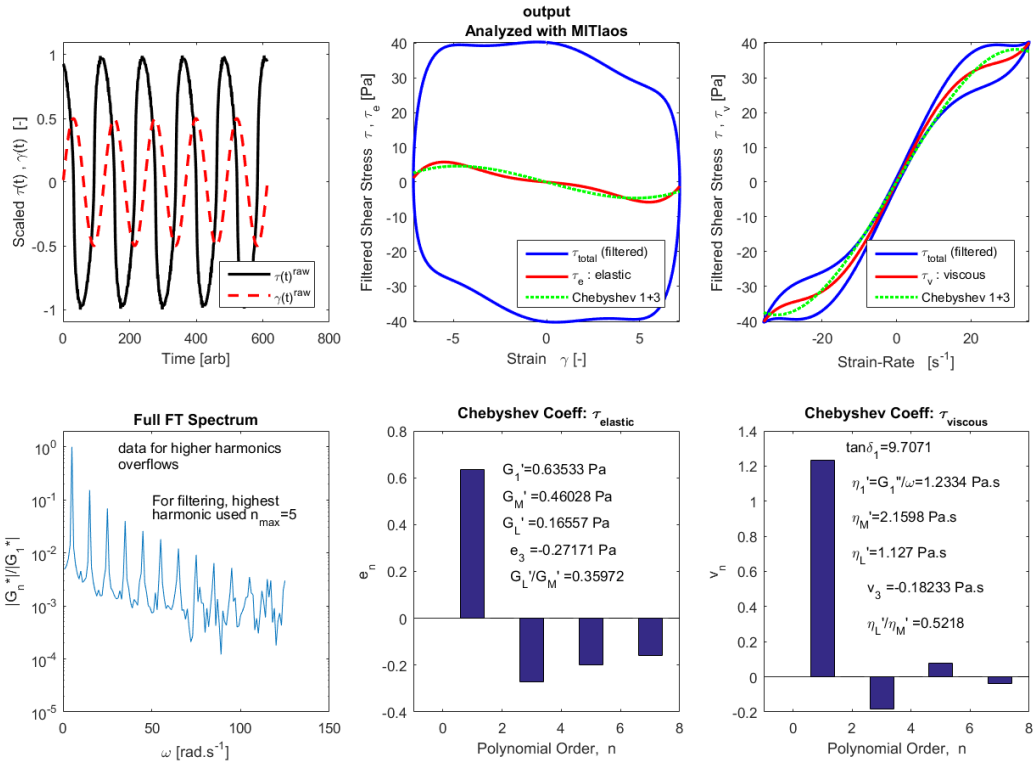

Strain 700%, frequency 5 rad/sec

APPENDIX 4

LAOS analysis with the variation of particle volume fraction

1. 2% Volume Fraction

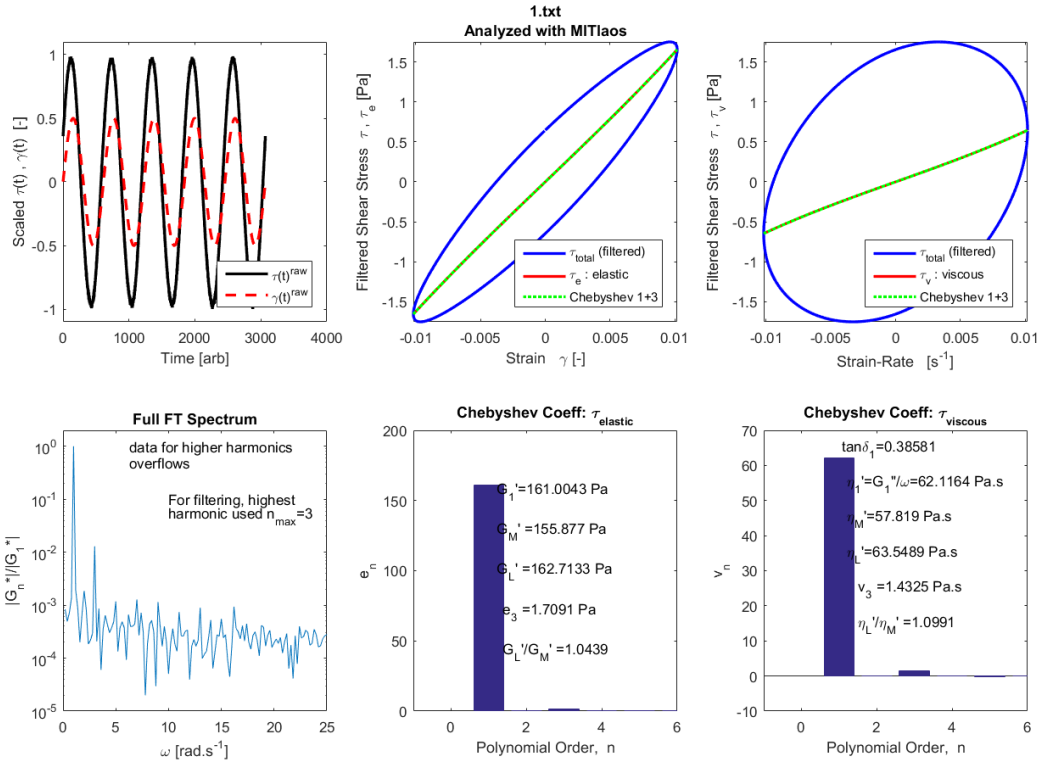

Strain 1%, frequency 1 rad/sec

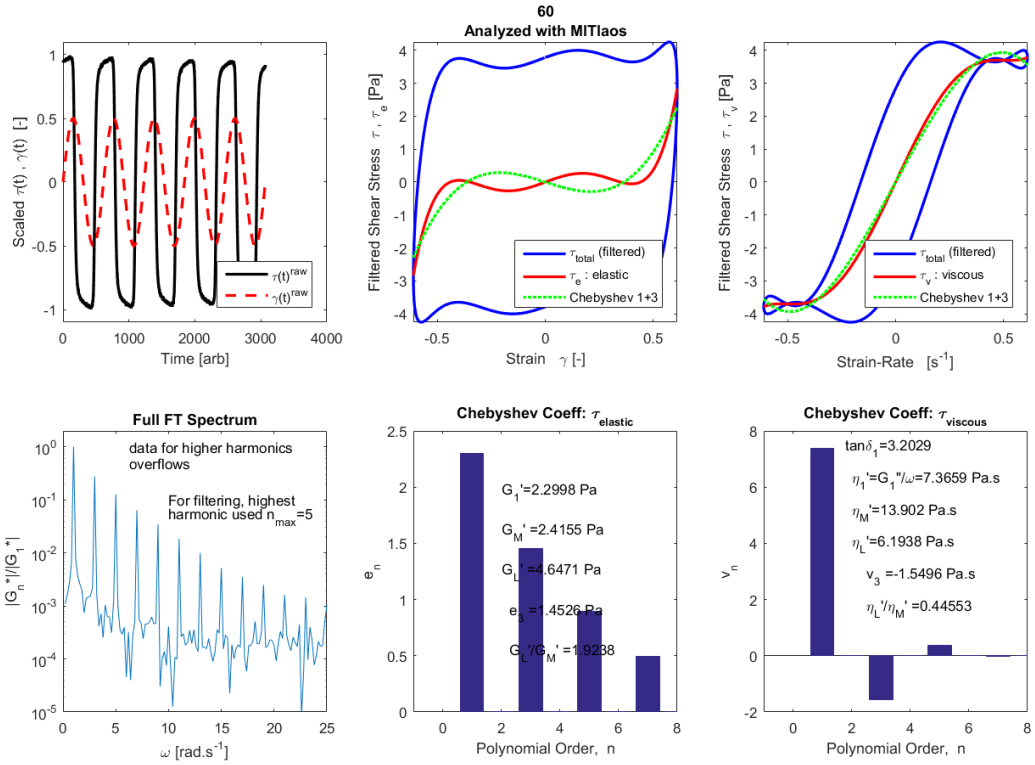

Strain 60%, frequency 1 rad/sec

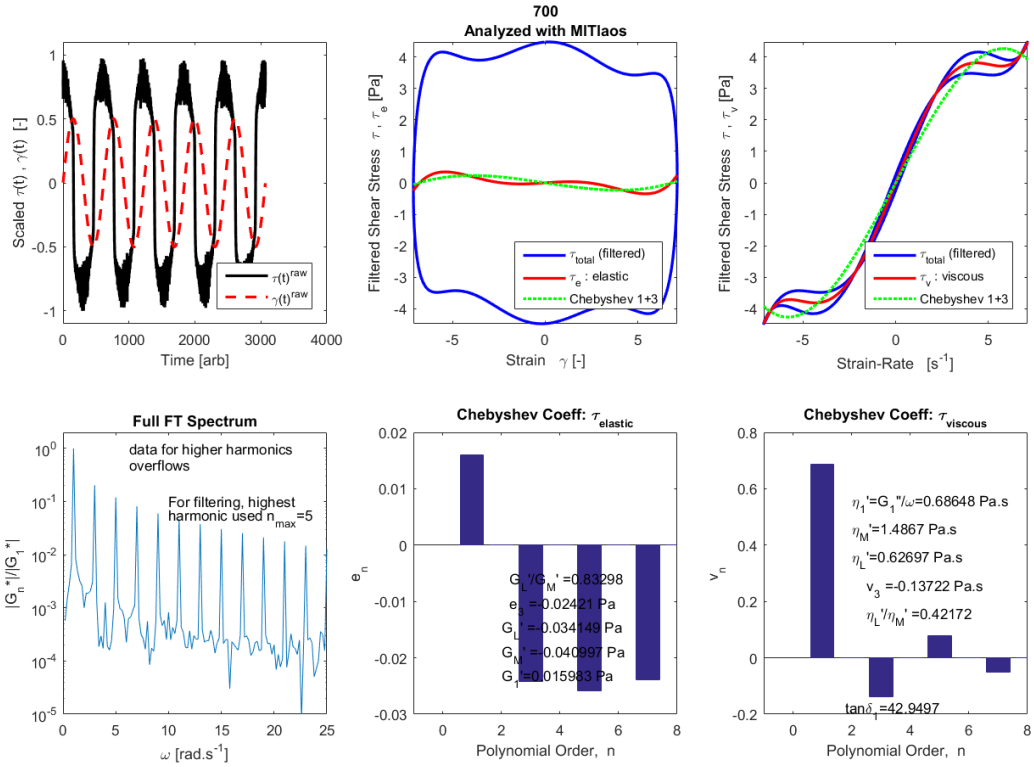

Strain 700%, frequency 1 rad/sec

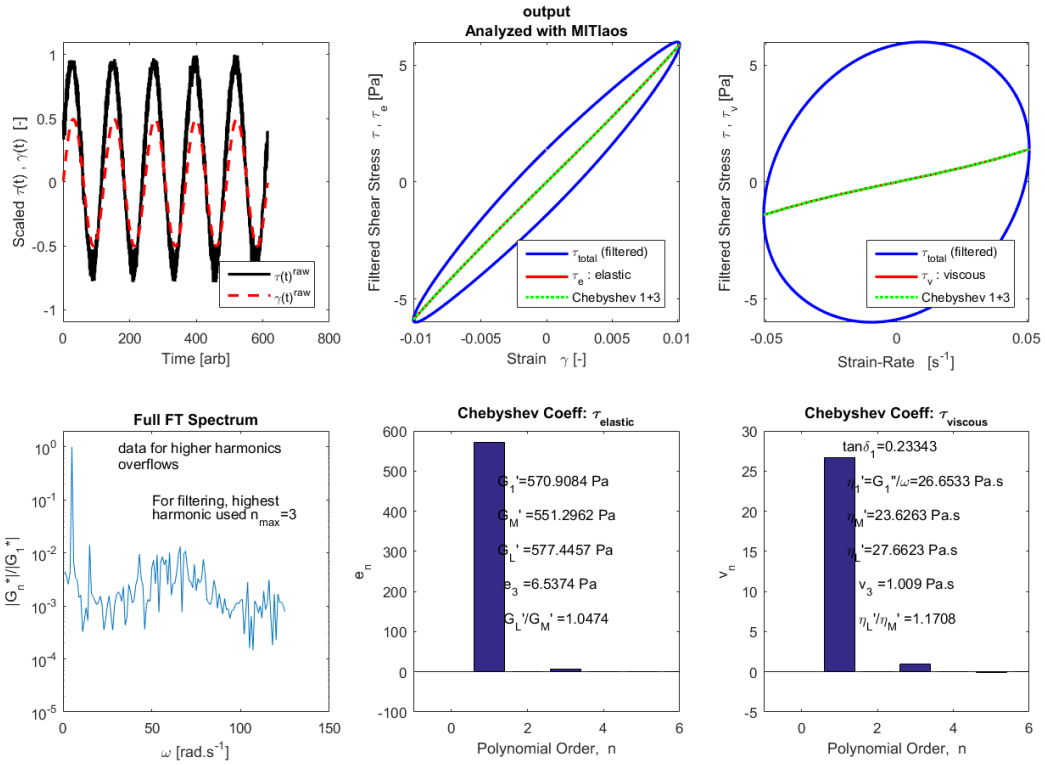

Strain 1%, frequency 5 rad/sec

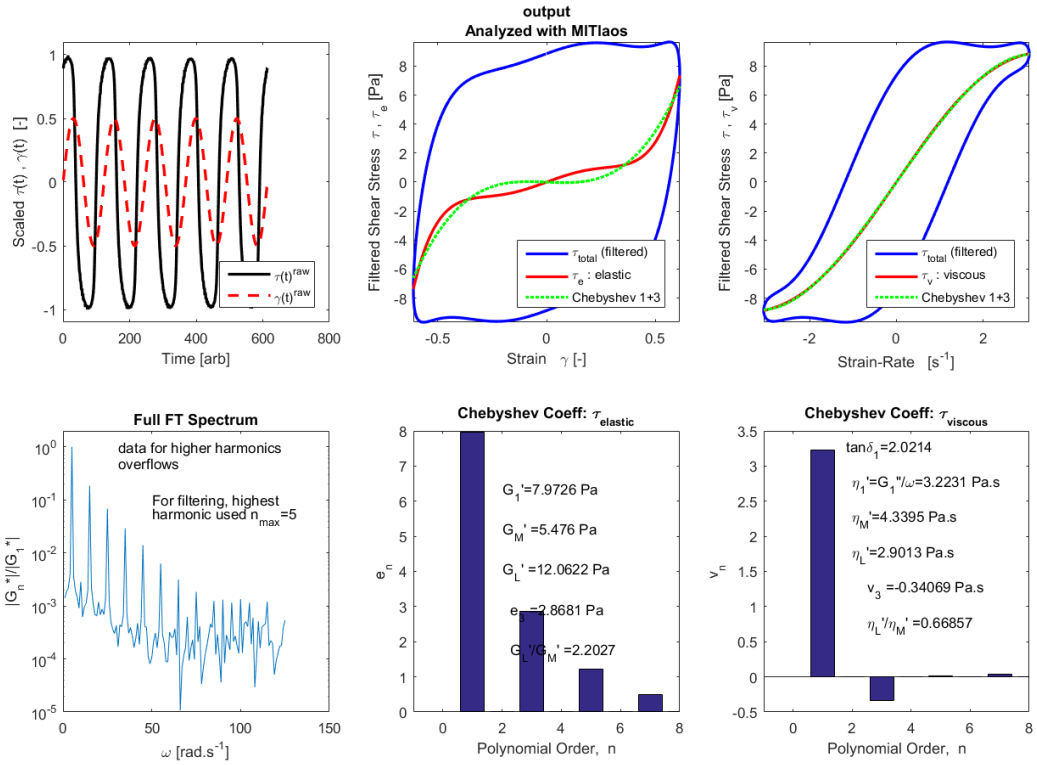

Strain 60%, frequency 5 rad/sec

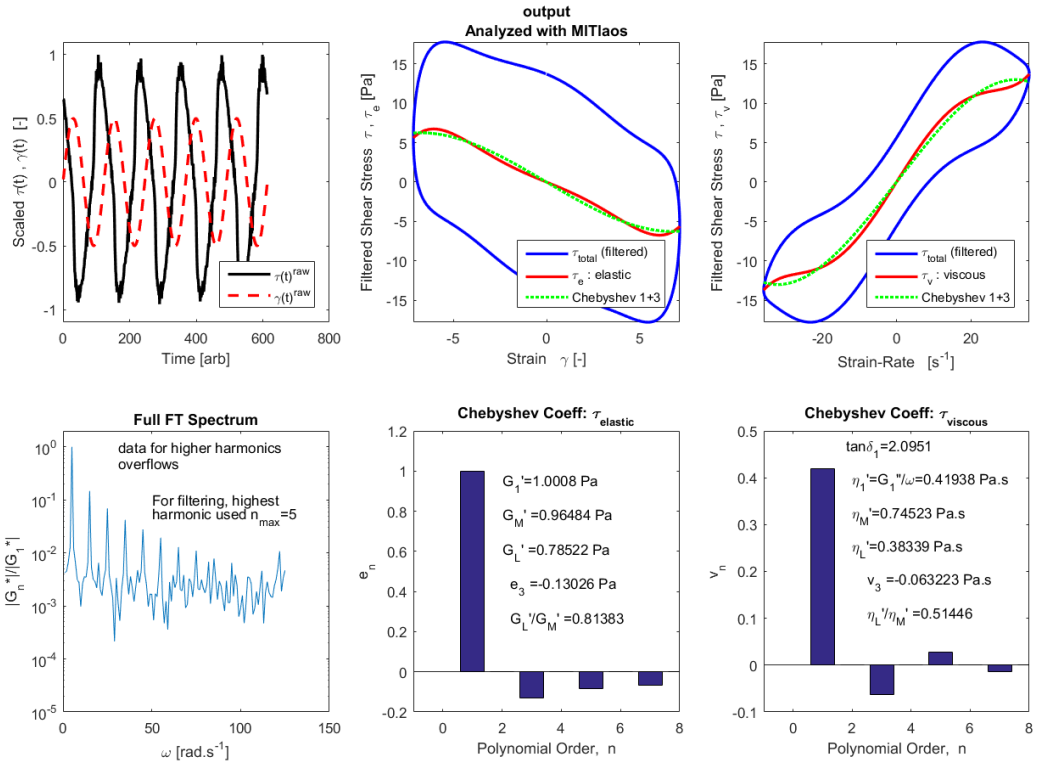

Strain 700%, frequency 5 rad/sec

2. 5% Volume Fraction

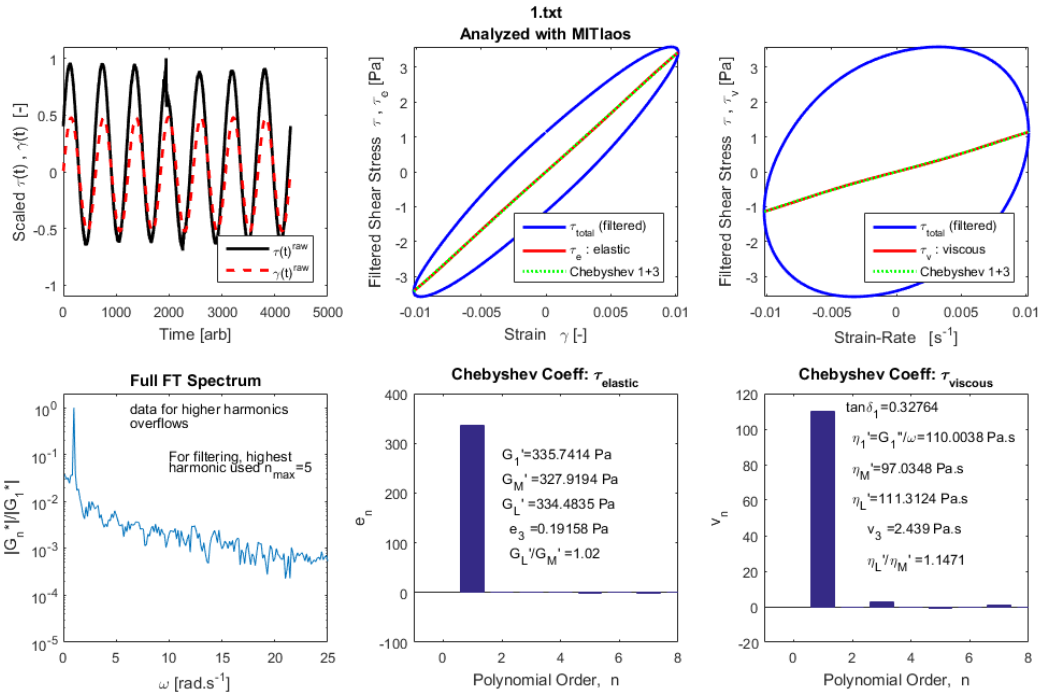

Strain 1%, frequency 1 rad/sec

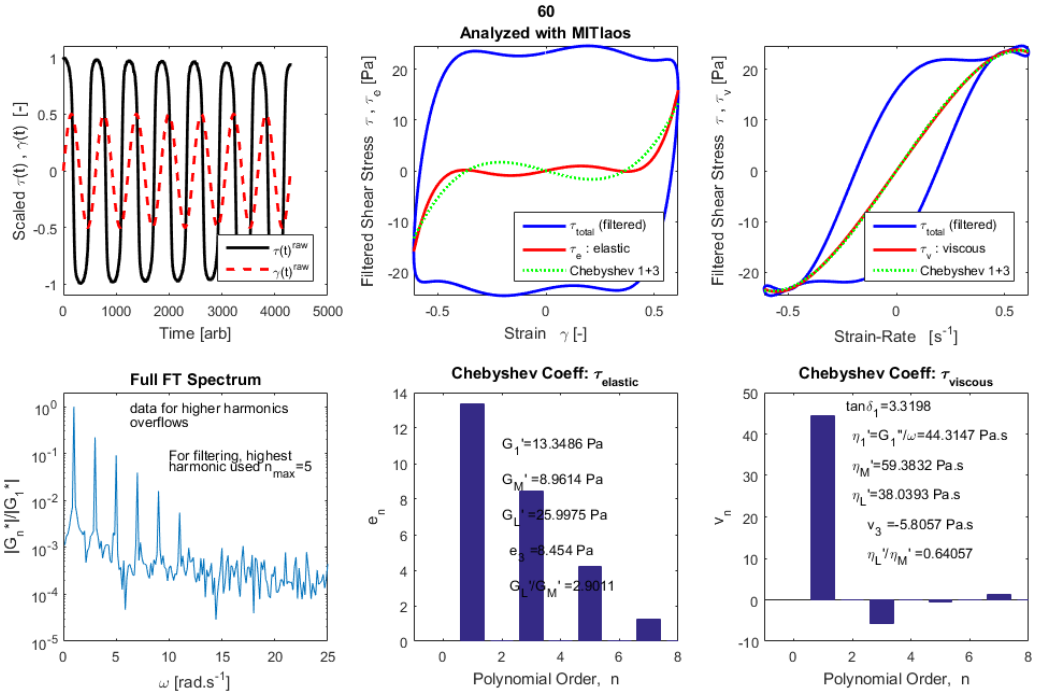

Strain 60%, frequency 1 rad/sec

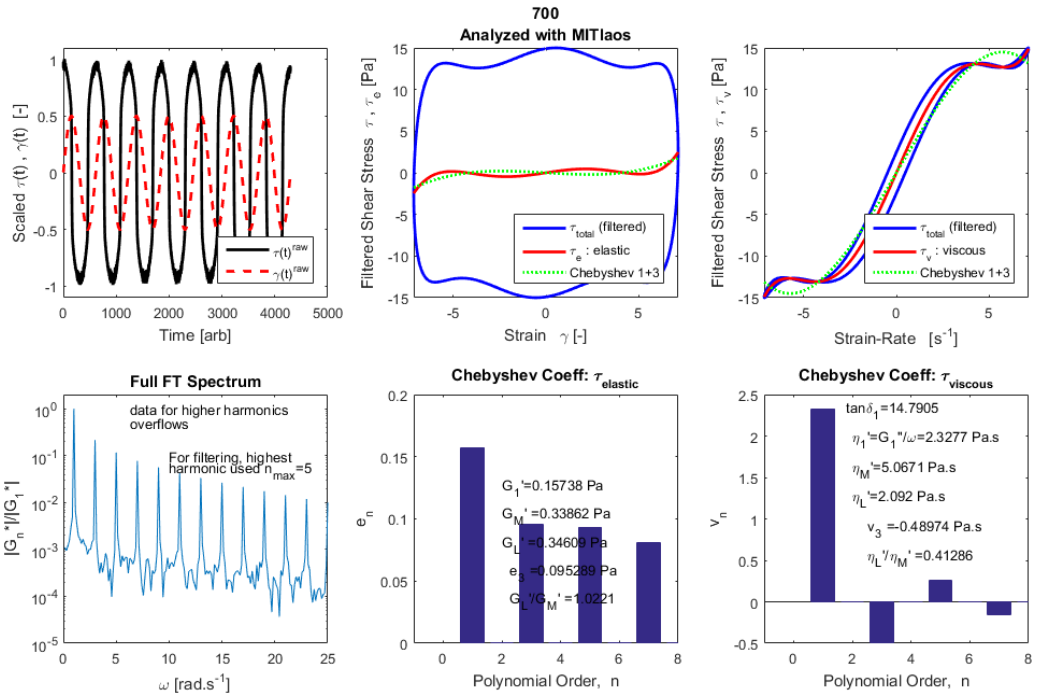

Strain 700%, frequency 1 rad/sec

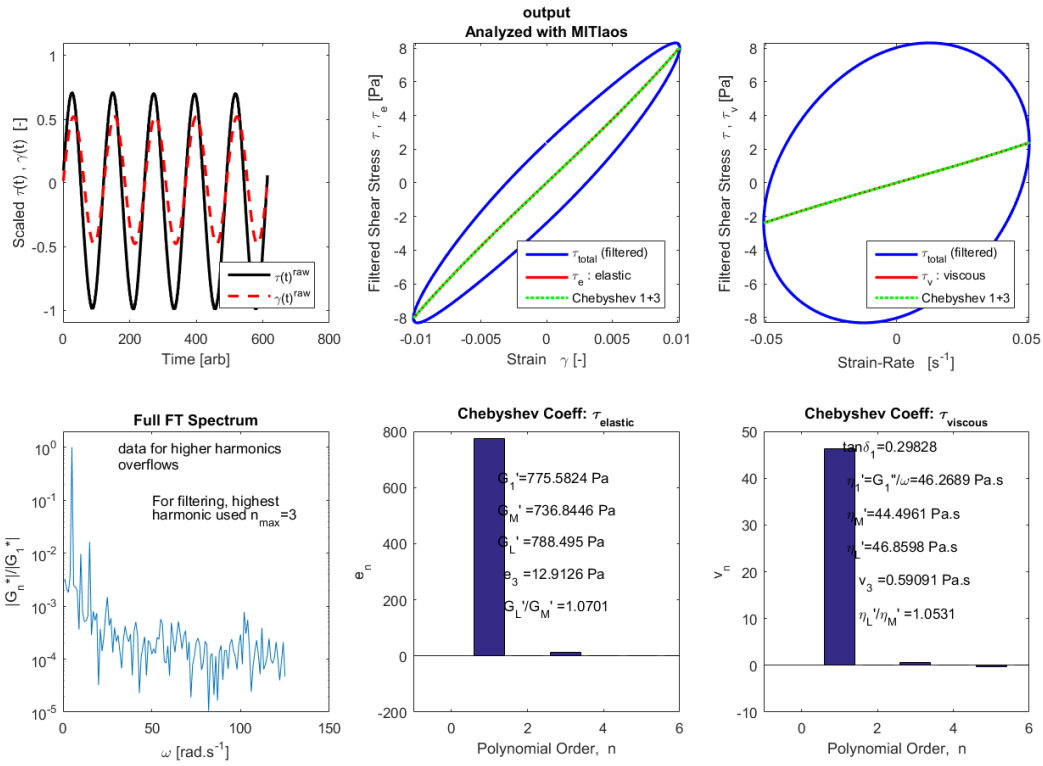

Strain 1%, frequency 5 rad/sec

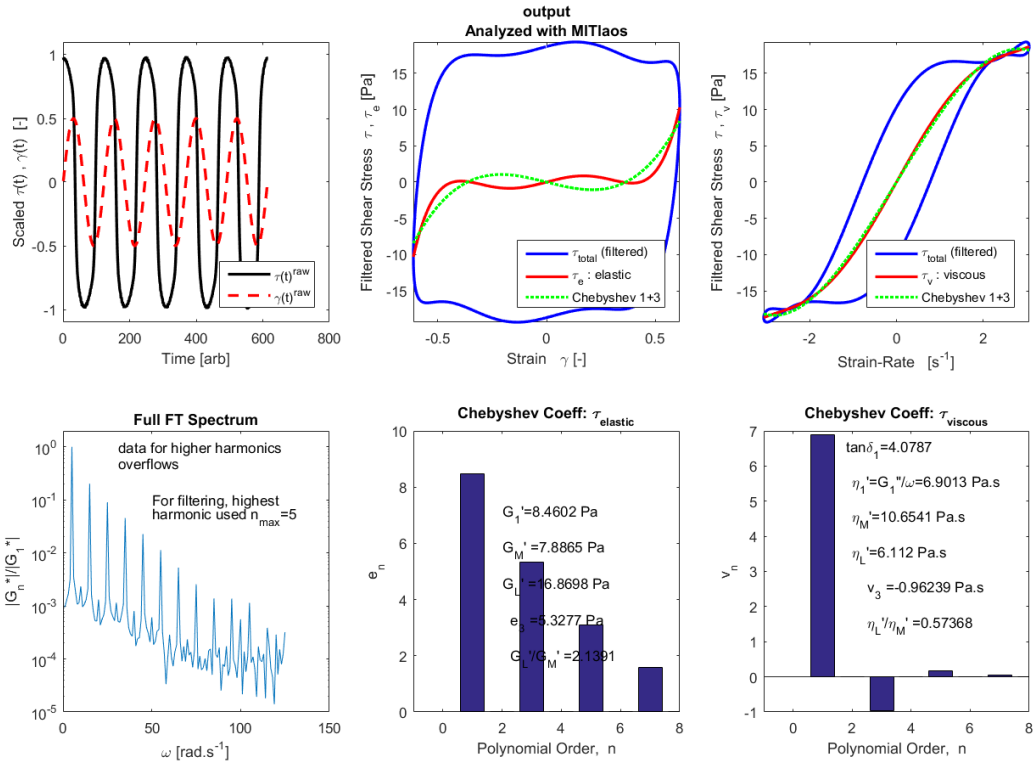

Strain 60%, frequency 5 rad/sec

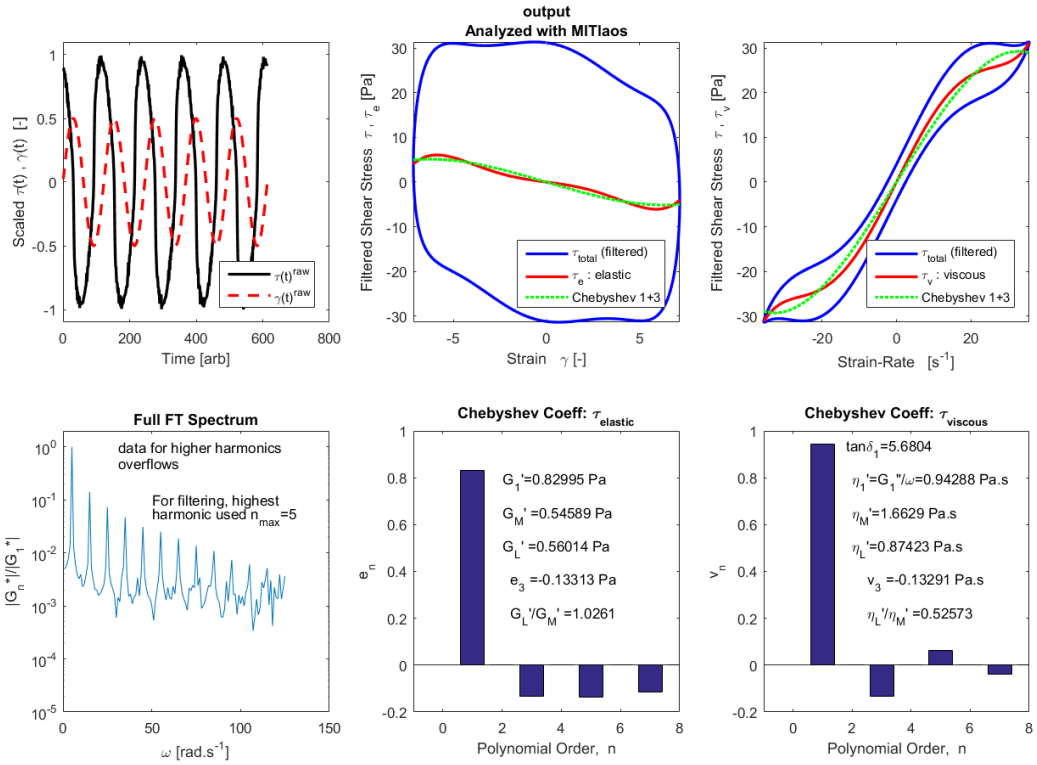

Strain 700%, frequency 5 rad/sec

REFERENCE

1. Tadros, T. F. (2009) Emulsion Science and Technology: A General Introduction, in Emulsion Science and Technology (ed T. F. Tadros), Wiley-VCH Verlag GmbH & Co. KGaA, Weinheim, Germany. doi: 10.1002/9783527626564.ch1
2. S. U. Pickering. *J. Chem. Soc. 1907, 91*, 2001.
3. Yves Chevalier, Marie-Alexandrine Bolzinger, Colloids and Surfaces A: Physicochemical and Engineering Aspects, Volume 439, 20 December 2013, Pages 23–34
4. Michiel Hermes and Paul S. Clegg, Soft Matter, 2013, 9, 7568
5. Stefan A. F. Bon, CHAPTER 1 : The Phenomenon of Pickering Stabilization: A Basic Introduction, in *Particle-Stabilized Emulsions and Colloids: Formation and Applications*, 2014, pp. 1-7
6. Studart, A. R. (2008), Book Review: Colloidal Particles at Liquid Interfaces. By Bernard P. Binks and Tommy S. Horozov (Eds.).. Adv. Mater., 20: 207. doi:10.1002/adma.200700947
7. Hyun, Kyu, Manfred Wilhelm, Christopher O. Klein, Kwang Soo Cho, Jung Gun Nam, Kyung Hyun Ahn, Seung Jong Lee, Randy H. Ewoldt, and Gareth H. McKinley. “A Review of Nonlinear Oscillatory Shear Tests: Analysis and Application of Large Amplitude Oscillatory Shear (LAOS).” Progress in Polymer Science 36, no. 12 (December 2011): 1697–1753.
8. Randy H. Ewoldt, A. E. Hosoi and Gareth H. McKinley, J. Rheol. 52, 1427 (2008); http://dx.doi.org/10.1122/1.2970095
9. Ewoldt, R. H., C. Clasen, A. E. Hosoi, and G. H. McKinley, “Rheological fingerprinting of gastropod pedal mucus and synthetic complex fluids for biomimicking adhesive locomotion,” Soft Matter 3, 634–643 (2007).
10. Barry N. Taylor and Chris E. Kuyatt, Guidelines for Evaluating and Expressing the Uncertainty of NIST Measurement Results, NIST Technical Note 1297, 1994 Edition
11. Eamonn Mullins: Statistics for the Quality Control Chemistry Laboratory, DOI: 10.1007/s00216-005-3184-6, 2005-07
12. Interlaboratory Testing Programs, Statistical Quality Control Principles, Saskatchewan Highways and Transportation
13. Steve Granick, Yingxi Zhu & Hyunjung Lee, *Nature Materials* **2**, 221 - 227 (2003) doi:10.1038/nmat854
14. Taha Sochi (2011) Slip at Fluid-Solid Interface Polymer Reviews 51: 4. 309-340